University Of Bahrain

College of Engineering



Department of Mechanical Engineering

Study of Drag and Lift on a Moving Aerodynamic Airfoil with Varying Winglet Geometry

A Thesis submitted in Partial Fulfillment of the Requirements of the Master's Degree in Mechanical Engineering

Submitted by

Ebrahim Kamal Seddiq

University number: 20121003

Supervised by

Dr. Mohamed Nabhan

(Associate Professor)

University of Bahrain

Kingdom of Bahrain

October, 2016

University of Bahrain
Graduate Studies Council

Thesis Discussion Committee Decision

Student Name: Ebrahim Kamal Seddiq	Student ID: 20121003
Department: Mechanical Engineering	College: Engineering
Program: Master's Degree in Mechanical Engineering	
Thesis Title: Study of Drag and Lift on a Moving Aerodynamic Airfoil with Varying Winglet Geometry.	
Supervisor Name: Dr. Mohamed Nabhan	Student GPA: 3.75

The Discussion Committee met on Thursday (day and date) 19/1/17 in Hall no. 14 (hall/room no.) 162. Upon discussing the student whose details are stated above in public, the discussion committee recommends the following:

The student awarded grade A- In the thesis subject MSc in Mech. Engineering

☐ Without making any changes to the thesis
☐ After making the modifications attached with this decision

Discussion Committee Members Approval:

Name		Signature
1. Mohd Nabhan	(Advisor)	
2. Ahmed Yousseb	(Internal Examiner)	
3. WALID CHAKROUN	(External Examiner)	

قسم الهندسة الميكانيكية
DEPT. OF MECHANICAL ENGINEERING
UNIVERSITY OF BAHRAIN

Declaration

I declare that this work is the result of my own investigation and that it has not already been accepted in substance for any degree, nor is it being currently submitted for any degree.

Signed: ..... Date: .....

Abstract

Aerodynamic characteristics of plain wing designed for Light Sport Aircraft has been studied. The fluid characteristics include induced drag and lift to drag ratio. Then, winglets are added to reduce the induced drag and increase the lift to drag ratio which are affected by the wing tip vortices. The theoretical, numerical, and experimental approaches are used to verify the results.

A rectangular untwisted 9.528 m wing spans with an Airfoil NACA 4412 was used for the basic design. Winglets are added with a tip airfoil of NACA 0012, side angle of 65° and new projected area of 10.328 m. Lift and drag coefficients are used as means to measure the improvement of the aerodynamic characteristics. The wing tip vortices increase the induced drag and spoil the lift over the wing's surface. The winglets design main objectives are:

1- Decrease the induced drag.

2- Decrease the fuel consumption.

3- Increase the flight safety, especially in take-off condition.

Multi trails have been tried on 3-D Foil Multi-Surfaces code to get the optimum design of the winglets. The 3-D model and the original models are manufactured at Polytechnic University using 3-D printer. The models were experimentally tested in C-15 wind tunnel at University of Bahrain. The tests repeated three times at 30%, 60%, and 90% fan speed power for each model and at different angles of attack namely: 0°, 5°, and 10°.

The second verification method was to simulate the 3-D models with Fluent Ansys 14 at 50 m/s velocity and (0^{o}, 5^{o}, and 10^{o}) angles of attack with laminar flow and Standard Boundary Conditions (S.B.C) such as 15^{o} Temperature, 101.325 Kpa atmospheric pressure and all other flow parameters as well.

The third verification method was also to simulate the 3-D models with 3-D Foil Multi-Surfaces code again with the same flow parameters. Finally, the last verification method was to solve the problem theoretically using the governing equations. The theoretical solutions were used as a base line for all other results.

The total drag reduction observed from the calculation is about

2% to 14.5 % during the takeoff regime, where the induced drag contributes about 60% of total drag of the wings. The lift to drag ratio improved also in our designed wing by a maximum of 18.6% from the plain wing design.

It was concluded that applying winglets to the base plain wing has achieved our objectives stated earlier. Recommendation is also made to continue the present work by applying winglets to different aircraft categories using different simulation codes for better results.

Dedication

I dedicate my dissertation work to my family, without them this could not have been achieved.

Acknowledgment

I would like to express my deep gratitude to my thesis supervisor Dr. Mohamed Nabhan for his support, guidance, and encouragement in the thesis work. I would also like to thank all Mechanical Engineering Department staff for their support to complete the thesis successfully.

Very special thanks go to Allah (s.w) who blessed me with a great family, who supported and motivated me to reach to where I am today.

Table of Contents

Subject		Page Number
Abstract		i
Dedication		iii
Acknowledgment		iv
Table of Contents		v
List of Tables		viii
List of Figures		x
List of Appendices		xiii
Nomenclature		xiv
Chapter One Introduction		
1.1	Overview	2
1.2	Research Questions	3
1.3	Research Objectives	3
1.4	Research Significance	4
1.5	Contribution	4
1.6	Research Setting	5
1.7	Research Terminology	6
1.8	Literature Review	10
1.9	Commentary on Literature Review	22
1.10	Research Hypothesis	22
Chapter Two Theory And Computational Simulation		
2.1	Introduction To Theory	24
2.2	Theoretical Framework	30

2.2.1	The Whole Aircraft Lift Curve	30
2.2.2	The Whole Aircraft Drag Polar	31
2.3	Wings	31
2.3.1	The Language	31
2.3.2	Wingtip Vortices	33
2.3.3	Downwash	35
2.3.4	Span wise Lift Distribution	37
2.3.5	Wing Induced Drag	38
2.3.6	Winglets and Tip Plates	39
2.4	Flight Regimes	40
2.5	Drag and Lift Analysis	41
	Chapter Three **Methodology**	
3.1	Introduction	44
3.2	Methodology Steps	47
3.3	Theoretical Work Setup	48
3.3.1	Plain Wing Theoretical Work Setup	48
3.3.2	Wing with Winglets Theoretical Work	50
3.4	Numerical Work Setup	53
3.4.1	Fluent Ansys 14Code Solution	53
3.4.1.1	Design Modeler	53
3.4.1.2	Meshing	54
3.4.1.3	Fluent Setup	56
3.4.2	3-D Foil Multi-Surface Code Solution	62
3.5	Experimental Work Setup	64
3.5.1	Wind Tunnel Setup	64
3.5.1.1	Electrical Interface Console	65
3.5.1.2	Electronic Manometer Bank	66

3.5.1.3	Lift and Drag Electronic Balance Device	67
3.5.2	Models Manufacturing	68
3.5.3	Testing and Calibrating the Models	69
3.6	Experimental Procedures and Uncertainty	70
3.6.1	Experimental Procedures	71
3.6.2	Uncertainty Analysis	72
3.7	Summary	73
	Chapter Four **Results and Discussions**	
4.1	The Research Results	76
4.1.1	Theoretical Results	76
4.1.2	Numerical Results	79
4.1.2.1	3-D Foil Multi-Surfaces Code Results	80
4.1.2.2	Fluent Ansys 14 Results	82
4.1.3	Experimental Results	87
4.2	Discussion of Results	88
4.2.1	Induced Drag and Lift to Drag Ratios Comparisons	88
4.2.2	Flow Characteristics Comparison	93
4.2.3	Wing's Pressure Comparison	96
4.3	Economical Study	99
4.3	Summary	101
	Chapter Five **Conclusions and Recommendations**	
5.1	Conclusion	104
5.2	Recommendations	107

List of Tables

NO.	Subject	Page
3.1	Comparison between Plain and Winglet Wings Meshing Data	56
3.2	Sandpaper Sizes	70
3.3	Experimental Tests and Parameters Performed for the Plain Wing and Wing with Winglet Models	72
4.1	Lift and Drag Coefficients versus Angle of attack for Plain Wing using Theoretical Relations	78
4.2	Lift and Drag Coefficients versus Angle of Attack for Wing with Winglets using Theoretical Relations	79
4.3	Lift and Drag Coefficients versus Angle of Attack for Plain Wing using 3-D Foil Multi-Surfaces Code	79
4.4	Lift and Drag Coefficients versus Angle of Attack for Wing with Winglets Wing using 3-D Foil Multi-Surfaces Code	80
4.5	Lift and Drag Coefficients versus Angle of Attack for Plain Wing using Fluent Ansys 14 Code	82
4.6	Lift and Drag Coefficients versus Angle of Attack for Wing with Winglets using Fluent Ansys 14 Code	83
4.7	Lift and Drag Coefficients versus Angle of Attack for Plain Wing and Wing with winglets using wind Tunnel C-15	87
4.8	The Percentage Difference in Induced drag between Plain Wing and Wing with Winglets Results for all Four Verification Methods at Different Angles of Attack	90

4.9	The Percentage Difference in Lift to Drag Ratio between Plain Wing and Wing with Winglets Results for all Four Verification Methods at Different Angles of Attack	93

List of Figures

NO.	Figure	Page
2.1	Plain Wing Geometry by Solid Works	25
2.2	Plain Wing as it appear in 3-D Foil Multi-Surfaces Code (a) Isometric View of the Plain Wing. (b)Top View of the Plain Wing.	26
2.3	Wing with Winglets in Isometric and Top Views (a) Isometric View of the Wing with Winglets (b)Top View of the Wing with Winglets	28
2.4	Wing with Winglets Top View by Solid Works	29
2.5	Isometric View for Wing with Winglets by Solid Works	29
2.6	Finite Wing Geometry Definitions	32
2.7	Wing Twist	33
2.8	Front View of Wing with Flow Around the Wing Tips	34
2.9	Downwash	34
2.10	Trailing Edge Vortices	35
2.11	Downwash Angle and Induced Drag	36
2.12	2-D and 3-D Lift Coefficient Curves	37
2.13	Elliptical Lift Distribution	38
2.14	(a): Three Induced Drag Reducing Wingtip Devices (b): Winglets on a C-17 (USAF Photo)	40
2.15	Flight Regimes	41
2.16	The Flight Drag Envelope	42

3.1	Jabiru Aircraft	45
3.2	Research Methodology	46
3.3	Generation of Negative Drag by Winglets	52
3.4	Ansys 14 Design Modeler Setup Page	54
3.5	Meshing's Final Shape	55
3.6	Closer View for Meshing	55
3.7	Fluent Main Setup	56
3.8	Fluent Model and Materials	57
3.9	Boundary Conditions	58
3.10	Other Boundary Conditions	59
3.11	Reference Values	60
3.12	Fluent Monitors Setup	61
3.13	Solution Methods and Initialization	61
3.14	Running the Calculations	62
3.15	3-D Foil Multi-Surfaces Simulation Features	63
3.16	C-15 Computer Controlled Subsonic Wind Tunnel	64
3.17	Stainless Steel Tubes Arrangement	65
3.18	(IFD 7) Electrical Interface Console	66
3.19	Electronic Manometer Bank	67
3.20	Lift and Drag Balance Device	67
3.21	(a) Plain Wing Model (b) Wing with Winglets Model	69
4.1	Top view for the Plain Wing and the Wing with Winglets	77
4.2	Front View for the Plain Wing and the Wing with Winglets	77
4.3	Plain Wing Drag Coefficient at 1000 Iterations at Zero Degree Angle of Attack	81

4.4	Plain Wing Lift Coefficient at 1000 Iterations at Zero Degree Angle of Attack	82
4.5	(a) Static Pressure Contours for Plain Wing (b) Total Pressure Contours for Plain Wing	84
4.6	(a) Static Pressure Contours for Wing with Winglets (b) Total Pressure Contours for Wing with Winglets	85
4.7	(a) Velocity Vectors for Plain Wing at $\alpha=10^{o}$ (b) Velocity Vectors for Wing with Winglets $\alpha=10^{o}$	86
4.8	Induced Drag (C_{Di}) Comparison for Plain Wing at Different Angles of Attack	89
4.9	Induced Drag (C_{Di}) Comparison for Wing with Winglets at Different Angles of Attack	89
4.10	Lift to Drag Ratio (C_L/C_D) Comparison for Plain Wing at Different Angles of Attack	91
4.11	Lift to drag ratio (C_L/C_D) comparison for wing with winglets at different angles of attack	92
4.12	Plain Wing Velocity Vectors at 10^{o} Angle of Attack	94
4.13	Wing with Winglets Velocity Vectors at 10^{o} Angle of Attack	95
4.14	Wing with Winglets Path Lines at 10^{o} Angle of Attack	96
4.15	Plain Wing Chord's Direction Total Pressure	97
4.16	Wing with Winglets Chord's Direction Total Pressure	97
4.17	Plain Wing's Wing Span Direction Total Pressure	98
4.18	Wing with Winglet's Wing Span Direction Total Pressure	99

List Appendices

NO.	Appendix
A	Uncertainty Analysis
B	3-D Foil Multi-Surfaces Optimum Model Trails
C	Fluent Ansys 14 Solution Iteration
D	Dimension 1200es 3-D Printer Specifications
E	C-15 Computer Controlled subsonic Wind Tunnel Specifications
F	Wind Tunnel Experiment Results

Nomenclature

a_o	The slope corresponds of a finite wing, *y/x*
a	The lift slope on infinite wing, *y/x*
AR	The Aspect Ratio, *m*
A_w	The reference area, m^2
b	The wing span, *m*
c	Chord length of an airfoil at any point along the wing span, *m*
C_D	The Drag Coefficient, $(D/0.5\rho V_\infty^2 A)$
C_L	The Lift Coefficient, $(L/0.5\rho V_\infty^2 A)$
C_L/C_D	Lift coefficient to drag coefficient ratio
$C_{D_{W_0}}$	The drag coefficient of the wing at zero lift, $(D_0/0.5\rho V_\infty^2 A)$
D	The Drag force, *N*
e	The geometry factor, m^{-1}
I_{sp}	The overall efficiency
K.	Constant of proportionality
L	The Lift force, *N*
L/D	Lift force to Drag force ratio
M	Mach Number, *M*
P	*Pressure, Pa*

S_w	Wing's wetted area, m^2
S	The whole wing's planform area, m^2
U_R	The uncertainty of the measured value R
U_{x_i}	The uncertainty of a given variables x_i
t	The wing tip chord, m
t_f	The flight time, s
V_∞	Uniform free air stream velocity, m/s
W_i	The initial weight, N
W_f	The final weight of vehicle, N
Re	Reynolds number, $(\rho V_\infty L/\mu)$

Greek Symbols:

α	The angle of attack, *degree*
α_{eff}	The effective angle of attack, *degree*
β	The side angle of the winglets
ρ	Density of air flow, kg/m^3
λ	The ratio of the chord length of the wing tip to the wing root
Λ_{LE}	The wing sweep angle, *degree*
δ	The induced drag factor
ΔC_{D_i}	The increment in induced drag coefficient value

Abbreviations:

CFD	Computational Fluid Dynamics
CFX	Ansys software solver for fluid dynamic, which uses the control volume finite element method
DWVG	The Delta Winglet Vortex Generators
LE	The Leading Edge of the wing
LSA	Light Sport Aircraft NACA National Advisory Committee of Aeronautics in United States of America
PC	Personal Computer
S.B.C	A differential equations together with a set of additional constraints, called the boundary conditions. A solution to a boundary value problem is a solution to the differential equation which also satisfies the boundary conditions.
TE	The Trailing Edge of the wing
UAV	Unmanned Aerial Vehicle
VLM	Vortex Lattice Method

Chapter One

Introduction

1.1 Overview

1.2 Research Question

1.3 Research Objectives

1.4 Research Significance

1.5 Contribution

1.6 Research Setting

1.7 Research Terminology

1.8 Literature Review

1.9 Commentary on Literature Review

1.10 Research Hypothesis

Chapter One

Introduction

1.1 Overview

Since the beginning of the age of aviation industry, developing and optimizing of aerodynamic characteristics were the main concern for all: users, manufactures and researchers. It can't be said that there is a perfect design, but we can say there are perfect approaches to the desired aerodynamic characteristics.

The basic forces on the airfoil are the lift and drag. All other forces and moments are resultant of the airfoil/ wing reactions with them. They depend on the shape of airfoil, wings and the aircraft body.

All researches in aerodynamics field consist of three main parts:

1. Experimental part using two dimensional or three dimensional wind tunnels.
2. Numerical part using simulation CFD programs.
3. Theoretical part using aerodynamic governing equations.

The flow near the tip of a three-dimensional wing tends to curl around the tip because the flow is forced from the high-pressure region underneath the tip to the low-pressure region above at positive lift condition. This tendency for the flow to leak around the tip causes a circulatory three-dimensional motion which trails downstream from the wing, the so-called wing-tip vortex. Aircraft that encounter or penetrate the wing-tip vortices of large preceding aircraft can experience severe upward or downward loads as well as over powering rolling moment, which is hazardous, especially during the take-off and landing phases of

flight. The wing tip vortex is also a source of the induced drag of three-dimensional wing. If the total strength of the wing tip vortex is reduced, then the induced drag of a three dimensional wing will then be reduced (Sohn & Chang, 2012).

The aerodynamic efficiency of an aircraft can be improved through a wingtip device which diffuses the strong vortices produced at the tip and thereby optimize the span wise lift distribution, while maintaining the additional moments on the wing within certain limits (Hossain, Rahman, Hossen, Iqbal, & Zahirul, 2011).

There are many studies discussing optimizing aerodynamic characteristics by using winglets. Sohn and Chang (Sohn & Chang, 2012) released a research: Visualization and PIV study of wing-tip vortices for three different tip configurations. Also (Hossain et al., 2011) released a research: Prediction of aerodynamic characteristics of an aircraft model with and without winglets using fuzzy logic technique.

1.2 Research Questions

Can the proposed winglet design improve the aerodynamic characteristics of an air craft wing?

1.3 Research Objectives

The aim of this project is to study the aerodynamic characteristics in low subsonic speeds (incompressible) laminar/ turbulent flow over airfoil NACA 4412 and straight rectangular wing which are designated to an Australian Light Sport Aircraft developed as touring/ training aircraft and manufactured by Jabiru Aircraft Company.

1. To investigate the effect of winglet geometry on induced drag and vortex flow.
2. To measure the lift and drag forces at various flow angles of attack.
3. To validate the obtained results by comparing the numerical CFD simulation results against the experimental results.

1.4 Research Significance

A renowned aircraft company (Jabiru) manufactures a light training aircraft without winglets installed on the wings. The winglet installation with various optimized geometrical configuration can have a positive effect on the reduction of total drag by minimizing the strength of the tip vortices on the wings span. The presence of winglet will result in the reduction of fuel consumption, energy savings, and provide larger range for this type of aircraft.

1.5 Contribution

The main contributions of this project are:

1. Introduce a complete study of effect of winglet geometry on induced drag and vortex flow.
2. Improvement of the measurements of Lift and Drag forces at various flow angles of attack.
3. Introduce a pilot study based on the validation of experimental results using CFD simulation, namely Fluent Code, and mathematical relations.

1.6 Research Setting

The results obtained from this project are presented into five chapters. This project is organized as follows:

Chapter 1 gives a general introduction and presents the problem statement, objectives, and contributions driven from this project. Comprehensive literature review and research's terminology are also discussed in this chapter.

Chapter 2 explores the key concepts of aerodynamics, especially winglets field and ideas surrounding the scope of the project, including results from previous researches, and their usefulness to the current work.

Chapter 3 highlights the research methodology. The research methodology was carried out in four steps. The main steps are to review the methodology used, research tools, design of the basic concept and suggested modified model, simulation, and testing and validation. The evaluation strategies and the data set used are also discussed.

Chapter 4 presents the design and experimental study of this project. The model has been designed using 3-D Multi-Surface Foil Code and solid works. While the numerical study is based on Ansys Fluent code and 3-D Multi-Surface Foil, the theoretical part is calculated by governing aerodynamic equations. Then, a two dimensional subsonic wind tunnel was used to verify the solution by experiments. Finally, results and discussions of this project were declared, as well as some comparisons have been discussed.

Chapter 5 includes the conclusion, recommendations, and suggestion for future work.

1.7 Research Terminology

1. Winglet: Winglets are a type of wing tip devices, which are used to enhance aerodynamic efficiency of wings. In general, a winglet produces a side force, which has a forward component because of the side wash produced by the wing tip circulation. This forward component of the lift acts as a thrust force reducing the aircraft induced drag, which is about 40% of the total drag in cruise and 80-90% of the total drag in the second climb segment (Kroo, 2005).

A winglet's main purpose is to improve performance by reducing drag (Maughmer, 2003). Other than that, flight mechanics are also influenced by winglets, as well as the flutter characteristics and the airplane's low speed performance (Hantrais-Gervois, Grenon, and Mann, 2009).

2. Aerodynamics: A part of fluid dynamics concerned with studying the motion of air, particularly when it interacts with a solid object, such as an airplane wing.

3. Aerodynamics Characteristics: In Aerodynamics, the four main forces which act on aircraft during the flight are Lift, Drag, Thrust and Weight. Drag is one of the most critical phenomena amongst all and is the opposing force of aircraft's forward motion. It could be divided mainly into parasite drag (not due to lift) and lift induced drag. The performance of a given airfoil profile as related to lift and drag, to angle of attack, and to velocity, density, viscosity, compressibility, and so on.

4. Airfoil: An airfoil is the shape of a wing, blade of a propeller, rotor, or turbine as seen in the view of cross-section. An airfoil designed body moves through air produces an aerodynamic force. The resultant

component of this force is divided into two main components: perpendicular to the direction of the flow direction is called lift. The component parallel to the flow direction is called drag. Subsonic flight airfoils have a characteristic shape with a rounded leading edge, and ended by trailing edge. Foils of similar function designed with water as the working fluid are called hydrofoils (Babinsky, 2003).

The lift on an airfoil is primarily the result of its angle of attack and geometry. When oriented at a suitable angle, the airfoil deflects the oncoming air (for fixed-wing aircraft, a downward force), resulting in a force on the airfoil in the direction opposite to the deflection. This force is known as aerodynamic force and can be resolved into two components: lift and drag. Most foil shapes require a positive angle of attack to generate lift, but cambered airfoils can generate lift at zero angle of attack. This "turning" of the air in the vicinity of the airfoil creates curved streamlines, resulting in lower pressure on one side and higher pressure on the other. This pressure difference is accompanied by a velocity difference, via Bernoulli's principle, so the resulting flow field about the airfoil has a higher average velocity on the upper surface than on the lower surface. The lift force can be related directly to the average top/bottom velocity difference without computing the pressure by using the concept of circulation and the Kutta-Joukowski theorem (Babinsky, 2003).

This airfoil shape can be different if the cross section taken at different locations on the wing. However, for any given cross section, we have a given airfoil. We can now think of the airfoil as an infinitely long wing that has the same cross sectional shape. Such a wing (airfoil) is called a two dimensional (2-D) wing. Therefore, when we refer to an airfoil, you can think of an infinite wing with the same cross sectional shape. Since

calculating lift and drag coefficients with a reference area of infinity would not make sense, we base airfoil lift and drag coefficients for airfoils on the plan form area, assuming the span is unity.

5. Airfoil Shape: It is the cross section of the wing. The lift force depends on the shape of the airfoil, especially the amount of camber (curvature such that the upper surface is more convex than the lower surface). Increasing the camber generally increases lift.

6. NACA Airfoils: Are airfoil shapes for aircraft wings developed by the National Advisory Committee for Aeronautics (NACA). The shape of the NACA airfoils is described using a series of digits following the word "NACA". The parameters in the numerical code can be entered into equations to precisely generate the cross-section of the airfoil and calculate its properties.

7. Light-Sport Aircraft (LSA): This is a small aircraft that is simple to fly and that meets certain regulations set by a national aviation authority restricting weight and performance. For example, in Australia the Civil Aviation Safety Authority defines a light-sport aircraft as a heavier-than-air or lighter-than-air craft, other than a helicopter, with a maximum gross takeoff weight of not more than 560 kilograms for lighter-than-air craft; 600 kilograms for heavier-than-air craft not intended for operation on water; or 650 kilograms for aircraft intended for operation on water.

8. Wind tunnel: This is a tool used in aerodynamic research to study the effects of air moving past solid objects. It is used to test prototypes. A wind tunnel consists of a tubular passage with the object under test mounted in the middle.

9. Subsonic Aircraft: Is an aircraft with a maximum speed less than the speed of sound (Mach 1). The term is sometimes, but not always, used to

describe an aircraft that flies below Mach 0.8. General Aviation aircraft, helicopters, and all modern airliners are subsonic aircraft.

10. Lift: A fluid flowing past the surface of a body exerts a force on it. The component of this force that is perpendicular to the oncoming flow direction.

11. Drag: A fluid flowing past the surface of a body exerts a force, which is the component of the resultant surface force parallel to the flow direction.

12. Induced Drag: Induced drag is an inevitable consequence of lift and is produced by the passage of an airfoil or wing through the air. Air flowing over the top of a wing tends to flow inwards because the decreased pressure over the top surface is less than the pressure outside the wing tip.

13. Computational Fluid Dynamics (CFD): Usually abbreviated as CFD, is a branch of fluid mechanics that uses numerical methods and algorithms to solve and analyze problems that involve fluid flows. Computers are used to perform the calculations required to simulate the interaction of liquids and gases with surfaces defined by boundary conditions.

14. Wing Tip Vortices: Vortices form because of the difference in pressure between the upper and lower surfaces of a wing that is operating at a positive lift. Since pressure is a continuous function, the pressures must become equal at the wing tips. The tendency is for particles of air to move from the lower wing surface around the wing tip to the upper surface (from the region of high pressure to the region of low pressure).

1.8 Literature Review

Cosin et al. (Cosin, Catalano, Correa, & Entz, 2010) worked on a wing with multi winglets, three small fins attached to the salmon timing different for each winglet were used. This device increases the aerodynamic parameters, with a 7.3% gain in efficiency. The aerodynamic characteristics of the process indicated improvements in lift and reduced expression of induced drag, represented by a 32% increase of the efficiency factor of Oswald.

Winglets belong to the class of wingtip devices aimed to reduce induced drag. Selection of the wingtip device depends on the specific situation and the airplane model. In the case of winglets, the reduction of the induced drag is accomplished by acting like a small sail whose lift component generates a traction force, draining energy from the tip vortices (Bento Mattos, Antonini Macedo, & Durval Silva Filho, 2003).

Beninati and Marshall. (Beninati & Marshall, 2005) stated that the vortex is characterized by extremely slow diffusion and persists for considerable distances downstream of the wing which gave it birth. With the arrival of the Boeing 747 airplane in the 70's the "Federal Aviation Administration" has established safe distances between aircraft based on their mass to limit the risk of incidents. These international standards define the minimum distance separation by class of aircraft, and these set a limit to the frequency of landings and takeoffs.

Winglets are a type of wing tip devices, which are used to enhance aerodynamic efficiency of wings. In general a winglet produces a side force, which has a forward component because of the side wash produced by the wing tip circulation. This forward component of the lift acts as a thrust force reducing the aircraft induced drag, which is about 40% of the

total drag in cruise and 80-90% of the total drag in the second climb segment (Kroo, 2005). A research tried to optimize winglet for minimum drag, while defining some constraints to avoid a huge weight penalty (Hantrais-Gervois et al., 2009). These constraints usually limit the wing root bending moment. However, using root bending moment is not a good indicator for the wings total weight, because it does not account for the effect of chord wise changes in the platform on the bending weight. Some researchers used low fidelity semi-empirical methods (Ning & Kroo, 2010) or high fidelity finite element analysis (Jansen, Perez, & Ra Martins, 2010) for wing weight estimation. In this research, a medium level of fidelity aerodynamic solver together with a medium level of fidelity weight estimation tool is used for winglet analysis. Using a medium level of fidelity allows reducing the computational time comparing to higher level of fidelity tools while keeping the level of accuracy high enough.

Drag is caused by the induced drag that is created by the downwash of airflow onto the upper surface of the wing at the wingtips thus producing vortices that trail in the aircraft's wake. The most important wingtip devise's functions is reduce the induced drag and consequently, the trailing vortex strength. By minimizing the induced drag, and thus the wingtip vortices produced by an aircraft's wing, the energy required to create the tip vortices can be conserved and the total drag on the wing reduced (Yahaya & Sheriff, 2012).

Belferhat, Meftah et al. (Belferhat, Meftah, Yahiaoui, & Imine, 2013) has focused their research on the flow of air at the wing tip and found that the vortices can be broken in order to reduce induced drag by small devices without disrupting the mass and the backbone of the wing. This device is called a winglet; it is a small vertical extension to the wing

tip to improve its efficiency by increasing its effective length. By recovering some of the energy of vortices, the winglet increases the aerodynamic efficiency of the wing. The persistence of the vortex responsible for the drag-induced lift is estimated at over a third of the total drag of the aircraft and half for low-speed takeoff and landing.

A research by NASA Langley research center developed the concept of winglet technology. According to Gimmestad, winglet could be described as the small wing like vertical structures which extends from the wingtip, aiming at reduction in induced drag when compared to other wing tip devices or extensions. He also claimed in his research that the winglet shows 20% reduction in induced drag when compared to tip extension and also improved lift-to-drag ratio. Unfortunately, his theory could not reduce the overall drag of aircraft despite reducing the induced drag. The increase in the viscous drag during cruise conditions outruns the reduction in induced drag (Gimmestad, 1981).

Ardonceau and Trapier. (Ardonceau & Trapier, 2005) has determined that the reduction of drag of a wing is made by the management of marginal separation by attaching a thin piece of salmon trigger the detachment with a reduction in total drag of about 1 % is observed with an increase in the lift without the increase in induced drag.

There is seven percent (7%) increase of the aircraft's range at cruise conditions (full speed conditions) for aircrafts with wings designed with winglet compared to wing without winglets. Other than that, wing with winglets or wingtip devices on commercial aircraft are found to have lower wing loading and better fuel consumption rates. All the advantages of the winglets and raked wingtip performances are due to its ability to

reduce the induced drag, or the drag generated during take-off by a 3-dimensional finite wing (Babigian & Hayashibara, 2009).

Studies concerning the efforts to decrease the fuel consumptions and lower emissions are the interest of the aviation industry, especially in the era of rising fuel prices and environmental issues. These researches are into a device that will provide longer range and more resourceful fuel consumption rates especially to commercial aircraft. It was found that there are two wingtip devices that will provide better fuel consumption rates and could provide longer range: the winglets and the raked wingtips (Babigian & Hayashibara, 2009).

The induced drag, or the drag generated during take-off is due to the difference in pressure of the upper and lower surfaces of an aircraft wings. The high pressure part is on the lower surface of the wing while the lower pressure part is located on the upper surface of the wing. The difference in pressure on the wing will form a net lifting force that is normal to the free stream airflow (Babigian & Hayashibara, 2009).

Considering winglets on jet-transports, a number of studies have been published, following the work of Gimmestad. Such a study is that of Meyer (Meyer Jr & Covell, 1986), who experimentally studied the effect of sideslip angle on winglet loads at high and low subsonic Mach numbers. An extensive work has also been done on winglet design for sailplanes by Maughmer at Penn State University (Maughmer, 2003, 2006). In his work, he notes that the design procedure is actually a trade-off study between reducing the induced drag and increasing the profile drag term. A large winglet will do a better job in reducing the induced drag but at the same time the increase in wetted area will cause the profile drag term to increase as well. Maughmer et al. designed a winglet airfoil

for high-performance sailplanes (Maughmer, 2006). Both theoretical and experimental results showed that the airfoil (PSU 94-097) performed better at a wide range of Reynolds numbers ($2.5x10^4$ to $1x10^6$).

The concept of wingtip device was first introduced by English engineer Frederick W. Lanchester. He patented the endplate concept in 1897 and his research results demonstrated that significant amount of induced drag could be diminished by placing vertical surface at the wingtip under high-lift condition. Although it was a promising approach to induced drag reduction technique, the benefits of this concept was suppressed because of large generation of profile drag at cruise condition.

Unfortunately, there wasn't any major contribution in the field of winglet concept until World War II. Dr. Sighard F. Hoerner, a German aeronautical engineer developed "Hoerner Tips" which was used in Heinkel He 162 jet aircraft. In 1952, he published a technical paper regarding drooped wingtips also called as "Hoerner Tips".

Nowadays, winglets are used in most commercial and military transport jets including the Gulfstream III, IV and V business jets, Boeing 747-400 and McDonnell Douglas MD-11 airliners, the McDonnell Douglas C-17 military transport and Embraer aircraft (Atique, Salam, Nafi, Probha, & Barman, 2015).

However, one of the major technical challenges still exists regarding incorporating winglet to the existing wing designs because of precipitating large profile drag is of great research interest. Beneficial factor in winglet performance is largely dependent on wing design, as well as the design of winglet itself. Basing on this fact, there has been many modifications of winglet, and these are conveniently being used by commercial aircraft manufacturers (Atique et al., 2015).

The vortex generators incorporated in fin-tube heat exchangers can be categorized based on their configurations with respect to heat transfer tubes, whether 'common flow down' and 'common flow up'. Fiebig (Schubauer & Spangenberg, 1960) contended that this configuration would delay flow separation and reduce drag. In the common flow up configuration, a pair of vortex generators is installed in front of the tube (at the upstream). Torii et al. (Torii, Kwak, & Nishino, 2002) speculated that this configuration accelerates the flow between a tube and its vortex generators as well as delays flow separation; thereby reducing the wake region behind the tube.

Other research by (Bojja & Garre, 2013), they considered the Boeing 767 wing, designed it in CATIA. The airfoil NACA 2213 coordinates are initially imported into CATIA from the design foil software. Then the coordinates are joined using spline, extruded and attached with a blended winglet structure. This wing without winglet is kept at 4°, 8°, 12° angles of attack and analyzed in Ansys software using the CFX workbench. The same procedure is followed for the other wing with circular winglet and wing without winglet. By analysis the performance of the wing with winglets can be estimated. The analysis is done for all the three wings using the Ansys-Fluent workbench by giving the initial and boundary conditions as pressure inlet and velocity outlet to find the coefficient of drag (C_d) for each wing. The flow on the wing without winglet, wing with blended winglet and wing with circular winglet is analyzed and the C_d is estimated.

Regarding Unmanned Aerial Vehicle (UAV), a recent research is that of Weierman and Jacob (J. R. Weierman & J. D. Jacob, 2010), who performed a winglet optimization study using Vortex Lattice Method (VLM). They examined the performance benefits of winglets attached on

the wingtips of a UAV and their impact on the vehicle's flight endurance and range. As they note, the predicted trends "compare very well to experimental data". However, as the in viscid calculations cannot predict drag due to viscous effects, separation and stall, the VLM results are "error prone" at higher angles of attack, whereas the predicted zero-lift drag values were estimated as much as 50% smaller than the actual ones, leading to the conclusion that the VLM can lead to "gross exaggeration of performance prediction".

In another UAV design-related research, Kontogiannis and Ekaterinaris employed Computational Fluid Dynamics (CFD) in the design procedure of a light UAV, including a winglet study as well (Kontogiannis & Ekaterinaris, 2013).

CFD has been used by various researchers for studying winglet performance, as it provides a reliable solution for modeling viscous effects as well. For example Azlin et al. (Azlin, Taib, Kasolang, & Muhammad, 2011) examined the performance of winglets at low subsonic flow. They studied two types of design, elliptical and semi-circular winglets with different angles, attached on a wing at various angles of attack. Takenaka etal. also used CFD in order to perform a multidisciplinary design exploration technique regarding winglets for a commercial aircraft (Takenaka, Hatanaka, Yamazaki, & Nakahashi, 2008). He stated that the winglet's (dihedral) angle and span length are the most important parameters when it comes to drag reduction.

The trends in the aeronautical engineering show a remarkably intensive effort concentration on the development and use of un-manned aerial vehicles. The Medium-Altitude-Long-Endurance (MALE) family can cover a wide variety of missions, and while the operating speed and

altitude is different for each design, they vary within a certain range. Therefore, optimizing the winglet geometry for a typical MALE UAV, such as the one being studied in this research, can help a long way in improving the performance of a large family of aircraft, in fact one of the largest in the UAV industry, including present and future designs (Panagiotou, Kaparos, & Yakinthos, 2014).

By installing the optimized geometry on the plane, a formidable increase in *L/D* has been achieved. Calculations show an increase in flight time equal to 1h, or10%. No changes were observed in pitch stability and stalling. As a first step, a combination of winglet airfoil, chord, height, and angle was enough for achieving the initial goals. However, the configuration can be further improved, as the effect of some parameters, such as toe angle and sweep angle, was not examined (Panagiotou et al., 2014).

Jacobi and Shah (Jacobi & Shah, 1995) reviewed previous works until the early 1990s. They explained physical phenomena and vortex characteristics associated with vortex generators on a fin as well as introduced experiments and analysis on the performance of heat exchangers with vortex generators. They categorized active and passive methods of vortex generation. Active methods generate vortices using external energy, such as electric or acoustic fields, mechanical device, or surface vibration. Passive methods generate vortices through structures and additional fluids. Regardless of method, vortex generators enhance heat transfer and simultaneous pressure drop due to form loss. The vortex generator has the interesting characteristic of having a small pressure loss compared with other interrupted fin designs. As such, most previous works focused on quantifying the improvement of heat transfer performance and additional pressure drop characteristics.

An experimentally studied heat transfer performance in a channel with vortex generators in a common flow down configuration. The Delta Winglet Vortex Generators (DWVG) increases convective heat transfer by developing a boundary layer, swirl, or vortices, as well as through flow destabilization or turbulence intensification. The delta winglet enhances heat transfer more than a rectangular winglet. The highest heat transfer coefficient was obtained at a 45° attack angle, which is defined as the angle between the flow direction and vortex generators. The effects of the vortex generators on fin-tube heat exchangers were similarly experimentally investigated. The DWVG were installed onto 3-row fin-tube heat exchangers in a common flow down configuration. The staggered and inline effects of tube arrays on the thermal-hydraulic performance of the DWVG were compared. At nearly the same heat transfer coefficient, the f-factor of the staggered array was smaller than that of the inline array in a range of $Re > 1300$. The DWVG can reduce the size and mass of a heat exchanger for a given heat load (Fiebig, Valencia, & Mitra, 1993).

Kwak et al. (Kwak, Torii, & Nishino, 2003) measured the heat transfer coefficient and pressure drop in 2, 3, 4, and 5-row fin-tube heat exchangers with a common flow up configuration DWVG in a range of $280 < Re < 2400$. The DWVG were only mounted on the first row. Compared with heat exchangers with plain fins, those with DWVG fins showed a 10% increase in heat transfer performance of the j-factor for all heat exchangers, and a 0%–10% increase of the f-factor for the 2, 4, and 5-row heat exchangers. For the 3-row heat exchanger, however, the f-factor dramatically decreased by 30%–50%. This was attributed to the effects of vortices, which were produced at the first row of the tube but did not reach the fourth and fifth rows.

Kwak et al. (Kwak, Torii, & Nishino, 2005) investigated the effect of the number of DWVG rows, as well as measured the heat transfer capacity and pressure drop of staggered array fin-tube heat exchangers that were identical except for the number of DWVG rows. The heat exchanger with a single DWVG row experienced 10%–30% larger heat transfer capacity and 34%–55% less pressure drop than the heat exchanger without the DWVG. For the heat exchanger with two DWVG rows, however, heat transfer capacity and the pressure drop increased by 6%–15% and by 61%–117%, respectively, compared with the heat exchanger with a single DWVG row. The DWVG in the second row obstructed and decelerated the air flow to produce an additional pressure drop.

Recently, Joardar and Jacobi (Joardar & Jacobi, 2008) investigated the effect of the number of DWVG rows in the inline array fin-tube heat exchangers. Single and three DWVG fin tube heat exchangers were compared with a plain fin tube heat exchanger. The DWVG was placed in a common flow up configuration. For the single DWVG, the heat transfer coefficient was enhanced by 16.5%–44% as pressure drop increased by less than 12%. For the case of three DWVG rows, the heat transfer coefficient was augmented by 29.9%–68.8% as the pressure drop penalty increased 26% at Re = 960 and 87.5% at Re = 220. DWVG arrays can significantly enhance the performance of fin tube heat exchangers with flow depths and fin densities typical of those used in air-cooling and refrigeration applications.

Allison and Dally (Allison & Dally, 2007) similarly examined the performance of the DWVG in flat fin tube heat exchangers, and compared the performance of two fin types. The first is a plain fin with a DWVG and the second is a louvered fin. The DWVG were installed in a

common flow up configuration. The j- and f factors of the heat exchanger with the DWVG were 87% and 53%, respectively, of the heat exchangers with a louver fin.

Researchers also investigated the performance of DWVG fins through numerical analyses. Min and Xu (Min & Xu, 2005) numerically evaluated and compared the performances of a plain, DWVG, and louver fins incorporated in a flat tube heat exchanger. When compared with the heat exchanger with a plain fin, that with a louver fin had a heat transfer capacity of about 114.1%–139.1% with a pressure drop penalty of 163.9%–171.7%. In the case of the DWVG fin heat exchangers, heat transfer capacity was about 46.5%–74.1% and the pressure drop was 46.1%–49.7%. The significant variation in pressure drop could be attributed to the louver fin undergoing flow decay at each slit, whereas the winglet fin had no flow decay.

The research done by (Kevadiya & Vaidya, 2013), focuses primarily on designing the blade for regions of low wind power density. The aerodynamic airfoils of wind turbine blades have crucial influence on aerodynamic efficiency of wind turbine. This involves the selection of a suitable airfoil section for the proposed wind turbine blade. In this research NACA 4412 airfoil profile is considered for analysis of wind turbine blade. Geometry of the airfoil is created using GAMBIT 2.4.6 and CFD analysis is carried out using Fluent 6.3.26 at various angles of attack from 0° to 12. The coefficient of lift and drag values are calculated for 1 $\times 10^5$ Reynolds number.

A study by (Manea & Galeriu, 2004), focuses on turbulence and the surface roughness influence on the laminar – turbulent transition in the boundary layer, for NACA 4412 airfoil, which have the chord

L = 0.6 m. The mean velocity distribution is experimental determinate in the aerodynamic tunnel, for attack angle $\alpha=0^{o}$.

Also, another study by (Babigian & Hayashibara, 2009) , serves as a preliminary investigation into the aerodynamic effects of different wingtip configurations on the wingtip vortices generated as a result of the induced drag on a wing. In addition, the advantages and disadvantages of 3-D finite wings with winglets and raked wingtip wing configurations were investigated. The results presented in this study reveal two methods for reducing wingtip vortices, and consequently, the induced drag on a 3-D wing. This study has shown that clean wing configurations, i.e., wings without wingtip devices, produce the highest vorticity magnitudes when compared to wing configurations that employ either winglets or raked wingtip designs. The vortex wake generated by clean wing configurations reduces the effective aspect ratio of the wing, thereby increasing the induced drag on the wing. The winglet design employed in this study demonstrate the potential to produce a component of force in the thrust direction of the aircraft by concentrating the otherwise turbulent and chaotic vortex flow behind the wingtips into a more energy-efficient flow, thereby counteracting the drag on the wing. Alternatively, raked wingtips reduce the overall magnitude of the tip vortices, thereby reducing the induced drag on the wing.. The results of this preliminary study suggest that wings designed with winglets or raked wingtips can indeed reduce the induced drag on a wing during cruise conditions. This reduction of the induced drag on an aircraft's wing offer advantages in terms of an aircraft's performance including improved fuel efficiency, increased range, and reduced wing loading (Babigian & Hayashibara, 2009).

1.9 Commentary on Literature Review

The literature review consists of a number of salient themes, frameworks, models, architectures and approaches important for this study. Notably from this review, the problem of drag and lift on a moving aerodynamic airfoil with varying winglet geometry is very complex and occurs in multiple levels. All previous researches are on commercial jets and un-manned aircrafts, which open the door for us to explore the other aircrafts categories fields.

The results of previous researches are used to determine the optimum approach into our winglet design. Optimizing induced drag, lift to drag ratio and fuel consumption are the trending research fields as concluded from literature review.

1.10 Research Hypothesis

Aircraft designers are performing research to improve the overall aircraft aerodynamics efficiency which would be beneficial for both aircraft manufacturer and the airlines. In case of aircraft design process, reducing the overall drag at a compromising level would be one of the challenging processes. Many experiments have been conducted in order to reduce the lift-induced drag. This chapter reports the wings aerodynamic drag estimation using simulation numerical codes, theoretical study and experimental approach. The experimental approach uses the wind tunnel. While the numerical codes uses 3-D Foil Multi-Surfaces and Ansys Fluent. The governing aerodynamics equations are the theoretical baseline.

Chapter 2: Theory and Computational Simulation

2.1 Introduction to the Theory

2.2 Theoretical Framework

2.3 Wings

2.4 Flight Regimes

2.5 Drag and Lift Analysis

Chapter 2: Theory and Computational Simulation

2.1Introduction to the Theory

The NACA airfoils are airfoil shapes for aircraft wings developed by the National Advisory Committee for Aeronautics (NACA). The shape of the NACA airfoils is described using a series of digits following the word "NACA". The parameters in the numerical code can be entered into equations to precisely generate the cross-section of the airfoil and calculate its properties. The NACA four-digit wing sections define the profile by first digit describing maximum camber as percentage of the chord, second digit describing the distance of maximum camber from the airfoil leading edge in tens of percent's of the chord and last two digits describing maximum thickness of the airfoil as percent of the chord. The airfoil used in Jabiru aircraft, which we are studying in this thesis is NACA 4412. And the wing is rectangular wing with no aerodynamic twist and constant chord. Noted that, there are no winglets are used in the wings.

The main objective of the design is to:

- Decrease induced drag resulting in a total drag decrease.
- Reduce the strength of the tip vortex.
- Increase the lift to drag ratio,
- Decrease fuel consumption.
- Increase the flight range.
- Increase safety by eliminating the effect of wing tip vortices.

The original design which comes as plain wing is shown in Figure (2.1) in recognizable format with actual dimensions ready to be exported to the simulation code: Ansys Fluent 14.

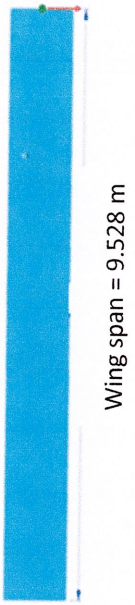
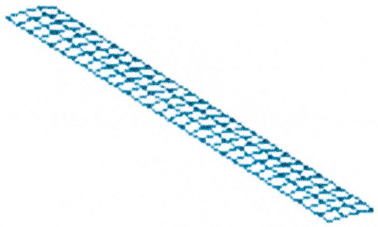
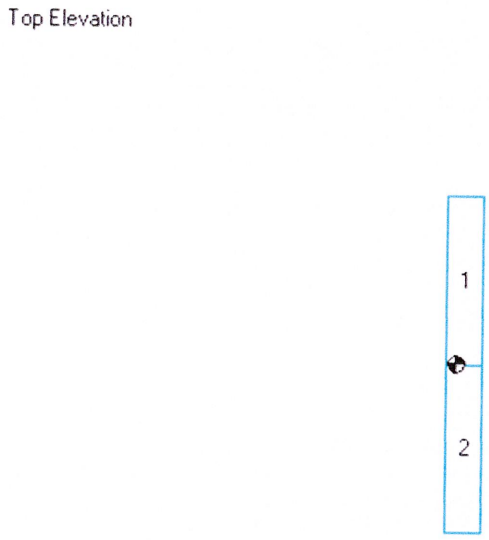


Figure (2.1) Plain Wing Geometry by Solid works

Another code is used to verify the simulation results got from Ansys Fluent 14 code is the 3-D Foil Multi-Surfaces. It is light simple version software uses the thin airfoil theory model. That made this code as verification code in our research but with moderate accuracy. Simplicity of this code allowed us to design the wing with winglet model. The suggested design needed around ten iterations to obtain the optimum design of the winglets. Then we proceeded to test it numerically, theoretically and experimentally. Figure (2.2) (a, b) shows the plain wing layout as it appears in 3-D Foil Multi-Surfaces.



(a) Isometric View of the Plain Wing



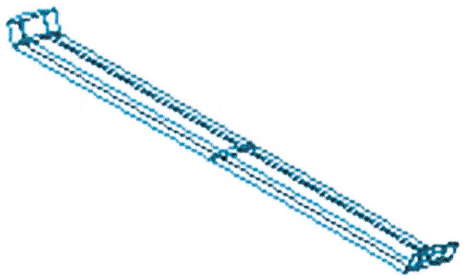
(b) Top View of the Plain Wing

Figure (2.2) Plain Wing as it appear in 3-D Foil Multi-Surfaces Code

The design iterations are listed in Appendix (B). The parameters changed in the design iteration are:

1. The span wise slope angle of the winglets to get optimum angle at $\beta = 65^{o}$.
2. The length of the winglets to be found optimum at 0.4 m.
3. Fixed chord of the airfoils from tip to the root of the winglets.
4. NACA 4412 airfoil for the winglets root, and NACA 0012 for the winglets tip.

The optimum design of wing with winglets is shown in Figure (2.3) for an isometric view and top views:



(a) Isometric View of the Wing with Winglets

Top Elevation



(b) Top View of the Wing with Winglets

Figure (2.3) Wing with Winglets in Isometric and Top Views

After obtaining the optimum design from the comparison with the 3-D Foil Multi-Surfaces code, Solid Works is used to draw the wing with winglet final model ready to export to Ansys Fluent 14 code. Figure (2.4) shows top view of the design, while Figure (2.5) presents the 3-D wing with winglet design.

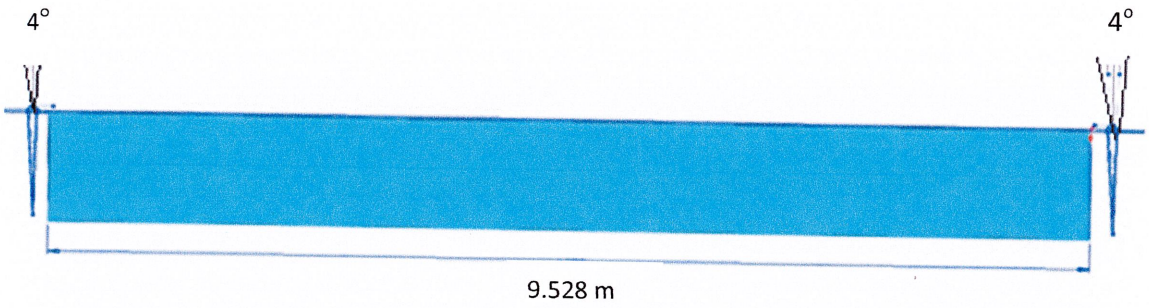


Figure (2.4) Wing with Winglets Top View by Solid Works

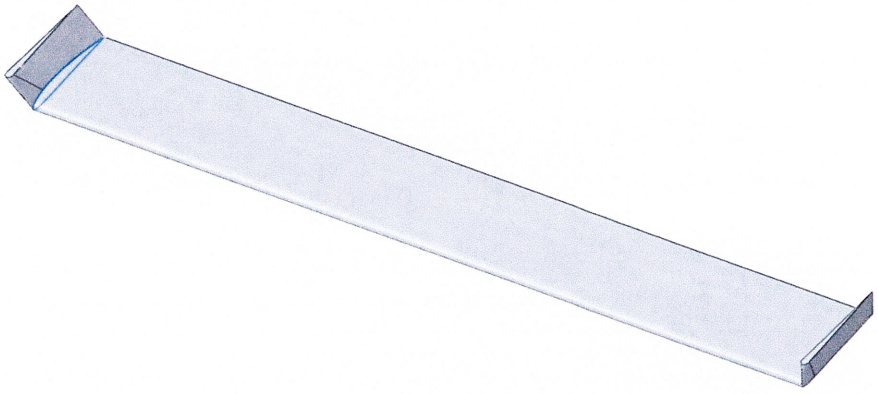


Figure (2.5) Isometric View for Wing with Winglets by Solid Works

2.2 Theoretical Framework

The study of airfoils in Chapter 1 gave insight into how wings generate lift, but it did not tell the whole story. The flow over a wing near the wingtips is very different from the two-dimensional flow around an airfoil. The differences have profound effects on the lift and drag generated by a wing. Understanding these effects is crucial to the aircraft designer who must shape an aircraft's wing to optimize its performance. Section 2.3 discusses wing lift and drag theory and analysis methods.

2.2.1 The Whole Aircraft Lift Curve

Other components besides the wing contribute to an aircraft's lift. The lift contributions of the aircraft's fuselage, control surfaces, high-lift devices, strakes, etc. must all be considered in order to accurately predict an aircraft's lifting capability. But in our case, we are analyzing a very low speed aircraft, with simple wing rectangular geometry located on top position of the aircraft, which make our assumptions in studying the wings aerodynamic characteristics instead of the whole aircraft closer to the reality. The aircraft's maximum lift coefficient is one of the governing factors in an aircraft's instantaneous turn capability, landing speed and distance, and takeoff speed and distance. Section 2.3 describes a variety of devices for increasing an airplane's maximum lift coefficient, while Section 2.4 presents methods for estimating the lift curve slope and maximum lift coefficient of a complete airplane, including the effects of strakes, high-lift devices, control surfaces, etc.

2.2.2 The Whole Aircraft Drag Polar

The drag of all aircraft components must also be included when estimating whole aircraft drag. The variation of an aircraft's drag coefficient with its lift coefficient is called the aircraft's drag polar. The drag polar is the key information about an aircraft needed to estimate most types of aircraft performance.

2.3 Wings

2.3.1 The Language

Figure (2.6) represents a view of a wing plan form with some of the important dimensions, angles and parameters used to describe the shape of an aircraft wing. The wing span, b, is measured from wing tip to the other wing tip. The symbol c is used for the chord length of an airfoil at any point along the wing span. The subscript r indicates the chord length at the wing root or the aircraft centerline. The subscript t denotes the wing tip chord. In our design, r=t because of the rectangular wing shape. The overbar, c denotes an average value of chord length for the entire wing. λ then can defined as the ratio of the chord length of the wing tip to the wing root, which equals to one in our project. The symbol AR is used for a parameter called aspect ratio. Aspect ratio indicates the effective area which is proposed to produce lift. The symbol Λ_{LE} is used for wing sweep angle with the subscript LE denoting the wing leading edge. In our design this angle equals 0^{o} because our wing is rectangular. The subscript *25* denotes the line connecting the 25% chord positions on each airfoil of the wing.

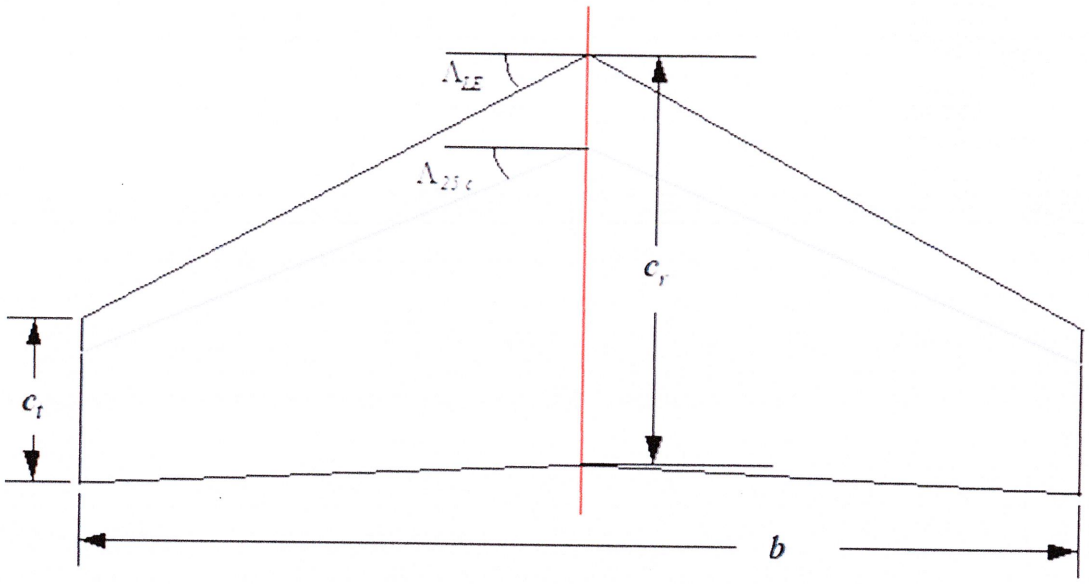


Figure (2.6) Finite Wing Geometry Definitions

Figure (2.7) illustrates a side view of the wing to illustrate the angle of twist. Wings which are twisted so that the wing tip airfoil is at a lower angle of attack than the wing root airfoil are said to have washout. Wing twist in the opposite sense from washout is washin. Wing twist of this sort is also called geometric twist. An effective twist of the wing can also be achieved by changing the airfoil shape along the wing span. If the airfoil at the wingtip has less camber than the airfoil at the root, this has much the same effect on the wing lift as if the airfoils were the same but the wingtip airfoil was at a lower angle of attack than the root. Changing airfoils along the wing span in this way is called aerodynamic twist. In our case we are studying rectangular wing which means that the sweep angle equals zero. Also there is no geometric twist. All of that leads to a simple design compatible to the purpose of this type of aircrafts (Light Sport Airplane) which should be in a reasonable low price of manufacturing and repairing.

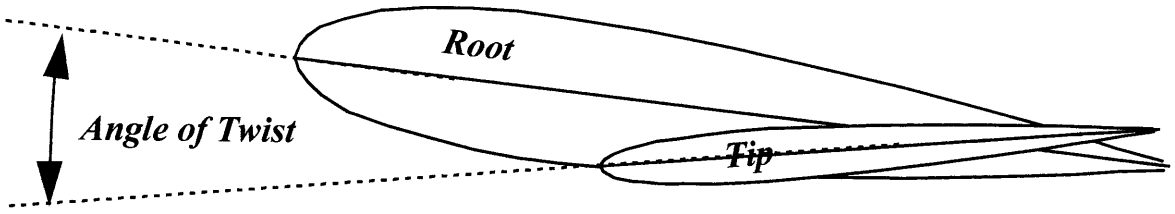


Figure (2.7) Wing Twist

2.3.2 Wingtip vortices

The flow around a wing section which spans the test section of a wind tunnel approximates the flow around a wing with an infinite span, no twist, and a constant chord length along its span. In this chapter, this type of flow was labeled two-dimensional, because flow properties did not vary in the z direction. The flow field around a finite wing or wing with a finite span is not two-dimensional. The majority of differences between the flow around a finite wing and that around an infinite wing result from flow phenomena which occur at the wingtips. Figure (2.8) represents a front view of the flow field around a finite wing. Note that the differences between the pressures above and below the wing which produce lift also produce a strong flow around the wing tip. The arrows in Figure (2.8) are intended to show a front view of flow streamlines in the plane of the 50% chord point on the wing. The lengths of the tails of the arrows do not indicate the magnitude of the velocity vectors. Of course, the actual magnitudes of the velocity vectors must be such that there is no flow through the surface of the wing.

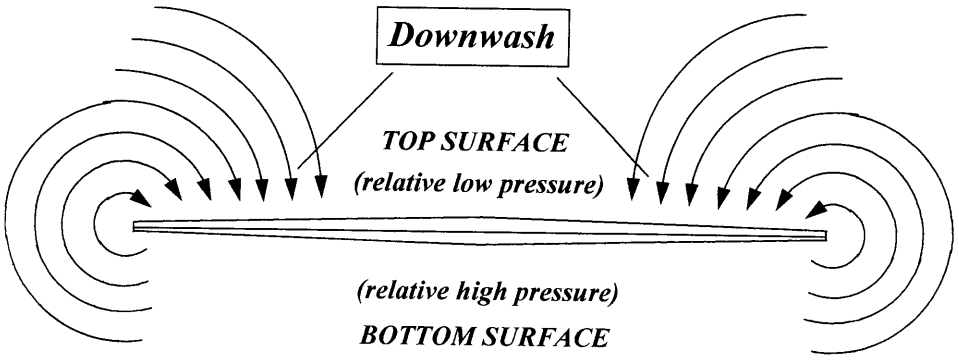


Figure (2.8) Front View of Wing with Flow around the Wing Tips

As shown in Figure (2.9), these circular flow patterns around the wing tips become concentrated into very strong tornado-like swirling flows known as wingtip vortices or trailing vortices. The trailing vortices generated by large aircraft persist for many miles behind them and can pose serious hazards to smaller aircraft which encounter them. Air traffic controllers must allow sufficient spacing between aircraft so that the action of air viscosity and turbulence can dissipate a preceding plane's trailing vortices before the arrival of the next one. This spacing requirement to allow vortex dissipation is the limiting factor on traffic density at most commercial airports.

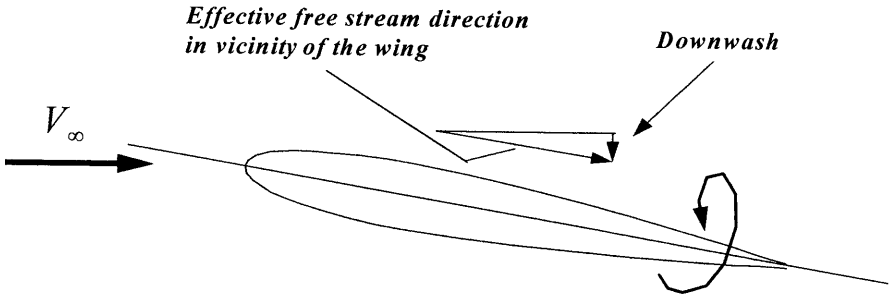


Figure (2.9) Downwash

2.3.3 Downwash

Figure (2.10) noted that the circular flow pattern around the wingtips results in a downward component to the flow over the wing. This downward flow component is called downwash. Figure (2.9) shows that downwash adds vectorially to the free stream velocity to change the direction of the flow velocity. Note that the resulting total velocity vector still results in flow parallel to the wing surface, but the orientation of the effective free stream velocity direction relative to the airfoil is altered.
The change in flow direction due to downwash is called the downwash angle, and is given the symbol ε. The angle between the airfoil chord line and the local flow velocity vector is called the effective angle of attack, α. Each individual wing section's lift, drag, and angle of attack vary with the airfoil's orientation to this local flow direction, but the whole wing's lift, drag and angle of attack must still be defined relative to the free stream direction.

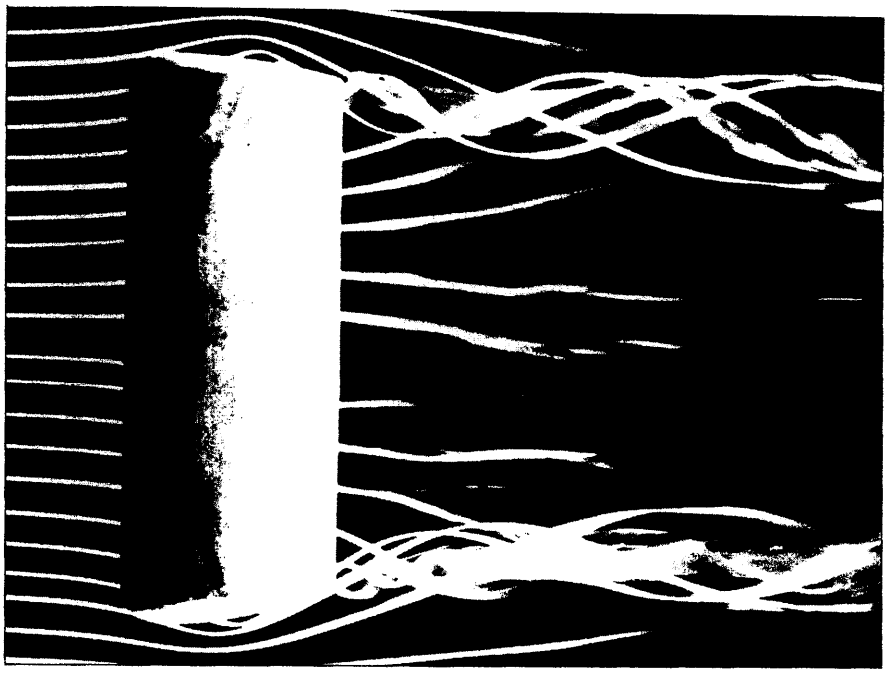


Figure (2.10) Trailing Edges Vortices (*Source:* Anderson, J. D. (2001). *Introduction to Flight* (5th ed.). New York: McGraw-Hill ,Page 397)

Figure (2.11) reveals that, as a consequence of the change in effective flow direction caused by the downwash, the effective angle of attack of the airfoil is reduced, and the lift generated by each airfoil has a component in the wing's drag direction. This component of lift in the drag direction is called induced drag. The reduction in effective angle of attack due to the downwash causes the wing to produce less lift than it would if there were no downwash.

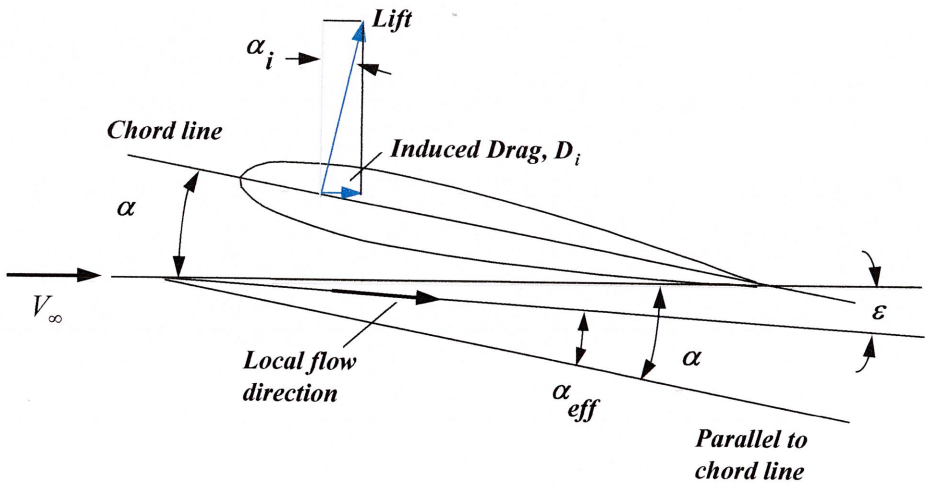


Figure (2.11) Downwash Angle and Induced Drag

Figure (2.12) illustrates the lift coefficient curves for an airfoil and for a finite wing with the same airfoil section shape. Note that C_L denotes two-dimensional airfoil lift coefficient while:

$$C_L = L / qS \qquad (1)$$

The same equation is used for the three-dimensional finite wing lift coefficient. This same convention will be followed for C_D and:

$$C_D = D / qS \qquad (2)$$

The reduction in effective angle of attack due to downwash decreases lift at any given α_{eff} and delays stall to higher values of α. Slopes of the lift curves 2-D and 3-D are defined respectively as:

$$c_{l_\alpha} \equiv \frac{\partial c_l}{\partial \alpha} \tag{3}$$

$$C_{L_\alpha} \equiv \frac{\partial C_L}{\partial \alpha} \tag{4}$$

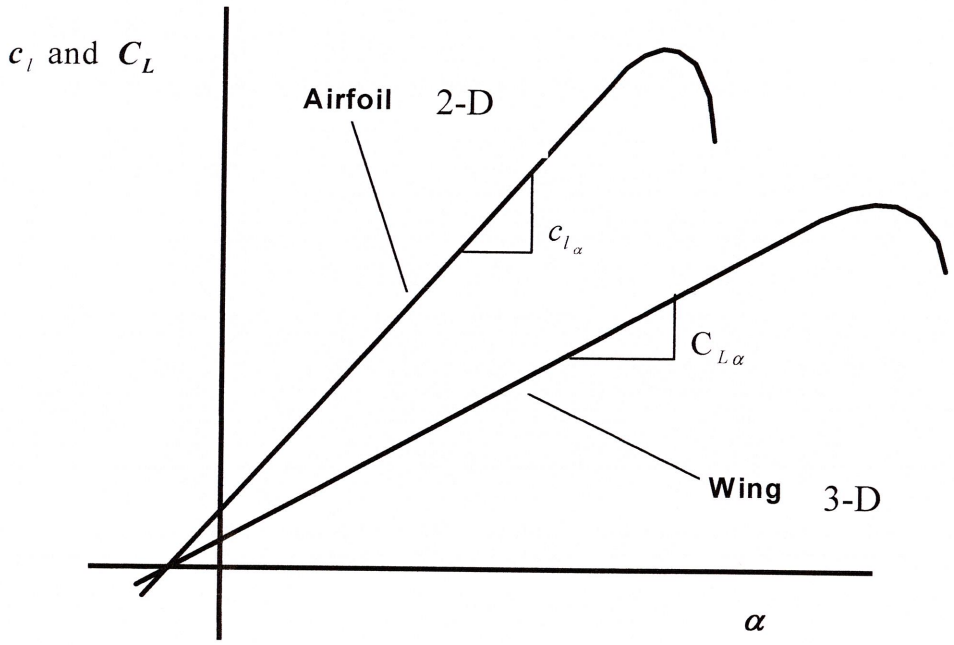


Figure (2.12) 2-D and 3-D Lift Coefficient Curves

2.3.4 Span Wise Lift Distribution

Unlike the two-dimensional flow around an airfoil in a wind tunnel, the flow around a finite wing varies in the span wise direction. This span wise variation is primarily due to the inability of the wing to support a pressure difference at its tips (the cause of trailing vortices). It may be influenced by wing taper, wing twist, or even differences in airfoil shape at different span wise positions on the wing. Span wise variation of airfoil shape is called aerodynamic twist. But even an un-tapered, untwisted, un-swept wing still has span wise variation of the flow field around it. This is because the trailing vortices on such a wing

have a stronger effect and produce more downwash near the wing tips than they do far from the tips. As a result, even though the wing is not twisted, increasing downwash reduces effective angle of attack and therefore lifts near the wing tips. Tapering the wing or giving it wash out can help reduce this effect. In fact, a wing which is tapered and/or twisted to give an elliptical span wise distribution of lift will have a constant downwash at every span wise position. Figure 12 represents an elliptical span wise lift distribution. An untwisted wing with an elliptical planform will have an elliptical lift distribution. As illustrated in Figure (2.13), the elliptical lift distribution is smooth and favorable. Elliptical lift distribution can be obtained from straight. The Elliptic and tapered wings are relatively complex and expensive to build, so straight-tapered wings are much more common.

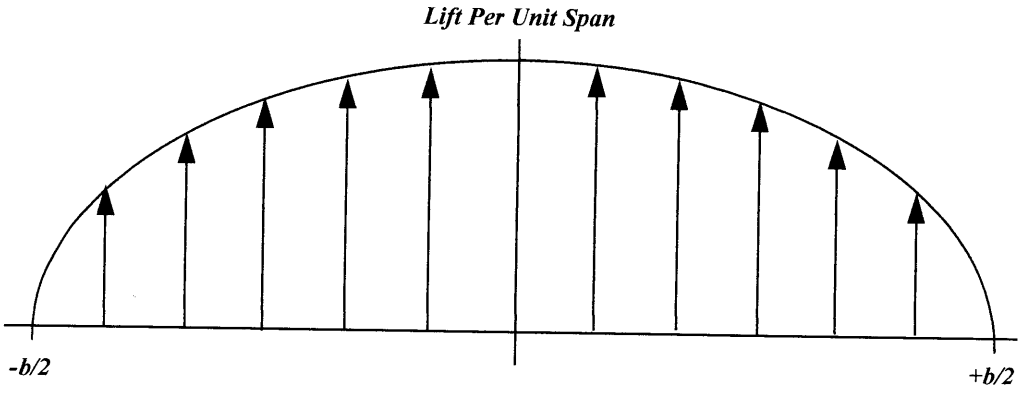


Figure (2.13) Elliptical Lift Distribution

2.3.5 Wing Induced Drag

Figure (2.11) represents the induced drag is a component of the three-dimensional lift in the drag direction:

$$D_i = L\sin\varepsilon \qquad \text{or} \quad C_{D_i} = C_L \sin\varepsilon \tag{5}$$

It can be shown that the induced angle of attack everywhere along the span of wings with elliptical lift distributions is given by:

$$\varepsilon = \frac{C_L}{\pi AR} radians = \frac{57.3C_L}{\pi AR} degrees \tag{6}$$

For ε small, $\sin\varepsilon \approx \varepsilon$ (in radians) and:

$$C_{D_i} = C_L\varepsilon = C_L\frac{C_L}{\pi\ AR} = \frac{C_L^{\ 2}}{\pi\ AR} \tag{7}$$

2.3.6 Winglets and Tip Plates

A variety of devices have been used on aircraft to reduce induced drag. Figure (2.14 a) illustrates three such devices. Of the three, the winglet is the most effective and most widely used. In addition, jet fighter aircraft which carry fuel tanks or air-to-air missiles on their wingtips experience a small reduction in induced drag when such wingtip stores are in place. All of these devices inhibit the formation of the wingtip vortices and therefore reduce downwash and induced drag. Figure (2.14 b) illustrates a winglet on the wingtip.

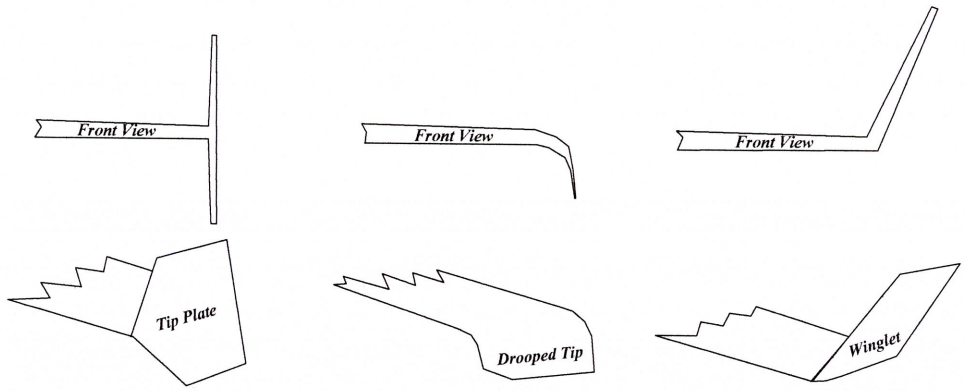


Figure (2.14 a) Three Induced-Drag-Reducing Wingtip Devices



Figure (2.14 b): Winglets on a C-17 (USAF Photo)

Of course, just extending the wing to increase its span and aspect ratio will have a similar effect. However, the increased lift far out at the end of the wing will increase the bending moment at the wing root and create greater loads on the wing root structure. The winglet increases wing span only slightly. It is preferred because it achieves an effective increase in aspect ratio without significantly increasing wing root structural loads.

2.4 Flight Regimes

The range of Mach numbers at which aircraft fly is divided up into flight regimes. The regimes are chosen based on the aerodynamic phenomena which occur at Mach numbers within each regime, and on the types of analysis which must be used to predict the consequences of those phenomena. Figure (2.15) represents these regimes. Mach numbers below M_{crit} are grouped together as the subsonic flight regime. Within this regime, compressibility effects are usually ignored for $M < 0.3$. In our study, the aircraft cruise speed is 50 m/s as designed by the manufacture, which is considered low subsonic speed $M < 0.3$. And we will use subsonic incompressible flow governing aerodynamics equations Brandt, S. A. (2004). *Introduction to Aeronautics: A Design Perspective* (2nd ed.). Alexandria, VA: American Institute of Aeronautics and Astronautics, Inc.

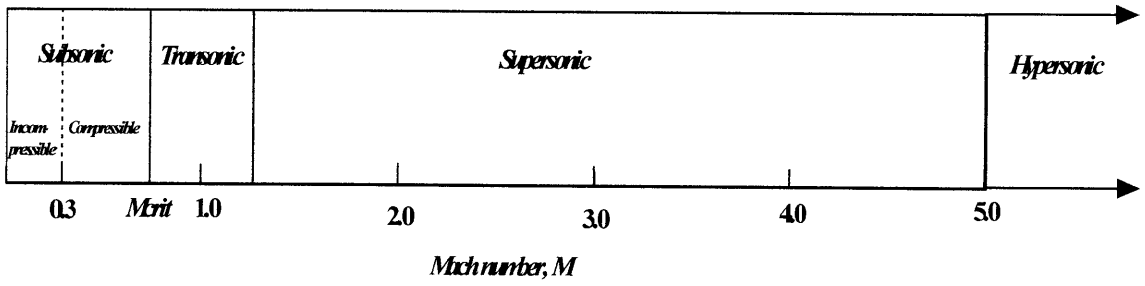


Figure (2.15) Flight Regimes (*Source*: Brandt, S. A. (2004). *Introduction to Aeronautics: A Design Perspective* (2nd ed.) P 135)

2.5 Drag and Lift Analysis

The base line of our calculations is the theoretical solution. We use the governing aerodynamics equations to analyze the original wing

parameters, then the modified design we got with winglets as explained in section 2.2.

We have selected 0^{o} and 5^{o} as the common angles of attack for the steady level flight or cruise flight. While 10^{o} angle of attack is the take-off angle of attack. The appearance of induced drag is severely affected in take-off with very low speeds. Figure (2.16) shows the flight envelope for the aircraft which explains these phenomena.

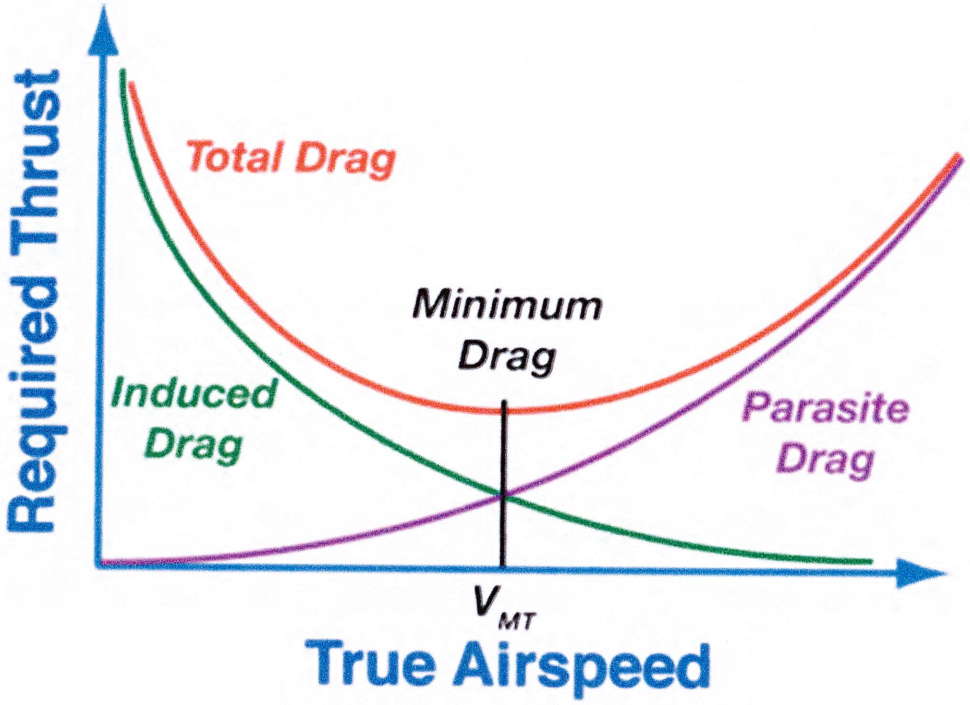


Figure (2.16) the Flight Drag Envelope

The numerical analysis was performed using two types of software: 3D Foil Multi-Surface code and Fluent Ansys 14 code. Firstly, to analyze the original wing (Plain wing), then to analyze the wing with winglet devices problem, the iteration process is used to obtain converged solution.

Chapter 3

Methods and Procedures

3.1 Introduction

3.2 Methodology Steps

3.3 Theoretical Work Setup

3.4 Numerical Work

3.5 Experimental Work setup

3.6 Experimental Procedures and Uncertainty

3.7 Summary

Chapter 3

Methods and Procedures

3.1 Introduction

Jabiru Light Sport Aircraft (LSA) widely used as private low cost jet. Also is used in basic pilots training. In both cases, there are favourable conditions to be assured:

1- Safety in flight.

2- Economical running cost.

Most of winglets researches are about commercial high subsonic speed jets, such as Boeing 737, 767,777 and Airbus 320, 330, 340, etc. These studies concluded remarkable benefits of applying winglets to those jets, reflected in increasing the range by decreasing fuel consumption. The flight safety can be improved by implementing the winglet to decrease the effect of wing tip vortices, especially in take-off and landing. These results lead to major change in aviation philosophy by applying the winglets to the new designed commercial jets.

New trend in winglets application should be those of LSA. Jabiru Rectangular-fixed chord-top positioned wing can be the best start of implementing this technique to this category of aircrafts. The wing span is 9.433 m with chord of 0.9 m. The cruise speed is 50 m/s. Figure (3.1) shows Jabiru LSA.



Figure (3.1) Jabiru Aircraft (LSA)

The success in decreasing induced drag and increasing the lift will result in increasing C_L/C_D then we will obtain better design. Theoretical governing aerodynamic equations are our base line in the solution. Ansys Fluent Code and 3-D Foil Multi-Surfaces Code will be also used to give us the Numerical solution. After that we will verify the results experimentally in the two dimensions wind tunnel C-15 Computer Controlled Subsonic Wind Tunnel, which is available in University of Bahrain.

An experimental work is proposed to study the fluid flow characteristics, namely lift and drag around an aerodynamic shaped airfoil model. The model will be positioned in a horizontal duct and shall be exposed to a varying upstream air velocity at various angles of attack. Fully developed laminar/turbulent air flow will be maintained in the test duct section which is to be connected to a sub-sonic wind tunnel. Induced drag and lift parameters will be studied at various winglet geometries and

simulation CFD work will be performed initially on the airfoil model to validate the experimental work.

This research shall be carried out in four steps as illustrated in the following research methodology phases as shown in Figure (3.2).

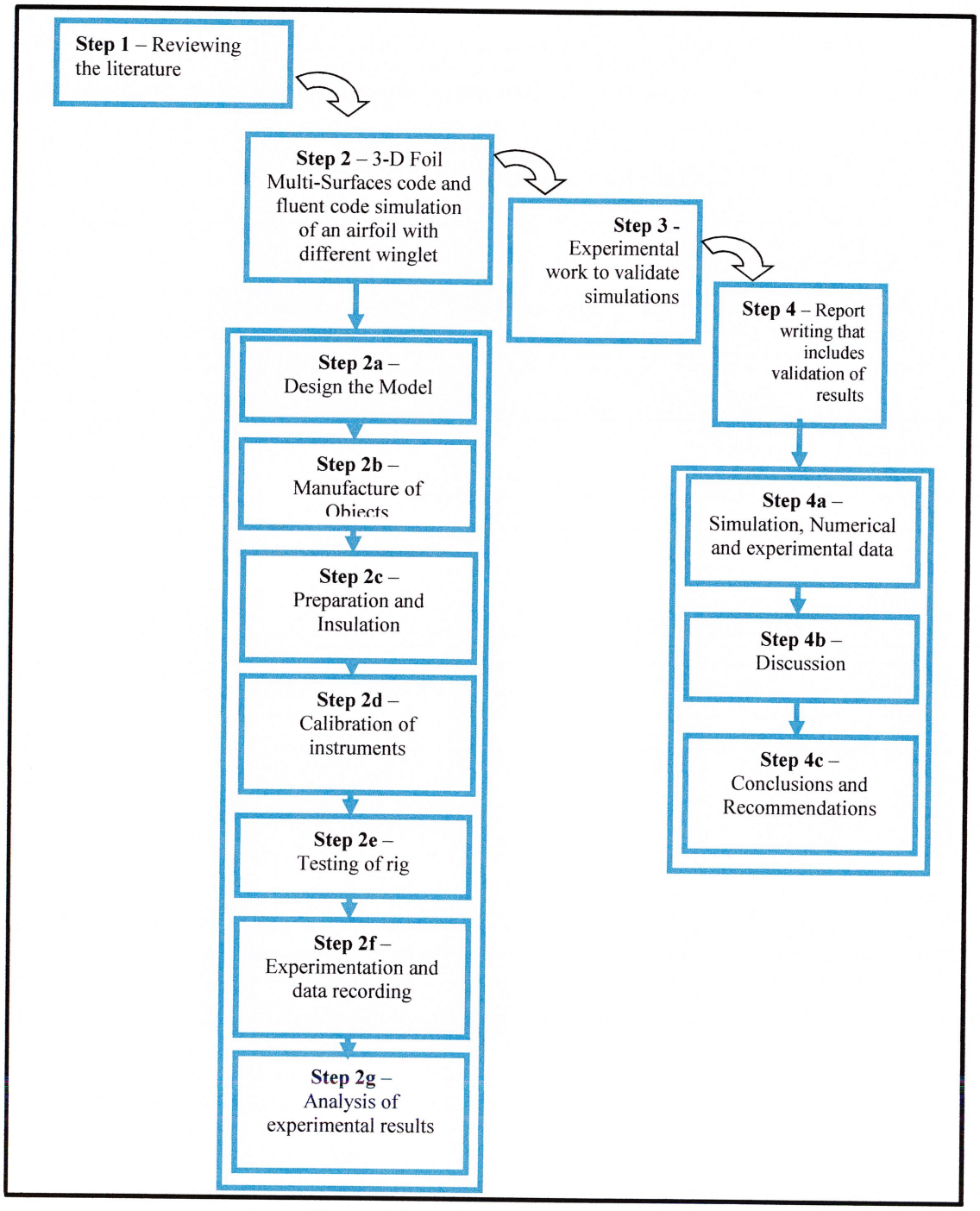


Figure (3.2) Research Methodology

A methodology is a formal approach to solve the problem of fluid flow, namely lift and drag around an aerodynamic shaped object based on its characteristics. Using a methodology ensures a rigorous process, and increases the likelihood of achieving the desired final objective.

3.2 Methodology Steps

This includes but not limited to the following methodologies:

1. Literature survey: Numerical solution of an airfoil and wing with different winglet geometry will be studied Using Fluent Ansys code, 3-D Foil Multi-Surface code and theoretical solution using numerical equations.
2. Experimental Work: To validate simulations; To design two models of wings by using suitable materials, dimensions, and tolerances. One of them is the original design which we call it Plain Wing, and the other one will be the designed Wing with Winglets.

The design reports and the wing aerodynamic lift and drag estimation using experimental approach and numerical study. The experimental approach uses two dimensional wind tunnels. The numerical study uses Ansys Fluent Code, 3D Multi-Surfaces Code and then theoretical governing equations. The experimental approach passes through the following steps:

1- Manufacture of object parts and assembly.
2- Preparation and installation of various instrumentations.
3- Calibration of instruments as advised in C-15 wind tunnel maintenance manual calibration steps.
4- Testing of rig to assess the performance of the wind tunnel as stated in C-15 operational manual
5- Experimentation and data recording.

6- Analysis of experimental results.
7- Report writing that includes validation of results (experimental, Simulation and numerical), discussions, conclusions and recommendation.

3.3 Theoretical Work Setup

Theoretical solution is set as the base line or first line of solution verification. Fundamentals of Aerodynamics by Anderson, J. D. (2003) text book is considered as the main reference. As the book contains the whole of governing equations for the selected boundary conditions using thin airfoil theory, the study updated with the latest corrections in figures and reference charts and values. But Anderson's equations do not cover the complex models of wings such as wings with winglets. So, we referred to Aerodynamics Aeronautics and Flight Mechanics text book by B. W. Mccormick as all winglets designs contribution in Aerodynamics parameters are determined in the governing equations. These winglets equations are added to the basic equations to get the Numerical solution for our suggested design: Wing with winglets.

3.3.1 Plain Wing Theoretical Work Setup

For low subsonic flow with Mach number ≤ 0.3, we can apply thin airfoil theory for laminar/ turbulent flow for viscous incompressible air. The aspect ratio will be calculated for rectangular wing geometry:

$$AR = \frac{S^2}{A} \qquad (8)$$

As discussed in Chapter (2), the total drag coefficient is the summation of the parasite drag coefficient and induced drag coefficient

contributions. The induced drag is called drag due to lift. So it depends mainly on the lift coefficient value. The parasite drag depends on the shape of the object generally, and the wing in our study. It contains the friction contribution also beside the boundary layer contribution. The summation of parasite and induced drag results in the total drag coefficient as stated in this equation:

$$C_D = C_d + C_{D_i} \tag{9}$$

The induced drag coefficient is proportional to the lift coefficient, and depends in the aspect ratio and the shape of the wing as well. The relation between the induced drag coefficient and the lift coefficient is:

$$C_{D_i} = \frac{C_L^2}{\pi\, e\, AR} \tag{10}$$

The geometry factor (e) has a mathematical formula. This formula is applied for all wings shapes: Elliptical, rectangular, swept back and trapezoidal wings. Noted that (δ) is the induced drag factor.

$$e = \frac{1}{1+\delta} \tag{11}$$

For finite wing of general planform, the next equation (12) is the best describing the value of the lift slope (a). Of most importance in equation (12) is the aspect ratio variation. Note that for low (AR) wings, a substantial difference can exist between the lift slope corresponds of a finite wing (a_o) and the lift slope on infinite wing (a). While (τ) is the wing's planform shape factor. The lift slope of the wing then can be determined as follow:

$$a = \frac{a_0}{1+\left(\frac{a_0}{\pi\, AR}\right)(1+\tau)} \tag{12}$$

Therefore, the lift coefficient of the wing is equal to the lift slope of the wing multiplied by the difference of the angles between the wing's angle of attack and the wing's zero lift angle of attack as follow:

$$C_L = a\,(\propto - \propto_{L=0}) \tag{13}$$

The induced angle of attack is explained in section (2.3.4). We calculate for airfoil NACA 4412.

$$\propto_i = \frac{C_L}{\pi\, AR} \tag{14}$$

As the effective angle of the wing is affected by the induced angle, then the effective angle will decrease by the calculated induced angle above to obtain:

$$\propto_{eff} = \propto - \propto_i \tag{15}$$

Finally, the lift coefficient of the airfoil is determined as follow:

$$C_l = a_0\,(\propto_{eff} - \propto_{L=0}) \tag{16}$$

From the NACA 4412 lift coefficient value, we can obtain the parasite drag of the wing using the proper Reynolds number (R_e) of 3.51×10^6.

3.3.2 Wing with Winglets Theoretical Work

The approximate analysis indicates that:

1. The reduction in C_D increases linearly with C_L^2.
2. At low C_L values, C_D will be increased by the addition of a winglet.
3. High winglet aspect ratio is desirable.

The severe limitations inherent in the assumptions leading to equation (17) must be recognized. For a given value of wing's wetted area to the whole wing's planform area (S_w/ S); it would appear that increasing the reference area (A_w) would always result in a smaller constant of proportionality, K.

$$C_D = C_d + [C_{D_i} + \Delta C_{D_i}] \tag{17}$$

As $C_{D_{W_0}}$ is the drag coefficient of the wing at zero lift, therefore, increment in induced drag coefficient value ΔC_{D_i} becomes:

$$\Delta C_{D_i} = -\frac{S_W}{S}\left[2\pi\left(\frac{A_W}{A}\right)^2 K^2 {C_L}^2 - C_{D_{W_0}}\right] \tag{18}$$

In Figure (3.3) we see the various forces acting on the wing tip with winglet. Figure (a) shows a view in direction of flight. Figure (b) is the plan view, and Figure (c) shows the forces acting on winglets. Outboard of the tip, the flow is nearly circular as air from beneath the wing flows outward along the span, around the tip, and inward on the upper surface. The velocities induced by the wing are shown. To these the free-stream velocity is vectorially added. The magnitudes of the induced velocities generally increase toward the tip. At given spanwise location, the induced velocities are highest close to the surface of the wing, just outside the boundary layer. Mccormick, Barens W. (1995). *Aerodynamics Aeronautics and Flight Mechanics* (2nd ed.)

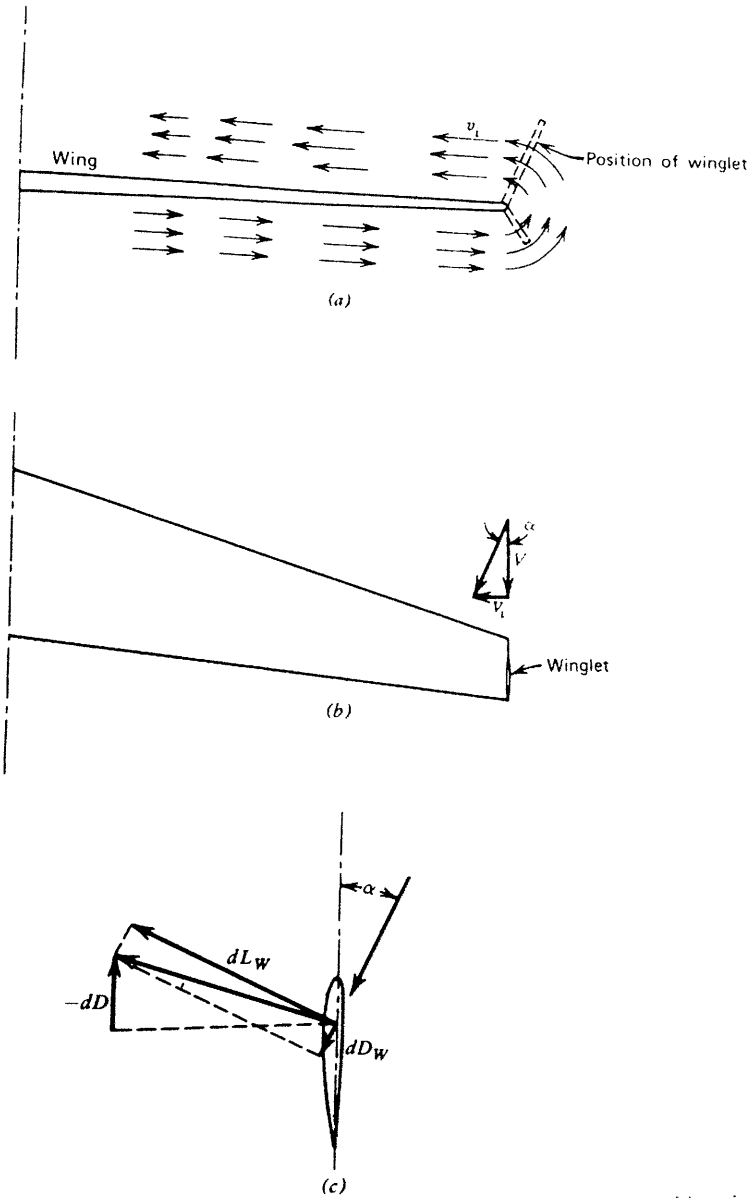


Figure (3.3) Generation of Negative Drag by Winglets (*Source:* Mccormick, Barens W. (1995). *Aerodynamics Aeronautics and Flight Mechanics* (2nd ed.). Page 189).

3.4 Numerical Work Setup

3.4.1 Fluent Ansys 14 Code

Fluent Ansys 14 code is the most powerful computational fluid dynamics (CFD) software tool available, empowering you to go further and faster as you optimize your product performance. Fluent includes well-validated physical modeling capabilities to deliver fast, accurate results across the widest range of CFD and multi-physics applications. Fluent Ansys 14 code software contains the broad physical modeling capabilities needed to model flow, turbulence, heat transfer, and reactions for industrial applications ranging from air flow over an aircraft wing to combustion in a furnace, from bubble columns to oil platforms, from blood flow to semiconductor manufacturing, and from clean room design to wastewater treatment plants. Special models that give the software the ability to model in-cylinder combustion, aero-acoustics, turbo-machinery, and multiphase systems have broadened its reach.

In Fluent Ansys 14, the plain wing is imported, then the designed wing with winglets is drawn in from Solid Works 2012 file to the Ansys 14 main page. Then start preparing the model for final drawing in the code design modeler, then apply meshing, and finally to the setup in fluent and running the results.

3.4.1.1 Design Modeler

In Figure (3.4) an envelope created around plain wing and around wing with winglet design in purpose to create the faces, nodes and surfaces for the models before the meshing step.

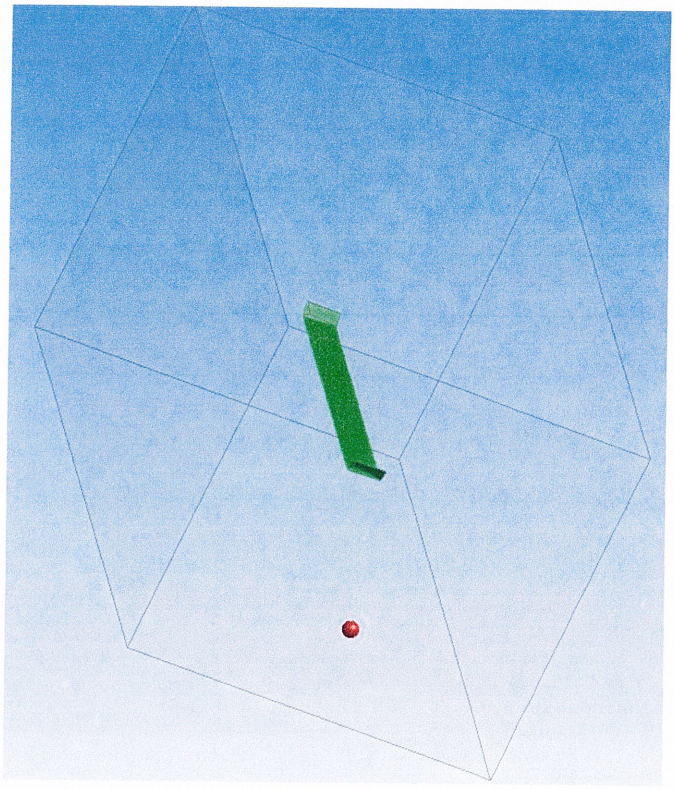


Figure (3.4) Ansys 14 Design Modeler Setup Page

3.4.1.2 Meshing

In Figure (3.5), the meshing final appearance will look alike for both plain and designed wings. The only difference is the number and sizes of the cells are more in the wing with winglet design because of the small edges created due to geometry. Other setup values are taken standard with high accuracy, fine meshing, high speed transition and triangular meshing cells.

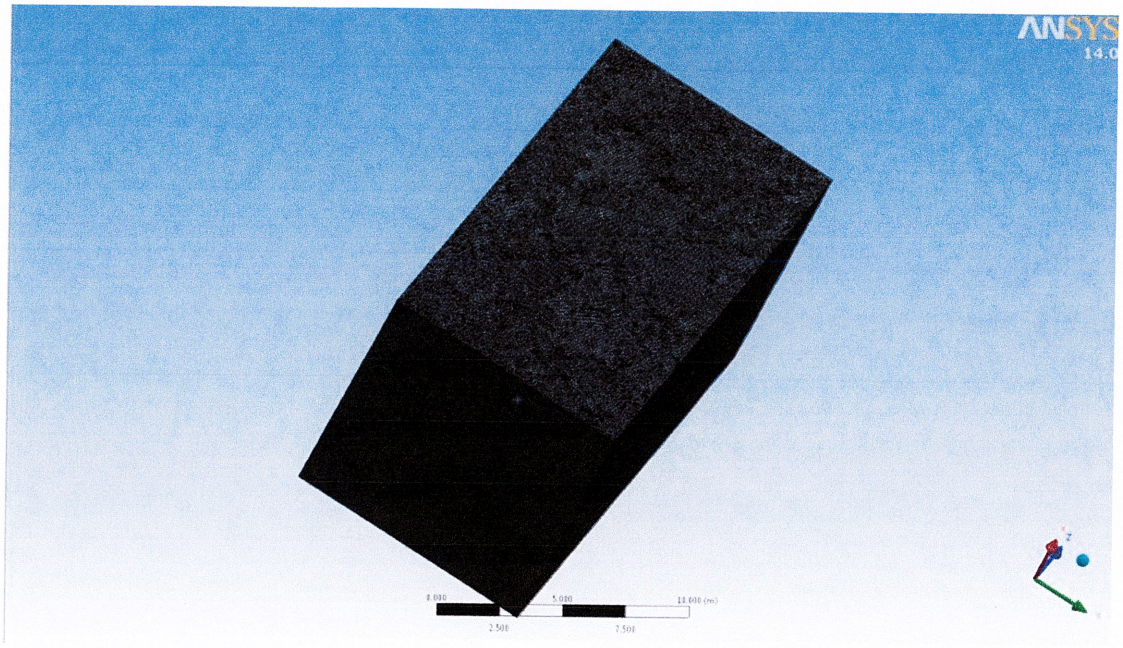


Figure (3.5) Meshing's Final Shape

Closer view in Figure (3.6) shows the shape of the meshing cells after final refinement. It is noticed that, 3-D meshing consumes huge data for calculations, which limits the mesh quality regarding computers memory and graphics.

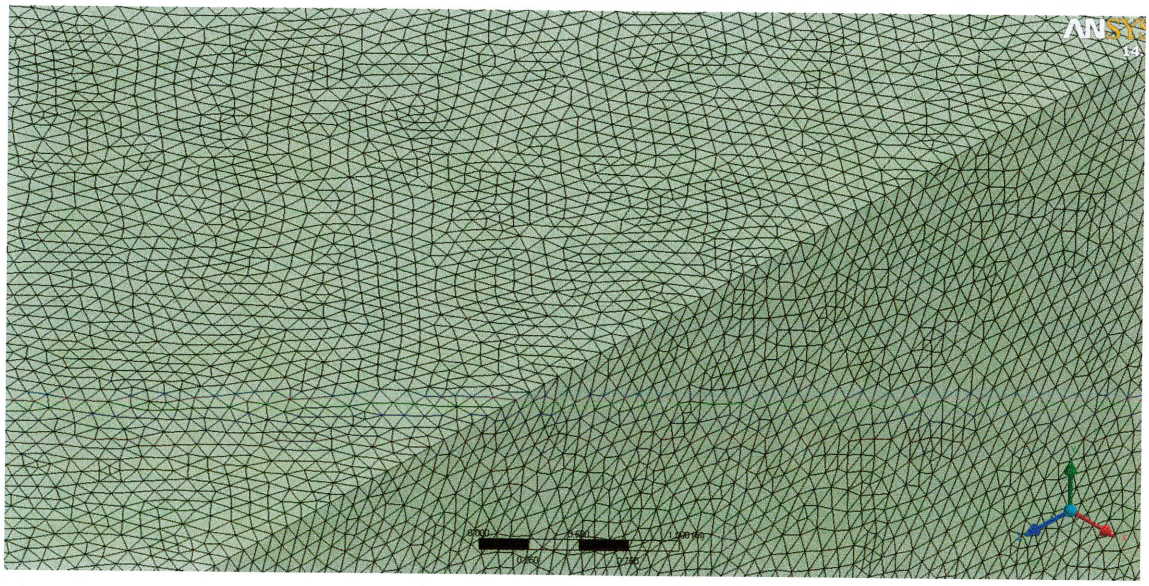


Figure (3.6) Closer View for Meshing

This methodology generates a high quality mesh. In Table (3.1) we can see the final meshing data for designed wing with winglets compared to the original plain wing. Noted that, all design aspects are greater in the Wing with Winglets than the Plain Wing. This is because of the small areas of the winglets design.

Table (3.1) Comparison between Plain and Winglet Wings Meshing Data

	Plain wing	Wing with winglets
Nodes	679745	773510
Elements	3675975	4211329
Faces	10	21
Edges	20	42
Vertices	14	26

3.4.1.3 Fluent Setup

In Fluent setup, the main setup as shown in Figure (3.7) is double precision method used for the best accuracy.

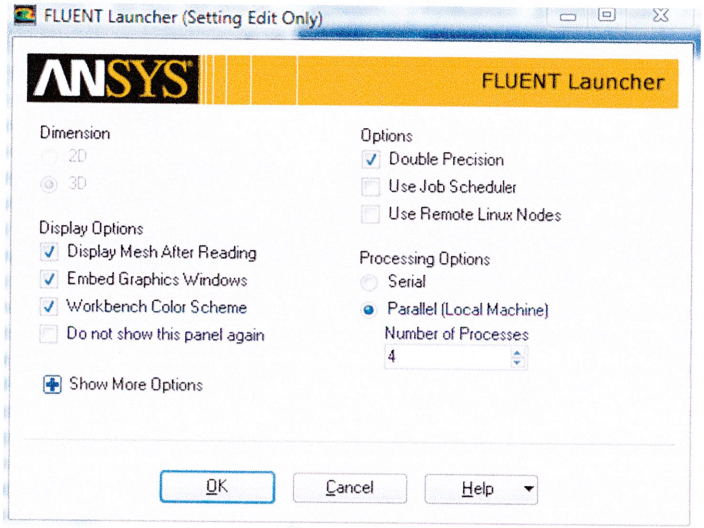
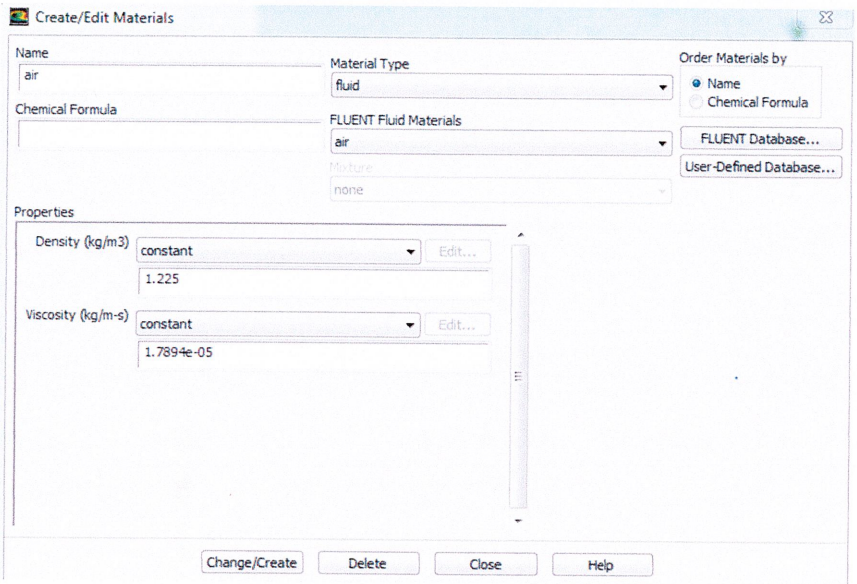
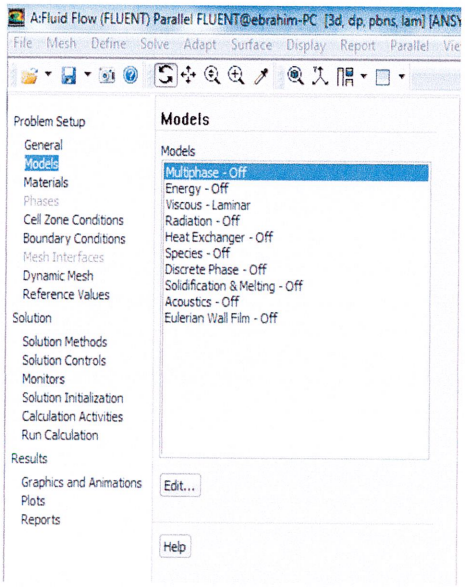


Figure (3.7) Fluent Main Setup

A steady pressure is selected based on absolute model for both plain wing and wing with winglets models. In Figure (3.8), we selected viscous laminar model because of very low speed and the simplicity of the 3-D model in Figure (3.8, a). The medium of the surrounding flow is air. The standard air properties as measured at 15° are selected for both models as seen in Figure (3.8, b).



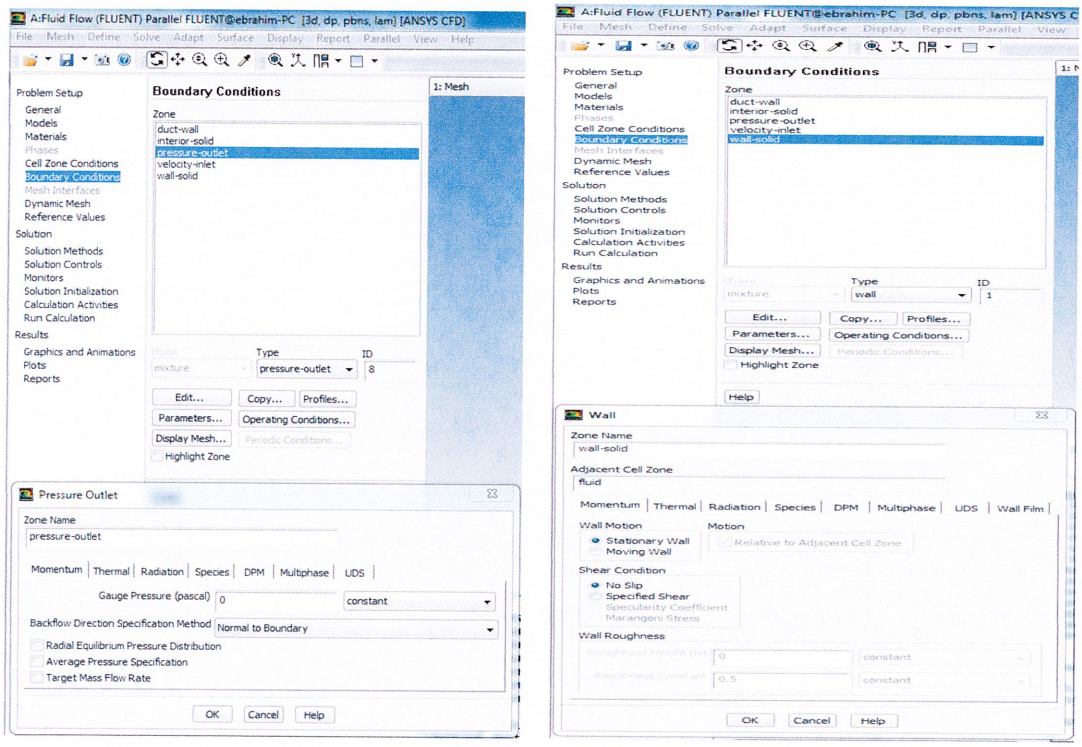
(a)



(b)

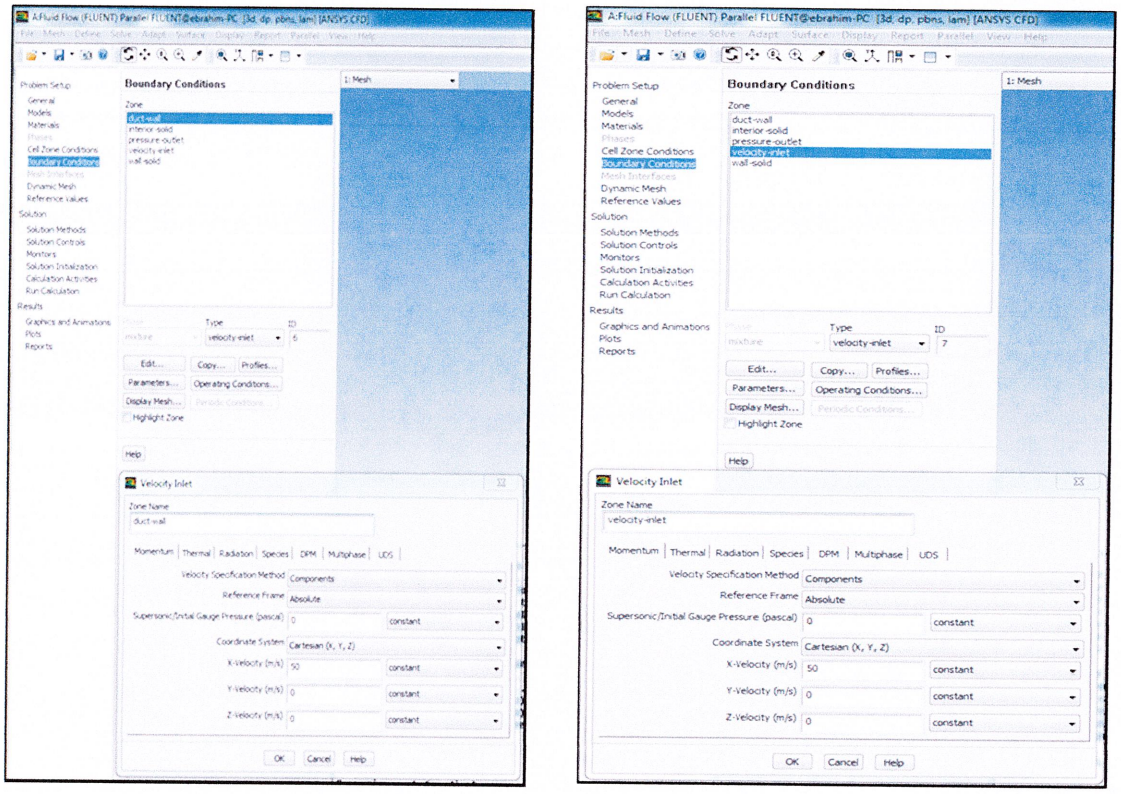
Figure (3.8) Fluent Model and Materials

The boundary conditions selected for both models are the same. Pressure outlet, velocity inlet, wing-walls and the duct walls are the main boundary conditions. Figure (3.9) shows the boundary conditions. The pressure outlet setup is shown in Figure (a). The wings walls considered to be smooth with no slip, while in (b) the figure indicates the standard condition selected for our wings. The remaining boundary conditions such as velocity inlet and duct walls are selected individually in three separate scripts. Each of them is designated to an angle of attack: 0^{o}, 5^{o} and 10^{o}. Figure (3.10): (c) and (d) show these boundary conditions for 0^{o} angle of attack. The velocity components only changed by changing the angle of attack in the two models: Plain wing and wing with winglets design.



(a) (b)

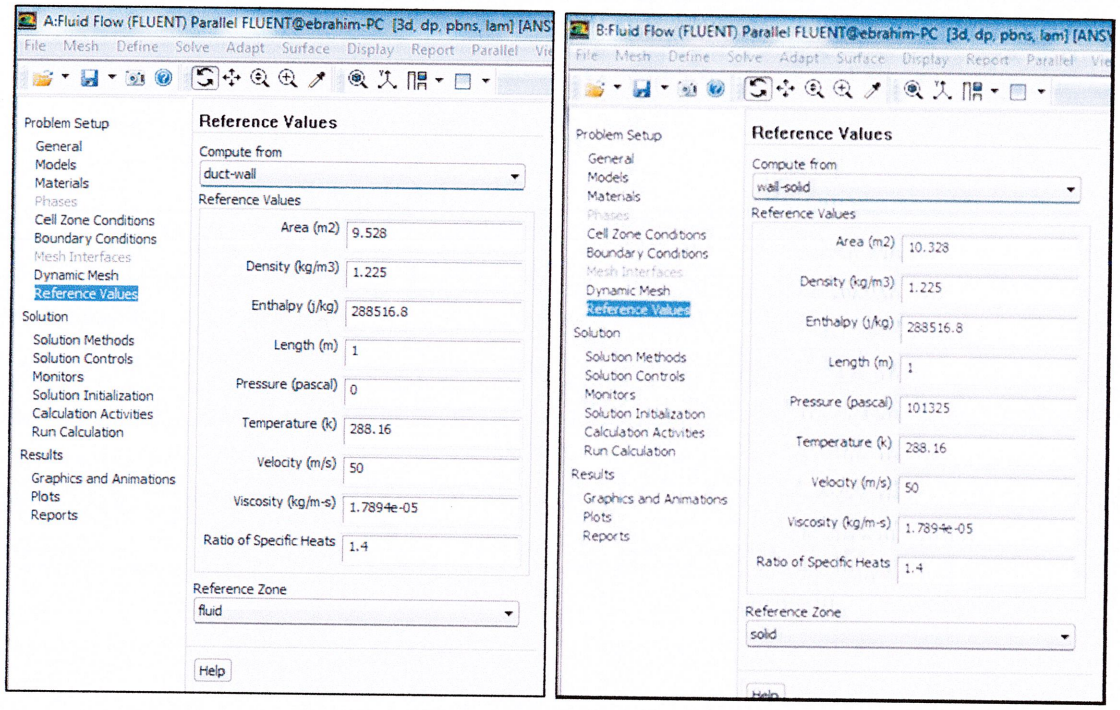
Figure (3.9) Boundary Conditions



(a) **(b)**

Figure (3.10) Other Boundary Conditions

As the reference values are measured at sea level condition. The only difference between the reference values in original model (Plain wing) and the designed model (wing with winglets) is the reference area. The reference area is the projected area of the top view of the wing. So, the winglets areas make slight increase in the wings projected area in the designed model. Figure (3.11) shows the reference values. Figure (a) For the plain wing, while Figure (b) shows the reference values of the wing with winglets.



(a) **(b)**

Figure (3.11) Reference Values

The monitors are adjusted to higher convergence accuracy for the solution. The drag and lift coefficients are added to the monitors. As the boundary conditions, the drag and lift coefficients calculation vectors adjusted to the three angles of attack 0, 5, and 10 degrees. Figure (3.12) depicts monitors port in Fluent.

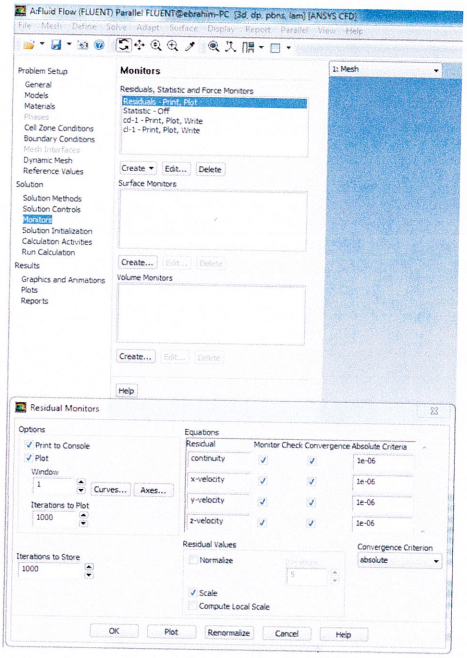
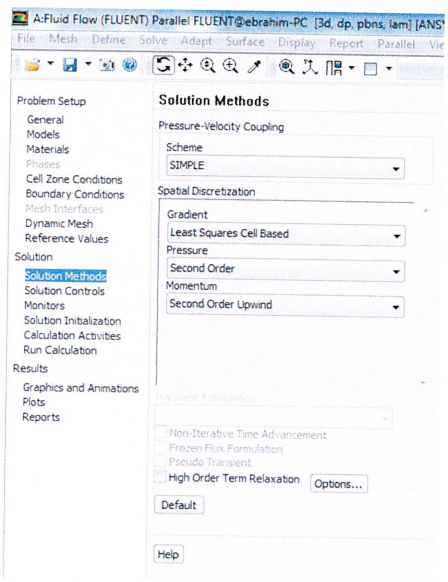
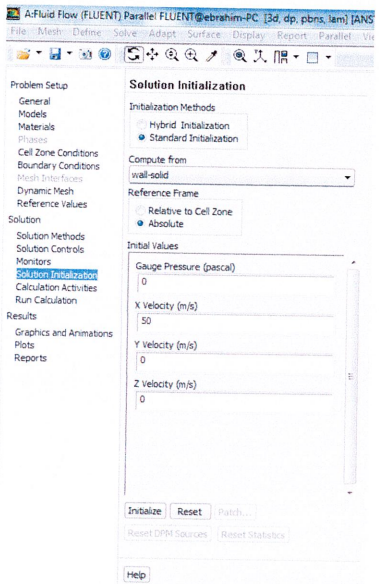


Figure (3.12) Fluent Monitors Setup

Finally, the solution initialization, calculation activities and running the calculations are set. Figure (3.13) (a) and (b) show these settings. And finally, the calculations are run as shown in Figure (3.14).





(a) **(b)**

Figure (3.13) Solution Methods and Initialization

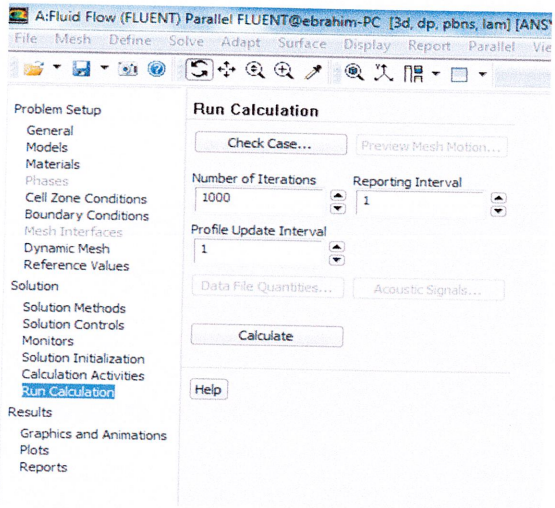


Figure (3.14) Running the Calculations

3.4.2 3-D Foil Multi-Surfaces Code

This airfoil/ wing simulation software is widely used in US navy aviation academies and other educational institutes. It is based on Thin Airfoil Theory but the reality of the results is less accurate than Fluent Ansys 14. We used it as a verification method. It is easy to deal with. Figure (3.15) shows the home page of the program software.

The 3-D Foil Multi-Surface code models complex wing geometries by using multiple tapered surfaces (8 surfaces). This code computes the values of lift, drag and pitch moment coefficients, the lift distribution, induced angle of attack distribution, angle of trim, lift to angle of attack curve (Cl-α) and pitch moment to angle of attack curve (Cm-α). The 3-D Foil Multi-Surfaces Code includes a body of revolution to simulate an airplane fuselage and other applications.

The 3-D Foil Multi-Surfaces Code is a light used by engineers, designers and students as an interactive tool to design and immediately

analyze aircraft wings, aircraft wing and body combinations and other aerodynamics objects directly on their personal computer.

3-D Foil is a lite version of Multi-Surface Aerodynamics. It excludes the body of revolution and has 8-surfaces (instead of 30). The remaining features of the full version are intact in 3-D Foil including the built-in tools, airfoil library and stability analysis.

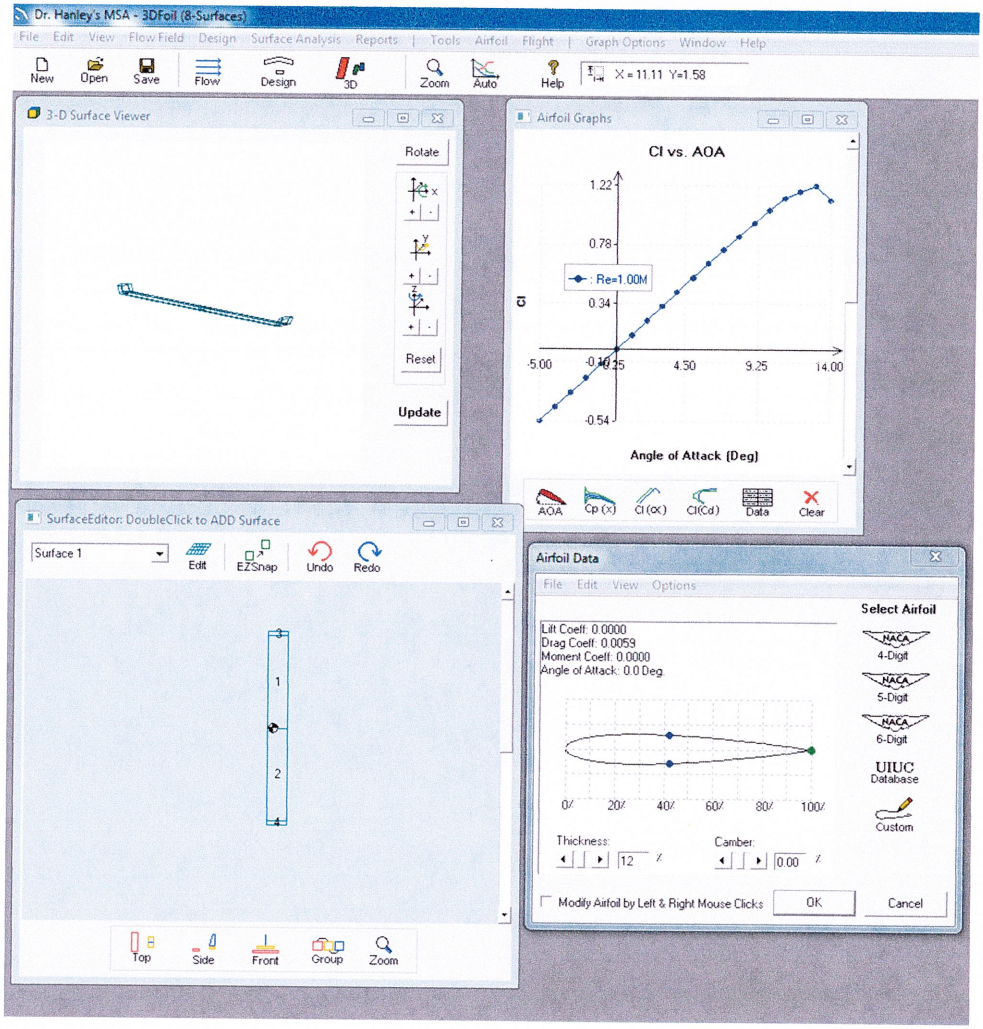


Figure (3.15) 3-D Foil Multi-Surfaces Code Simulation Code Features

3.5 Experimental Work Setup

The experimental solution is used to verify both of numerical and theoretical solutions.

3.5.1 Wind Tunnel Setup

Basically, the wind tunnel as shown in Figure (3.16) contains three main parts:

a- The entry section: Transparent working section with uniform cross section and outlet diffuser.

b- The main accessories associated with the wind tunnel: The balance device and electronic manometer bank which are connected with electrical console (IFD 7) and software model (C15-304).

c- The main computer: Connected to the wind tunnel and equipped with software for measuring and analysing the wind tunnel processed input data.

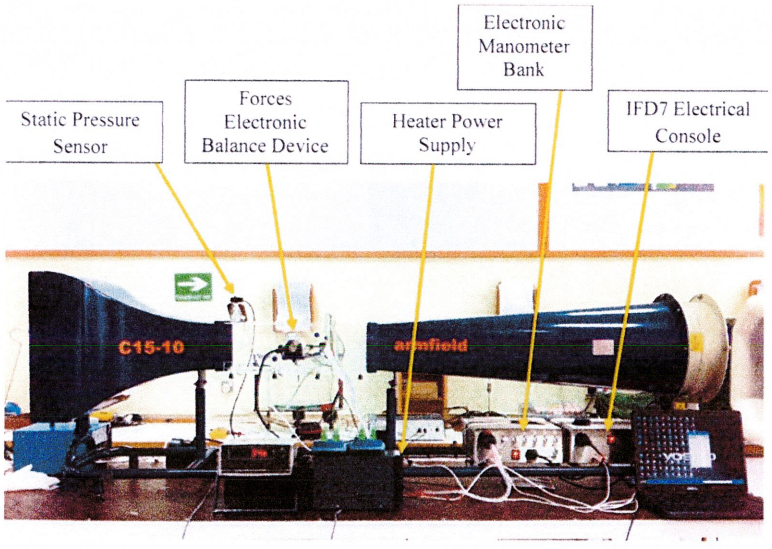


Figure (3.16) C15 Computer Controlled Subsonic Wind Tunnel

The limitation of using 2-D wind tunnel can be eliminated by scaling the model to fit the pitot tubes (10 stainless steel probes) at 90% of the wingspan which is exposed to the severest effect of induced drag. Mccormick, Barens W. (1995). Figure (3.17) shows the stainless steel tubes arrangement.

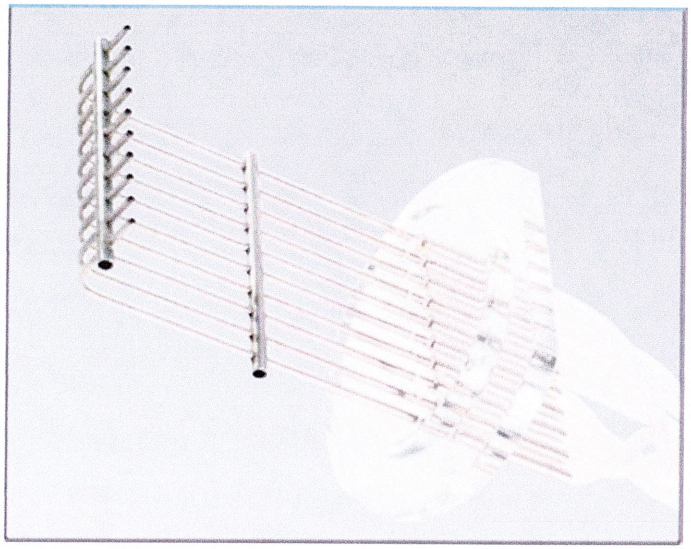


Figure (3.17) Stainless Steel Tubes Arrangement

Figure (3.15) shows the C15 Computer Controlled Subsonic Wind Tunnel used in our experimental work. Appendix (E) lists the wind tunnel specifications.

3.5.1.1 Electrical Interface Console

Electrical interface console IFD 7 transfers the data of drag, lift and rotational sensors in the balance device to the main (PC) computer via the computer's USB port. Also it provides the power to the electronic manometer bank and for the wind tunnel motor fan. In addition, the IFD 7 provides a connection to the computer which allows the fan to be

controlled from the PC using USB ports. Figure (3.18) illustrates the IFD 7 with the necessary connection from the device.

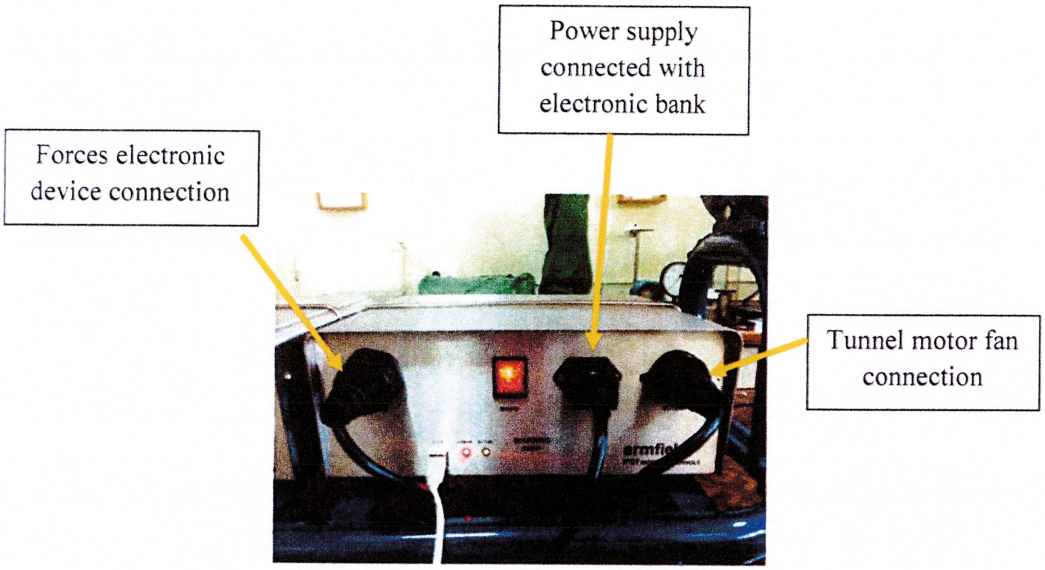


Figure (3.18) IFD 7 Electrical Interface Console

3.5.1.2 Electronic Manometer Bank

Through this electronic device, the differential pressures head in the wind tunnel are measured and recorded via the PC computer in the wind tunnel.

An electronic console operates 16 differential pressure sensors, each with a range of 0-178 mm H_2O. These sensors connected to the control PC using a second USB port, and the readings are integrated with the wind tunnel control (PC). All sensors designed to be referenced to atmospheric pressure. Quick release connectors lead to the best connection of models and instruments. Figure (3.19) shows the electronic manometer bank as it appears in the C-15 wind tunnel.

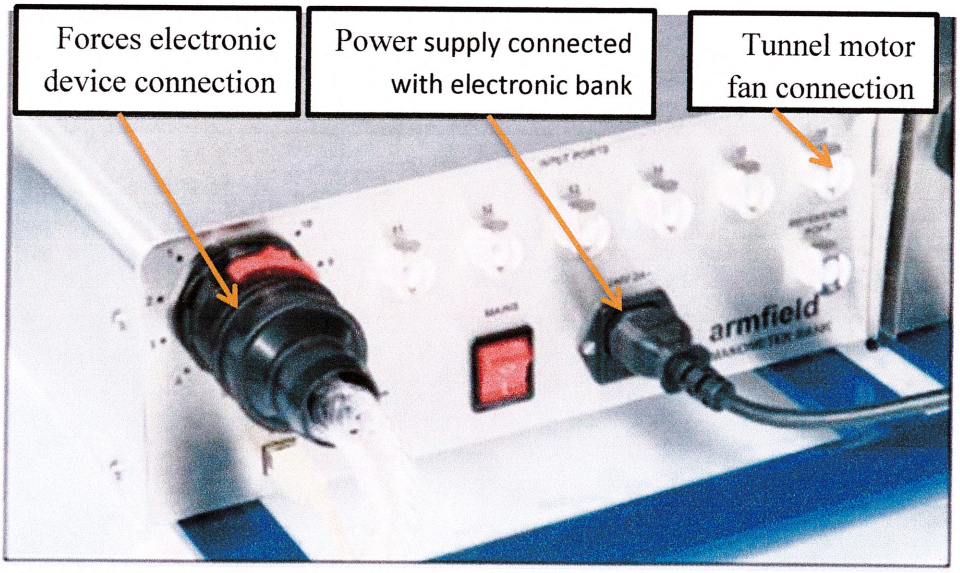


Figure (3.19) Electronic Manometer Bank

3.5.1.3 Lift and Drag Electronic Balance Device

The electronic balance device shown in Figure (3.20) used to measure both of lift and drag on the both models:

a. Plain wing model.

b. Wing with winglets model.

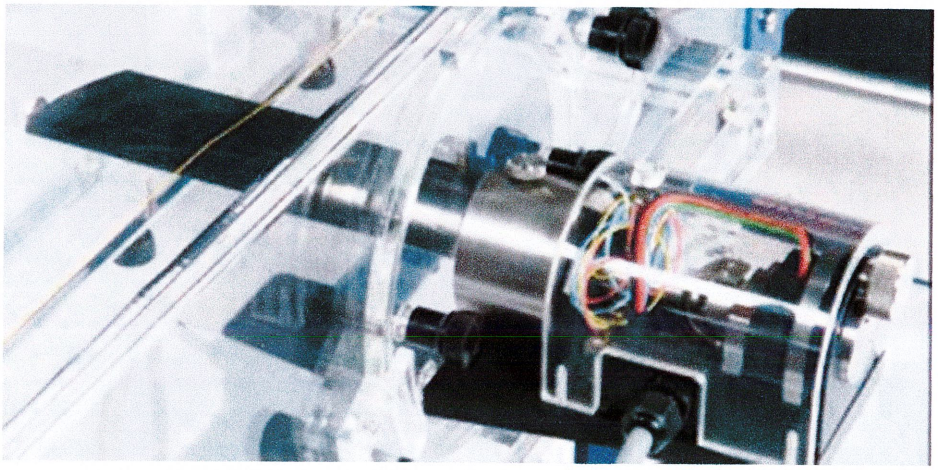


Figure (3.20) Lift and Drag Balance Device

The lift and drag prototypes are connected to the balance using a regular fixture that ensures proper orientation of the models. Electronic sensors are used in the lift and drag forces measurements, the drag being measured directly, and the lift by considering the model weight. The models can be adjusted in different inclinations on the fixture and the angle of rotation measured precisely electronically. The data collected from the models from the lift and drag sensors and the rotation sensor are displayed on the (PC) screen, and are available for data logging. The balance is designed to accommodate the C-15 but can also reads the data of alternative models manufactured by the user as done in the investigations.

3.5.2 Models Manufacturing

The complex shape of the airfoil and the addition of the winglets narrowed our options in manufacturing the 3-D models for both plain and designed models. 1:100 scale reduction used for both models in purpose to fit them into the 2-D tunnel as mentioned in section 3.5. These small dimensions can be manufactured by the 3-D printer Dimension 1200 available in the Polytechnics College at Isa Town Campus. The models were manufactured with 20 μm surface finish.

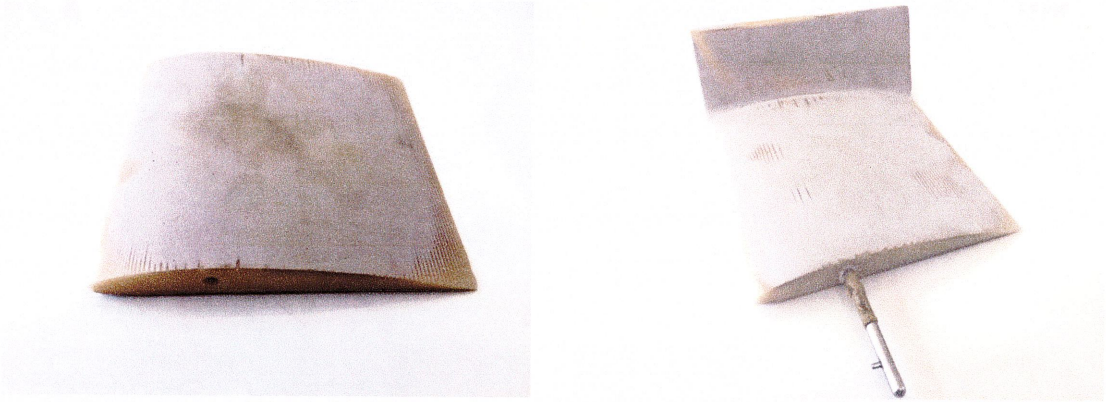
Original design is uploaded; Plain Wing, and the designed wing; Wing with Winglets script files drawn in Solid Works program into the 3-D printer. It took around 3 hours for producing each model. 3-D printer specifications are listed in Appendix (D).

3.5.3 Testing and Calibrating the Models

The models are 9.57 × 10 cm and 10.328 × 10 cm. They are scaled sections at the wing tip. The reasons that we couldn't make a full length model are:

1. The limitation of having only 2D wind tunnel.
2. The limited number of 2D probs (10 probs) placed 8 cm from the edge of the walls and the small cross section of 10 × 10 cm of the wind tunnel.

We got two models as shown in Figure (3.21). The models were rough and needed surface treatment.



(a) **(b)**

Figure (3.21) (a) Plain Wing Model and (b) Wing with Winglet Model

The treatment took place at Royal Bahraini Airforce (RBAF) in the Sheet Metal Work shop. Table 2 shows types and sizes of sandpapers used in refining the models. After sanding, the models are polished with thin layers aviation filler. We have used ultrafine polishing process on the model surfaces.

Table (3.2) Sandpaper Sizes

MACROGRITS	ISO/FEPA Grit designation	CAMI Grit designation	Average particle diameter (μm)
Very Fine (sanding finishes between coats)	P240		58.5
		240	53.0
	P280		52.2
	P320		46.2
	P360		40.5
Extra fine, start polishing of wood		320	36.0
	P400		35.0
	P500		30.2
		360	28.0

The wind tunnel is run through three different speeds: 10 m/s, 20 m/s and 30 m/s which are the maximum speed it can got from fan speed control unit at 30%, 68% and 96% from the maximum fan speed power. We set the models at 0 degree, 5 degrees, 10 degrees and 15 degrees angle of attacks and then operated the wind tunnel fan. The test is repeated 10 times for each of the two models.

3.6 Experimental Procedures and Uncertainty

In our experiments, three stages of calculations and analysing criteria are considered:

1. Stated theoretical equations.
2. Numerical simulation programs: Ansys 14 Fluent code and 3-D Foil Multi-Surfaces Code.
3. C-15 Wind tunnel experiment.

All boundary conditions are fixed in all stages such as: velocity, pressure, temperature, Reynolds number and boundary layer calculation method. Although of that, differences appeared between results obtained from each method. Because of that, the uncertainty percentage is set for our experiment and simulation results.

The maximum air speed in the wind tunnel was affected by the model shape, blockage area and the inclination angles. The maximum speed obtained was 30 m/s through over all trails.

3.6.1 Experimental Procedures

1. In the beginning, all necessary connection and arrangements should be prepared such as:
    a. Both (IFD 7) Figure (3.17) and Electronic Manometer Bank Figure (3.18) and USB cables are connected to the (PC).
    b. Both models: Plain wing model and the designed wing with winglets model shown in Figure (3.21) are connected to the fixing bar.
    c. The models are fixed without a gap between them and the fixture side of the wall. And free from the other side with a gap of 2 cm. This gap is sufficient to generate the wing tip vortices.

d. The stainless steel pitot tubes set are positioned as mentioned in section (3.5.1) at position of 90% from the wingtip edge, to get the worst wing tip vortices situation results.

2. The wind tunnel software programme in the (PC) is switched in running mode.
3. The (IFD 7) and Electronic Manometer Bank are switched ON.
4. Through the wind tunnel software programme, the values of drag forces are set to zero before starting the experiment for the best desired conditions. Then switched on the fan to the standby mode. The value of fan speed will reset to zero value. Also the lab ambient temperature reading is set to 19 degree Celsius.
5. The fan power percentage and the inlet velocity are calculated for different angels of attacks as show in the next Table (3.3).

Table (3.3) Experimental Tests and Parameters performed for the Plain Wing and Wing with Winglet Models

Plain wing/ wing with winglet angles of attack (α) inside the wind tunnel: (1) $\alpha = 0^{o}$, (2) $\alpha = 5^{o}$, (3) $\alpha = 10^{o}$, (4) $\alpha = 15^{o}$	
Inlet velocity (m/s)	Fan power percentage (%)
10	30
20	60
30	90

3.6.2 Uncertainty Analysis

In order to check the accuracy and the error percentage of our measurements, the same experiment is repeated three times for every setting to ensure the accuracy of the obtained results. Also, the

uncertainty was done for the numerical solution of Ansys 14 Fluent code and 3-D Foil Multi-Surfaces.

The inlet velocity differences in the experiments were 2 to 3 %. Vibrations on the models occurred in the experiments due to the wing tip vortices which caused differences in the values of drag and lift coefficients at 3 %. Appendix (F) illustrates all experiments trail done in our investigations.

Moreover, a standard uncertainty was performed for each measurement and analysed in details as shown in Appendix (A). The uncertainty of drag measurements was found to be approximately ± 0.502 % for the plain wing and ± 0.691 % for the wing with winglets. The drag coefficient uncertainty measured at zero angle of attack was found to be ± 2.308 % for the plain wing and ±3.005 % for the wing with winglets. While the lift coefficient found ± 4.053 % for the plain wing and ± 6.438 % for the wing with winglets.

The calculated results of the total drag and lift coefficients will involve uncertainties due to fluctuation of errors. These uncertainties were obtained from the formula stated by (Beckwith et al., 2007).

$$U_R = \pm \sqrt{\sum_{i=1}^{n} \frac{\partial R}{\partial x_i} U_{x_i}} \qquad (19)$$

Where U_R is the uncertainty of the measured value R, and U_{x_i} is the uncertainty of a given variables x_i upon R is based.

3.7 Summary

This chapter discusses the research methodology that is carried out in four steps. In Phase 1, the research plans and methods are reviewed and our proposed model components are formulated. The proposed model is based on synthesized component extracted from earlier literature

review. The literature reviewed a number of salient themes, frameworks, models, architectures and approaches important for this study. From this review believed that, the problem of drag and lift on a moving aerodynamic airfoil with varying winglet geometry is very complex and occurs in multiple levels.

Ansys 14 Fluent Code, 3-D Foil Multi-Surface Simulations and numerical solution of an airfoil/ wing with different winglet geometry are studied in Phase 2.

In Phase 3, an experimental work to validate simulations, which comprises the design of symmetrical airfoil/plate object using a suitable material, dimensions, and tolerances, manufacture of object parts and assembly, preparation and installation of various instrumentation, calibration of instruments, testing of rig, experimentation and data recording, and analysis of experimental results are discussed.

Chapter 4

Results and Discussions

4.1 Research Results

4.2 Discussion of Results

4.3 Summary

Chapter 4

Results and Discussions

4.1 Research Results

4.1.1 Theoretical Results

The lift and drag coefficients results are calculated at 0^{o}, 5^{o}, and 10^{o} angles of attack. The total drag as discussed in Chapter 2 is a combination of: Parasite drag and induced drag. All the boundary conditions measured at sea level, ambient temperature and Reynolds Number $Re = 3.519\times10^{6}$ for free stream velocity of 50 m/s.

Reynolds numbers are used in airfoil design to determine "Scale Effect" when computing flow characteristics. Aerodynamics Reynolds number, Re, $Re = Vc/v$ .where V is the velocity, c is the chord length, and v is the kinematic viscosity of the air surroundings the airfoil, which is 1.460×10^{-5} m^2/s for the air at sea level.

By using 3-D Foil Multi-Surfaces and Solid Works codes, the final drawings for the two models as mentioned in Chapter 3 were obtained. For a constant airfoil NACA 4412, the plain wing is 9.57 m span and, 1 m chord, with the side angle of the winglets $\beta=65^{o}$. While the wing with winglets as seen from top (The reference area view) is 10.28m span, 1m chord, $\beta=65^{o}$, constant airfoil NACA 4412, the tip of the winglets airfoil is NACA 0012, and the length of the winglet is 0.379m for each side. Figure (4.1) shows the top view of both models. Both wings are merged in one view to simplify the dimensions of the original and designed models.

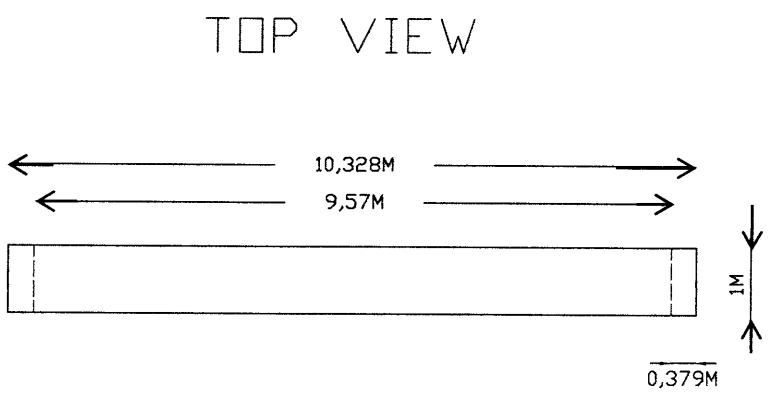


Figure (4.1) Top view for the plain Wing and the Wing with Winglets

In the front view, the plain wing with 9.57m span is seen. The winglets with the optimum side angle $\beta = 65^{o}$ as determined from 3-D Foil Multi-Surface code was added, but with a different winglets tip airfoil. Both wings have a constant maximum camber through all the geometry of 0.12m. Figure (4.2) shows the front view of the combined models.

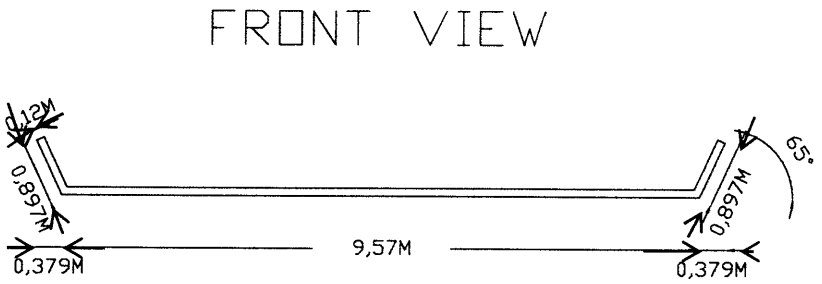


Figure (4.2) Front View for the Plain Wing and the Wing with Winglets

Tables (4.1) show the results of lift and drag coefficients versus angle of attack for plain wing using theoretical equations. C_L stands for the lift coefficient of the 3-D wing. While C_d presents the values of the profile drag, which are discussed in Chapter 1. C_{Di} is the value of the induced drag for the wing. The summation of all drag listed under C_D. These theoretical data are the base line in our thesis and uncertainty analysis as mentioned in appendix (A).

Table (4.1) Lift and Drag Coefficients versus Angle of Attack for Plain wing using Theoretical Relations

	C_L			C_d			C_{Di}			C_D		
Plain Wing	0^0	5^0	10^0	0^0	5^0	10^0	0^0	5^0	10^0	0^0	5^0	10^0
Theoretical Solution Results	0.357	0.863	1.368	0.0076	0.0112	0.0203	0.0047	0.0275	0.069	0.0123	0.0387	0.0894

Table (4.2) shows the results of lift and drag coefficients versus angle of attack for the designed wing with winglets using theoretical equations. All boundary conditions are exactly the same in both cases of theoretical calculations.

Table (4.2) Lift and Drag Coefficients versus Angle of Attack for Wing with Winglets using Theoretical Relations

	C_L			C_d			C_{Di}			C_D		
Wing with winglet	0^0	5^0	10^0	0^0	5^0	10^0	0^0	5^0	10^0	0^0	5^0	10^0
Theoretical Solution Results	0.364	0.880	1.395	0.0077	0.0115	0.0238	0.0043	0.0247	0.0590	0.01195	0.0362	0.0828

4.1.2 Numerical Results

4.1.2.1 3-D Foil Multi-Surfaces Code Results

The results of this code are based on the thin airfoil theory. Results of Plain Wing are listed in Table (4.3), while results of the Wing with Winglets are listed in Table (4.4). The results are for Figure (4.1) and Figure (4.2) which is given in section 4.1.1.

Table (4.3) Lift and drag coefficients versus angle of Attack for Plain Wing using 3-D Foil Multi-Surfaces Code

	C_L			C_d			C_{Di}			C_D		
Plain Wing	0^0	5^0	10^0	0^0	5^0	10^0	0^0	5^0	10^0	0^0	5^0	10^0
3D Foil Multi-Surfaces Code Solution Results	0.255	0.679	1.1	0.0075	0.0073	0.0110	0.0023	0.0154	0.040	0.0098	0.0227	0.0510

Table (4.4) Lift and Drag Coefficients versus Angle of Attack for Wing with Winglets wing using 3-D Foil Multi-Surfaces Code

	C_L			C_d			C_{Di}			C_D		
Wing with winglet NACA4412	0^0	5^0	10^0	0^0	5^0	10^0	0^0	5^0	10^0	0^0	5^0	10^0
3D Foil Multi-Surfaces Code Solution Results	0.246	0.660	1.07	0.0075	0.0073	0.011	0.0020	0.0141	0.0369	0.00945	0.0214	0.0477

4.1.2.2 Fluent Ansys 14 Results

The results of Ansys 14 are detailed and very close to the theoretical results. Flow direction and vortices are monitored as well as drag and lift coefficients results.

1. Lift and Drag Coefficients

The convergence of the solution is the sign for stable and précised results for both of drag and lift coefficients. The convergence could not got due to many reasons, like the shape of wings and boundary conditions. Figure (4.3) illustrates the drag coefficient iterations. Noticed that the solution stabilized after 50 iterations, but did not reach convergence accuracy which is set at (10^{-6}).

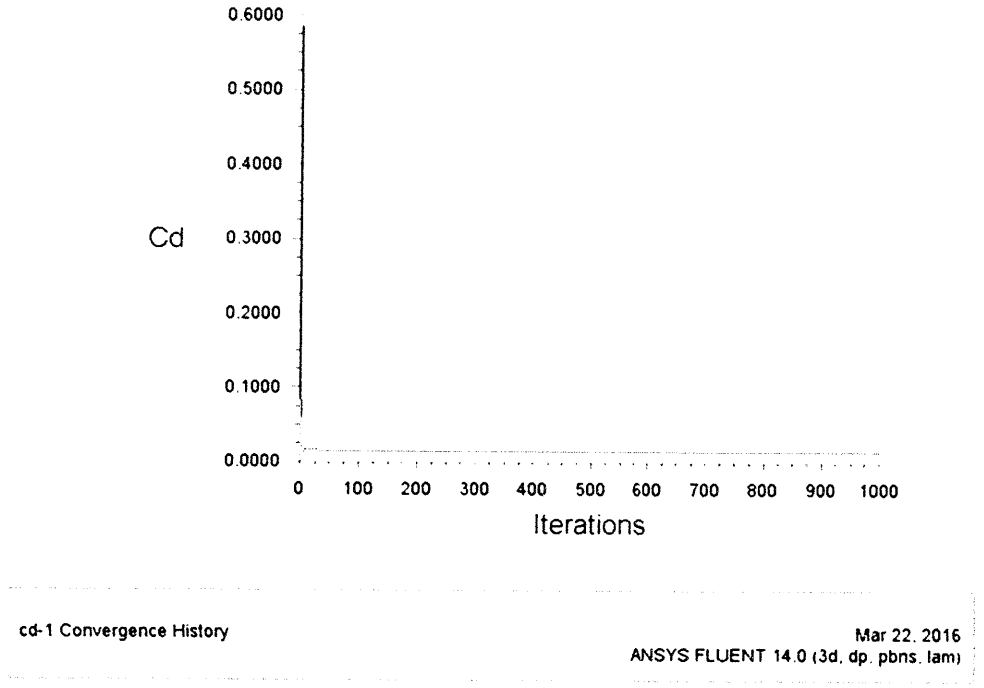


Figure (4.3) Plain Wing Drag Coefficient at 1000 Iterations at Zero Degree Angle of Attack

The lift coefficient needed 150 iterations to reach stabilization point. Figure (4.4) shows the iterations of the lift coefficient of the plain wing at zero degree angle of attack.

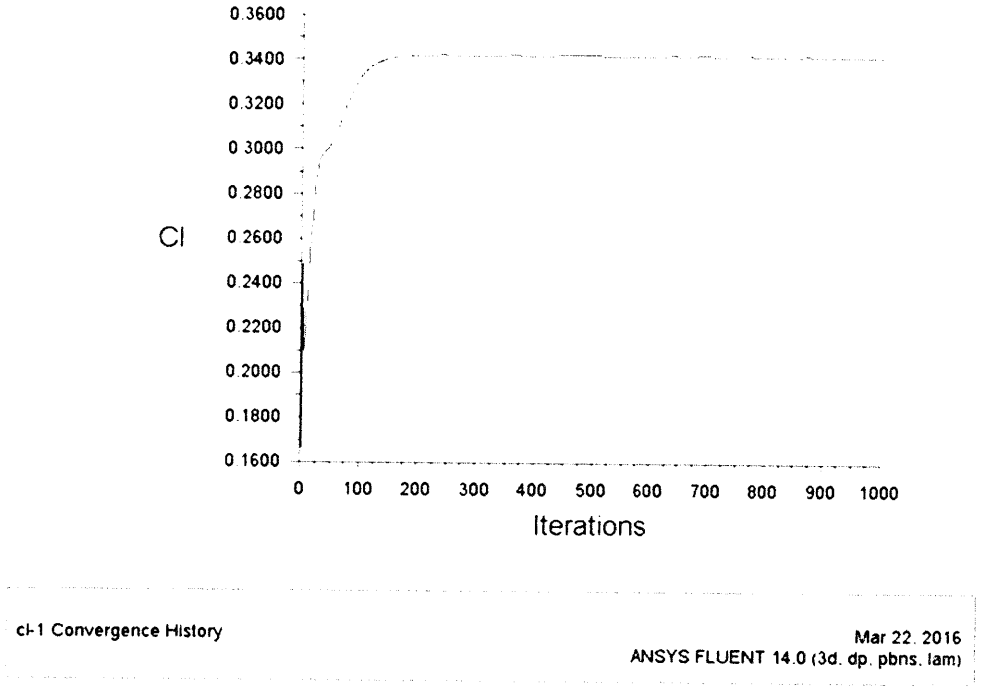


Figure (4.4) Plain Wing Lift Coefficient at 1000 Iterations at Zero Degree angle of Attack

Fluent Ansys 14 have been operated separately with different settings as mentioned in Chapter 3 for each of the plain wing and wing with winglets. All parameters and boundary conditions remained the same except the angle of attacks. Angles of attack of 0°, 5° and 10° have been changed in each solution script data. Table (4.5) and Table (4.6) show these results.

Table (4.5) Lift and Drag Coefficients versus angle of Attack for Plain Wing using Fluent Ansys 14 Code

	C_L			C_d			C_{Di}			C_D		
	0^0	5^0	10^0	0^0	5^0	10^0	0^0	5^0	10^0	0^0	5^0	10^0
Plain Wing	0.342	0.768	1.165	0.0075	0.0100	0.0240	0.0069	0.0229	0.0457	0.0144	0.0329	0.0697

Table (4.6) Lift and Drag Coefficients versus Angle of Attack for Wing with Winglets using Fluent Ansys 14 Code

	C_L			C_d			C_{Di}			C_D		
	0^0	5^0	10^0	0^0	5^0	10^0	0^0	5^0	10^0	0^0	5^0	10^0
Wing with winglet	0.329	0.747	1.333	0.0075	0.0101	0.0180	0.0067	0.0219	0.0492	0.0142	0.0318	0.0673

2. Static , Total Pressure, and Velocity Results

Static and total pressures contours are shown in Figure (4.4) (a,b) and Figure (4.5) (a,b) for plain wing and wing with winglets at angle of attack $\alpha = 0^o$ and $\alpha = 10^o$ respectively.

It is noticed that the pressures are affected by the wings geometry at different angles of attack. The plain wing is affected more than the designed wing with winglets with an increase in the angle of attack from $\alpha = 0^o$ to $\alpha = 10^o$ as shown in the Figures (4.5) and (4.6). These phenomena will be explained in the discussions. The velocity contour results at $\alpha = 10^o$ for both geometries are shown in Figure (4.7) (a, b). It is noticed that the velocity values decrease when winglets are used, thus leading to a reduction in the induced drag. This will be further discussed in the discussions section.

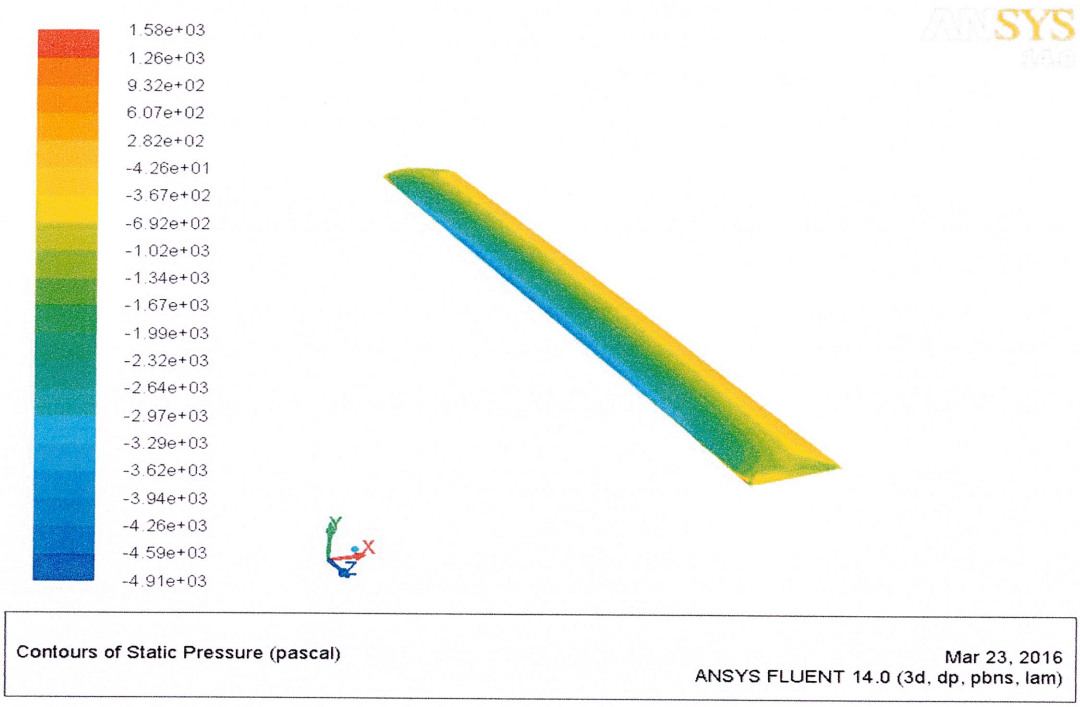


Figure (4.5) (a) Static Pressure Contours for Plain Wing

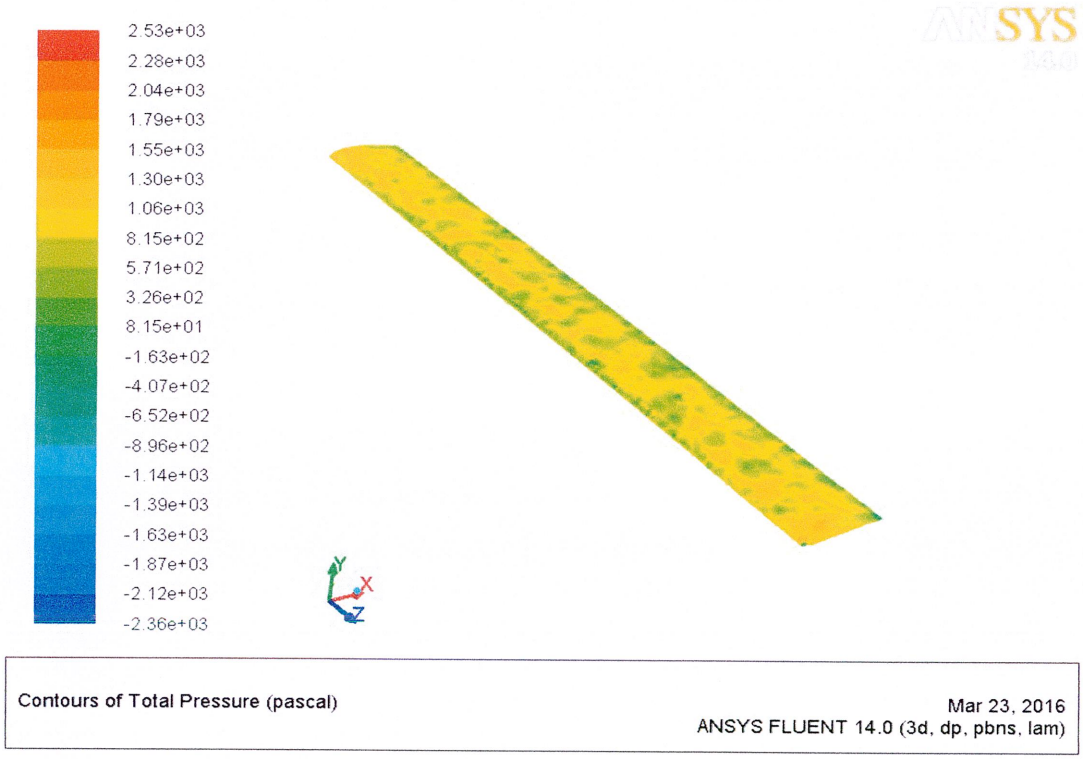


Figure (4.5) (b) Total Pressure Contours for Plain Wing

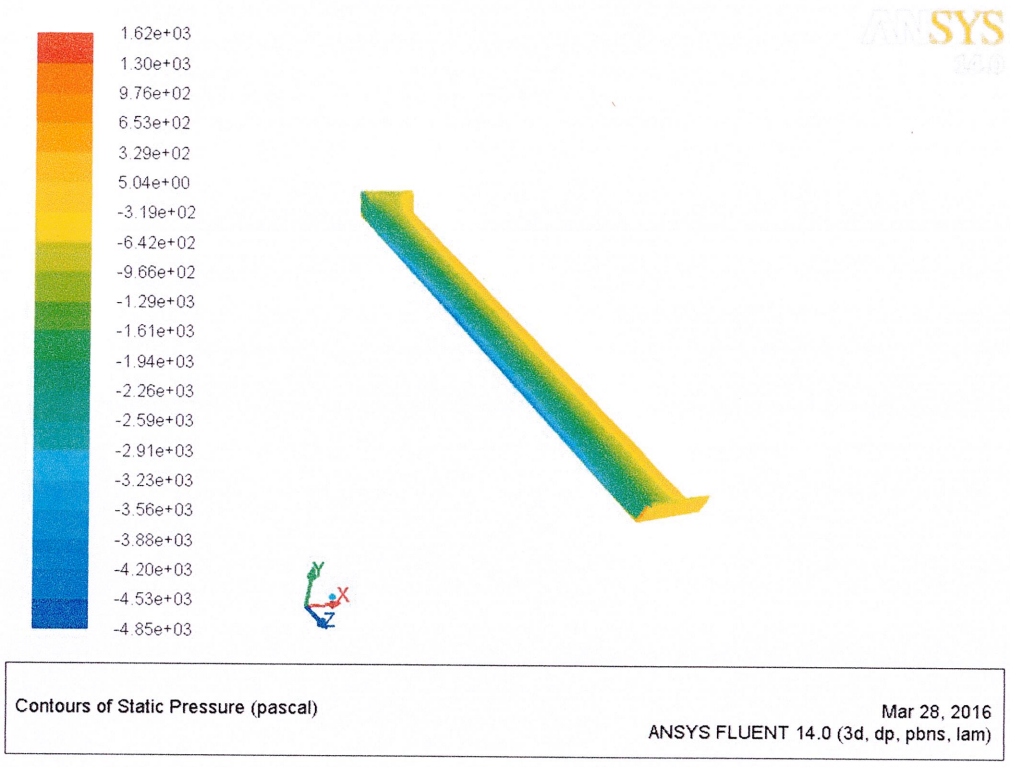


Figure (4.6) (a) Static Pressure Contours for Wing with Winglets

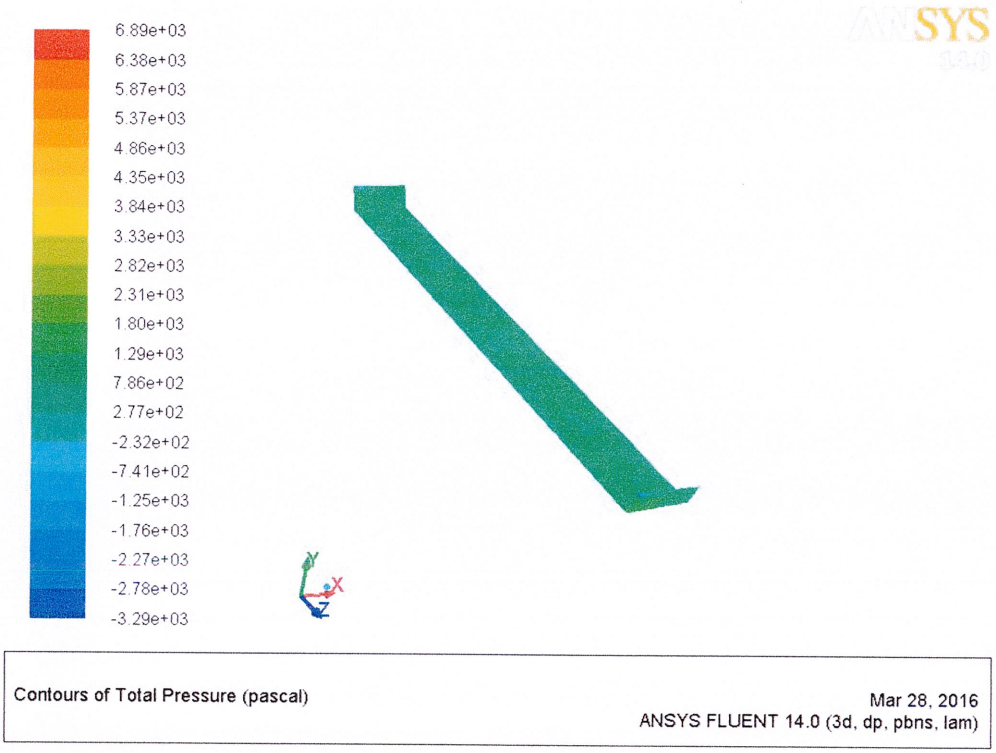


Figure (4.6) (b) Total Pressure Contours for Wing with Winglets

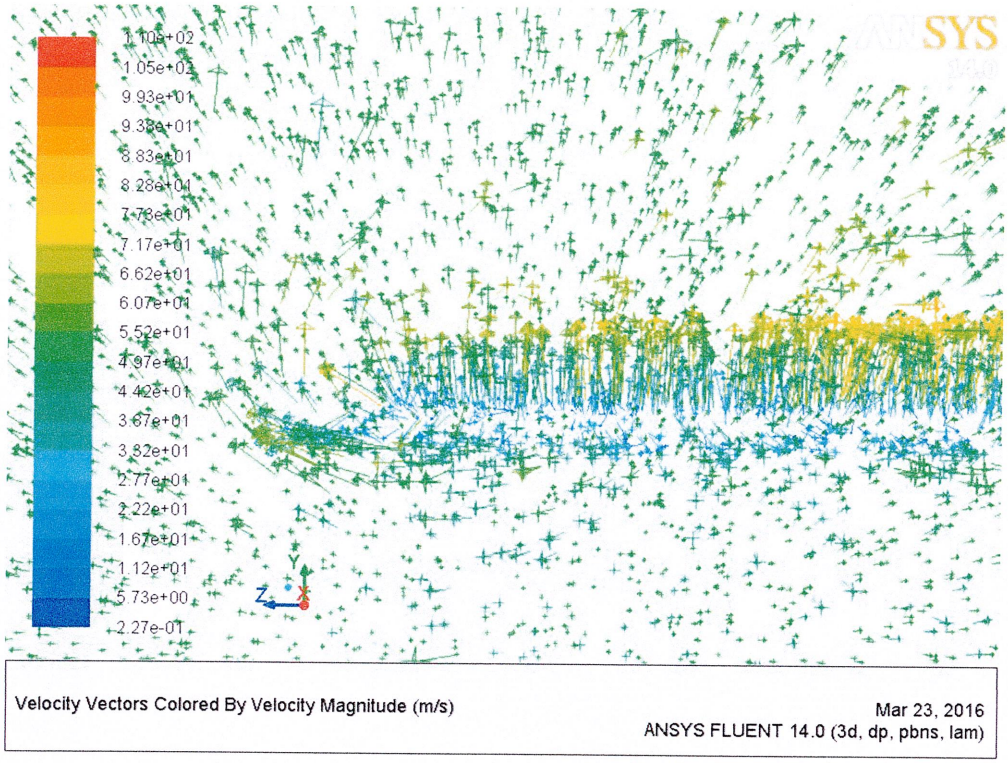


Figure (4.7) (a) Velocity Vectors for Plain Wing at α=10°

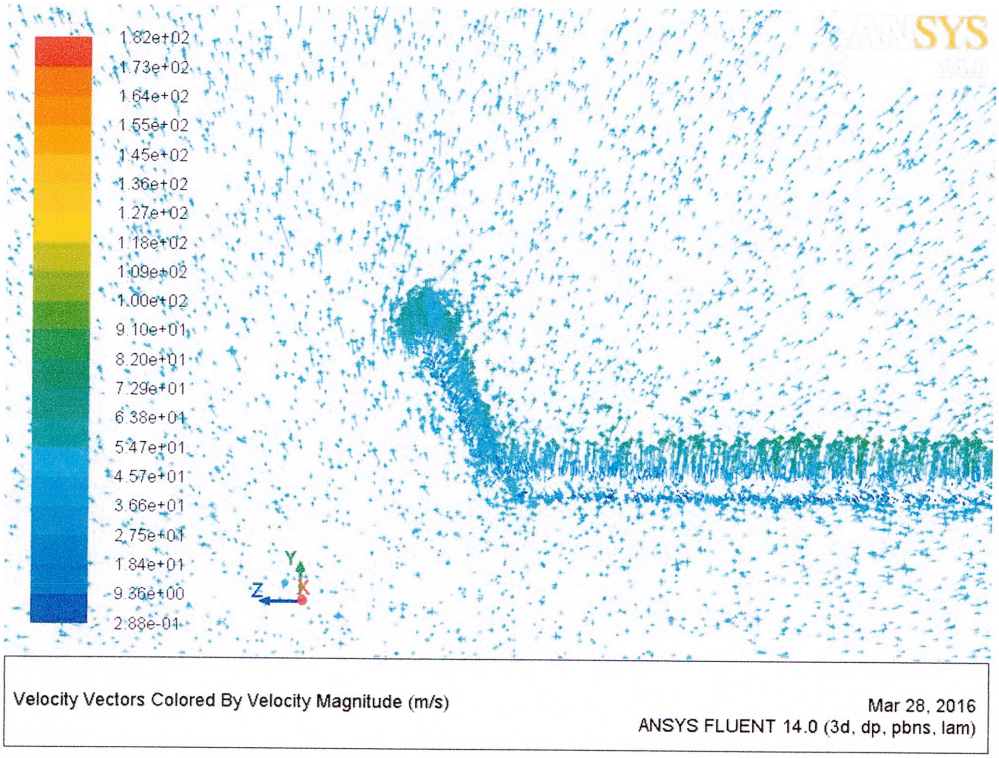


Figure (4.7) (b) Velocity Vectors for Wing with Winglets at α=10°

4.1.3 Experimental Results

The experimental results are varied in each experiment. The wind tunnel is run for the plain wing model and repeated it for 6 times. The best result assumed to be the second trail because of the model stabilization during the experiment and the results also was very close to theoretical and numerical results. For the wing with winglet model, it was easier to get the model stabilized and that obviously due to the winglets effect. But the results were little far from the obtained theoretical and numerical results. That is explained by the nature of the 2-D wind tunnel used and the wind tunnel walls effect on the complex shape of the winglets. But still accepted results obtained after ten trails. The optimum result was the sixth trail results.

1:100 scaling factor is used in processing all the results. Table (4.7) shows the experimental results for the plain wing and wing with winglets.

Table (4.7) Lift and Drag Coefficients versus Angle of Attack for Plain wing and wing with winglets using Wind Tunnel C-15

	C_L			C_d			C_{Di}			C_D		
	0^0	5^0	10^0	0^0	5^0	10^0	0^0	5^0	10^0	0^0	5^0	10^0
Plain wing	0.249	0.587	0.805	0.006	0.013	0.016	0.004	0.019	0.036	0.011	0.032	0.052
Wing with winglets	0.256	0.581	0.917	0.007	0.008	0.018	0.003	0.017	0.031	0.010	0.025	0.049

The maximum air speed was approximately 30 m/s, so the calculations done again with flow parameters are slightly different from

the numerical and theoretical work. Flow parameters corrections were done and results recalculated with the same input parameters and boundary conditions of both numerical and theoretical work to get the final results.

4.2 Discussion of Results

4.2.1 Induced Drag and Lift to Drag Ratios Comparisons

The comparison of the results between plain wing and the designed wing with winglets is divided into two main sectors:

1- The Induced Drag Comparison: One of the objectives in this study is to decrease the amount of the induced drag, which is set as the main objective in chapters 1 and 2. The Induced drag is noticeably decreased in the designed wing with winglets in comparison to the original plain wing for numerical methods work, and experimental work as shown in Figure (4.8) and Figure (4.9) against the angles of attack.

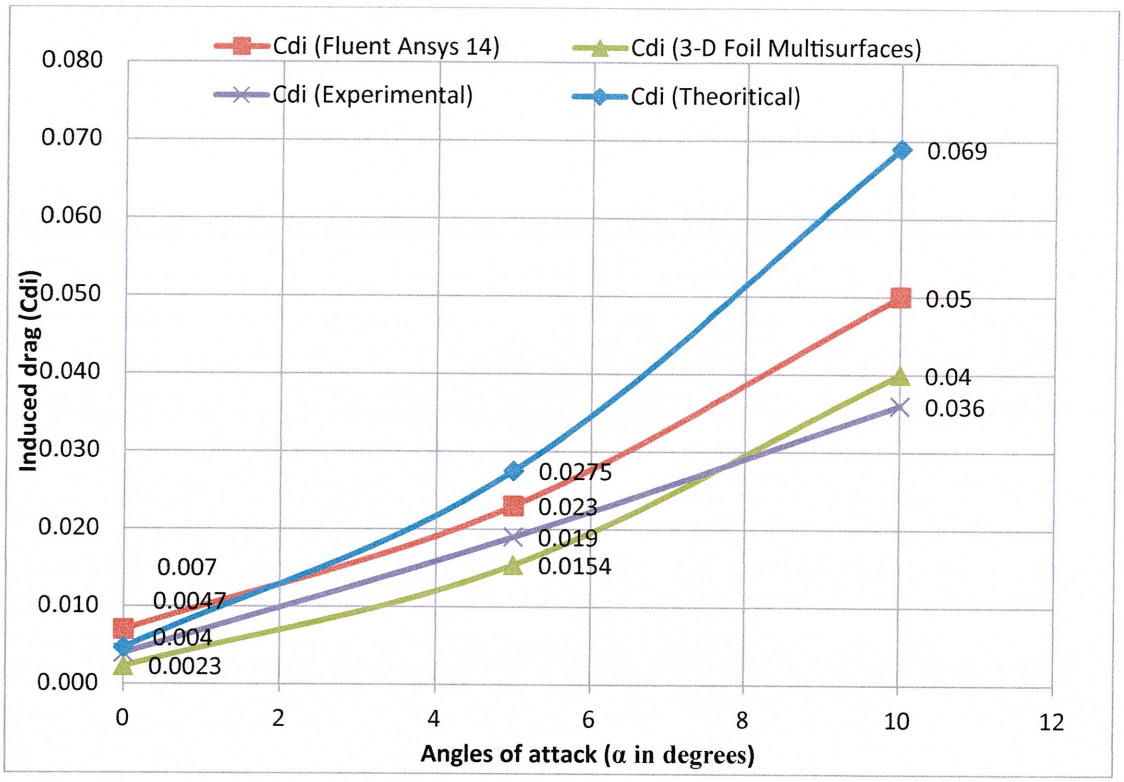


Figure (4.8) Induced Drag (C_{Di}) Comparison for Plain Wing at different Angles of Attack

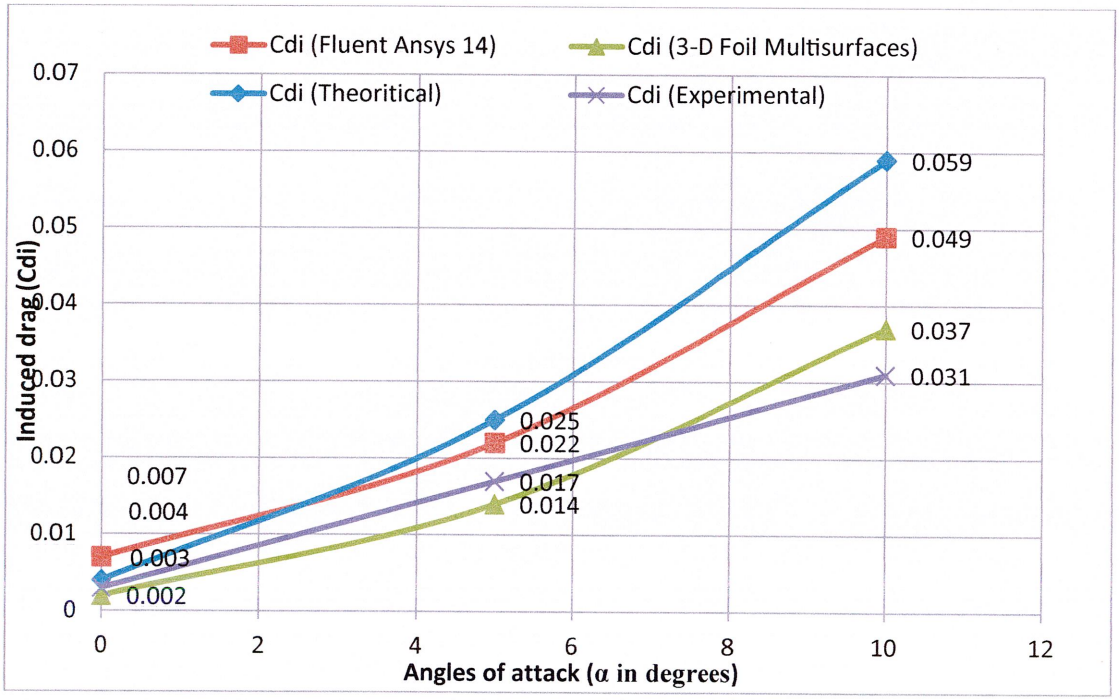


Figure (4.9) Induced Drag (C_{Di}) Comparison for Wing with Winglets at different Angles of Attack

The overall results shows that the induced drag values successfully decreased in all solutions between 0 % as minimum change in Fluent Ansys 14 result and 25 % as maximum change in the experimental results for 0^{o} angle of attack. Then the results varied, but still with decrease in induced drag for 5^{o} angle of attack between minimum change of 9% in 3-D Foil Multi-Surfaces results and maximum of 20 % in Fluent Ansys 14 results. Finally, for 10^{o} angle of attack the results of induced drag decreased between minimum of 2 % for Fluent Ansys 14 and maximum of 14.5 % in the theoretical results. The percentage difference in induced drag between plain wing and wing with winglets results for all four verification methods in the different angles of attack are shown in Table (4.8).

Table (4.8) The Percentage Difference in Induced Drag between Plain Wing and Wing with Winglets Results for all four Verification Methods at Different Angles of Attack

α / The method	0^{o}	5^{o}	10^{o}
Theoretical	**-14.9 %**	**-9.1 %**	**-14.5 %**
Fluent Ansys 14	**0 %**	**-20 %**	**-2 %**
3-D Foil Multi-Surfaces	**-13 %**	**-9 %**	**-7.5 %**
Experimental	**-25 %**	**-11 %**	**-13.9 %**

The designed winglets improved the aerodynamic characteristics of the wing by decreasing the induced drag values at different angles of attack.

2- The Lift to Drag Ratio Comparison: The second main objective of our study is to show that the winglets design has a significant effect in improving the lift to drag ratio. This ratio has increased especially at high angles of attack due to the reduction of the amount of the induced drag, which allow the total drag coefficient to decrease and the lift coefficient to increase at the same time. Different results obtained from each working method. Those results for plain wing are shown in the graphs presented in Figure (4.10) and the designed wing with winglets results are given in Figure (4.11).

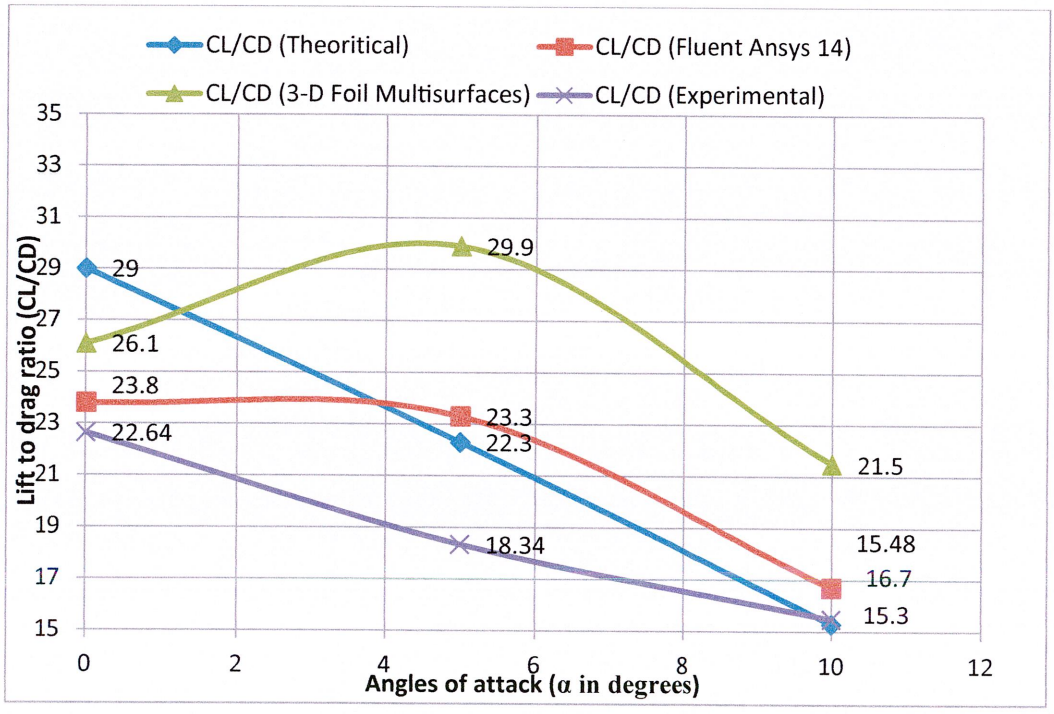


Figure (4.10) Lift to Drag Ratio (C_L/C_D) Comparison for Plain Wing at Different Angles of Attack

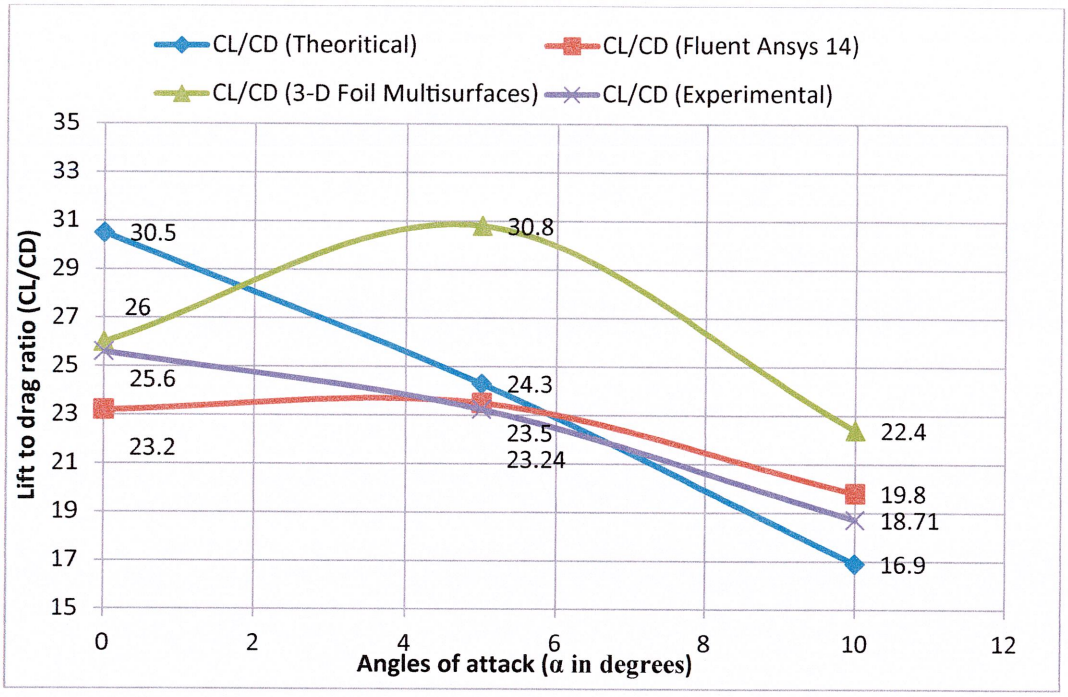


Figure (4.11) Lift to Drag Ratio (C_L/C_D) Comparison for Wing with Winglets at Different Angles of Attack

From the previous figures the results show that at 0^o angle of attack, the maximum improvement of the lift to drag ratio is 13.1 % in the winglet model experimental results, while this ratio decreases to 2.5 % using Fluent 14 simulation. This is due to addition of winglets in the wing's geometry which increases the parasite drag and thus the total drag that leads to an increase in the lift to drag ratio. At higher angles of attack, the effect of the induced drag become obvious due to aerodynamic characteristics as explained in Chapter 2. Table (4.9) illustrates the percentage difference in lift to drag ratio between plain wing and wing with winglets results for all four verification methods at different angles of attack. At $\alpha>0$, all methods show an increase in the C_L/C_D ratio for the use of winglet geometry in the wing.

Table (4.9) The Percentage Difference in Lift to Drag Ratio between Plain Wing and Wing with Winglets Results for all Four Verification Methods at different Angles of Attack

α / The Method	0^o	5^o	10^o
Theoretical	**+5.1 %**	**+9 %**	**+10.5 %**
Fluent Ansys 14	**-2.5 %**	**+0.9 %**	**+18.6 %**
3-D Foil Multi-Surfaces	**-0.4 %**	**+3 %**	**+4.2 %**
Experimental	**+13.1 %**	**+26.7 %**	**+12 %**

4.2.2 Flow Characteristics Comparison

When a wing produces lift, the pressure difference between the upper and lower sides of the wing generates a vortex. Near the ends of a wing, the high pressure air on the underside tends to slip off the ends and rounded to the side of low pressure forming wing tip vortices. Generally, in aviation, the intensity of this vortex is considered very dangerous for air traffic and its dissipation is estimated to average two minutes (Daniel, 1989). This time interval is considered as an interval between two takeoffs or two landings. So the vortices are considered a significant factor in the design of airplanes.

In Fluent Ansys 14, after the solution is processed, it is noticed that the 3-D shape of the velocity vectors which best describes the air molecules around the wings. As we started the calculations with the plain wing in the three angles of attack 5^o, 10^o, and 15^o at velocity magnitude of 50 m/s, it is clearly observed how the air circulates around the wing's tip forming wing tip vortices. Those vortices has unfavorable effect as

discussed in Chapter 2 which spoil the lift around the wing tips area and may extends further more to nearly 30 % of the total wings area (Allen, 1981). Also, it creates a resistance which is called induced drag or drag due to lift. The resultant of these phenomena is decreasing the efficiency and the overall lift to drag ratio with a major flight safety concern of losing the stability and even the maneuverability especially at high angles of attacks. Figure (4.11) simulates the real flow pattern around the plain wing tips at 10^{o} angle of attack. The flow is clearly seen circulating around the wing's tip from the high pressure region to the low pressure region.

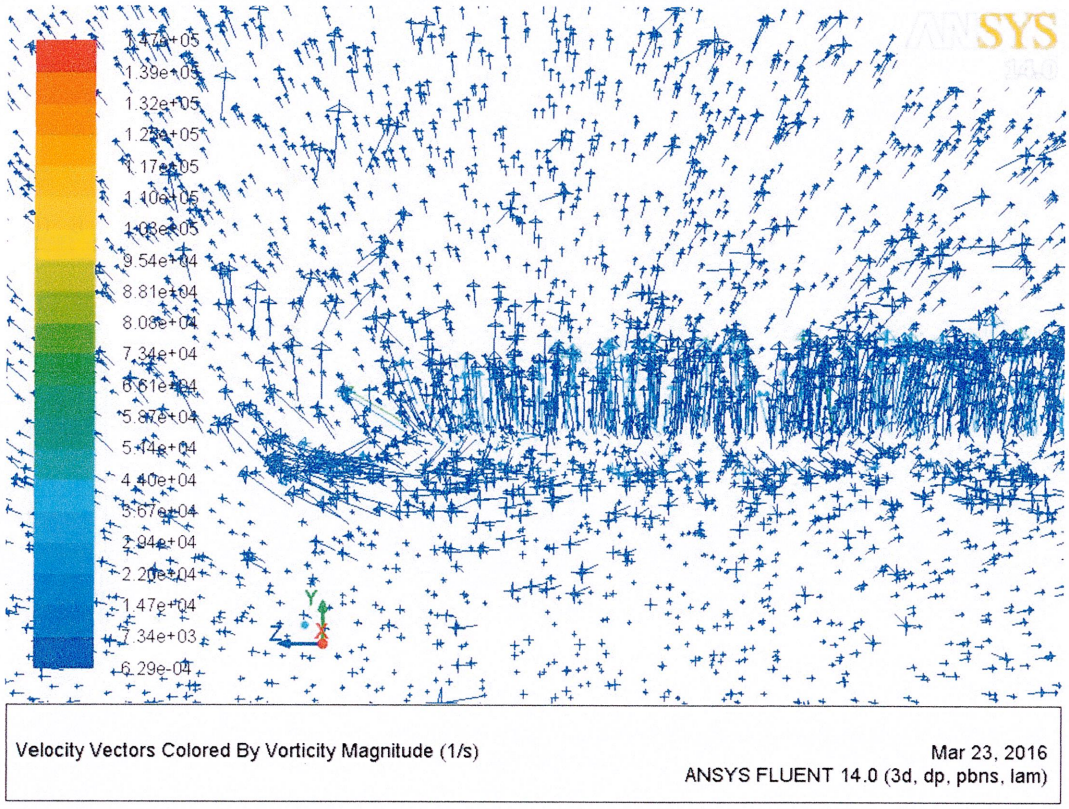


Figure (4.12) Plain Wing Velocity Vectors at 10^{o} Angle of Attack

After processing the solution of the designed wing with winglets in Fluent Ansys 14, it is shown that the flow characteristics of the wing will

be improved after applying the winglets with the optimum winglet's geometry as discussed in Chapter 3. The vortices are shifted to the edge of the winglet as seen in Figure (4.12). This shift moves all the vortices to the winglets instead of the wing tips. Because of this effect, the stability and maneuverability increase at high angles of attack. The Induced drag decreases due to that as well as the lift to drag ratio increases. The tip vortices in this case will not spoil the lift on the wing tips and the resistance will decrease. The fuel consumption then will decrease also. Figure (4.13) shows the particles pathlines simulation around the wing's tip at 10^{o} angle of attack.

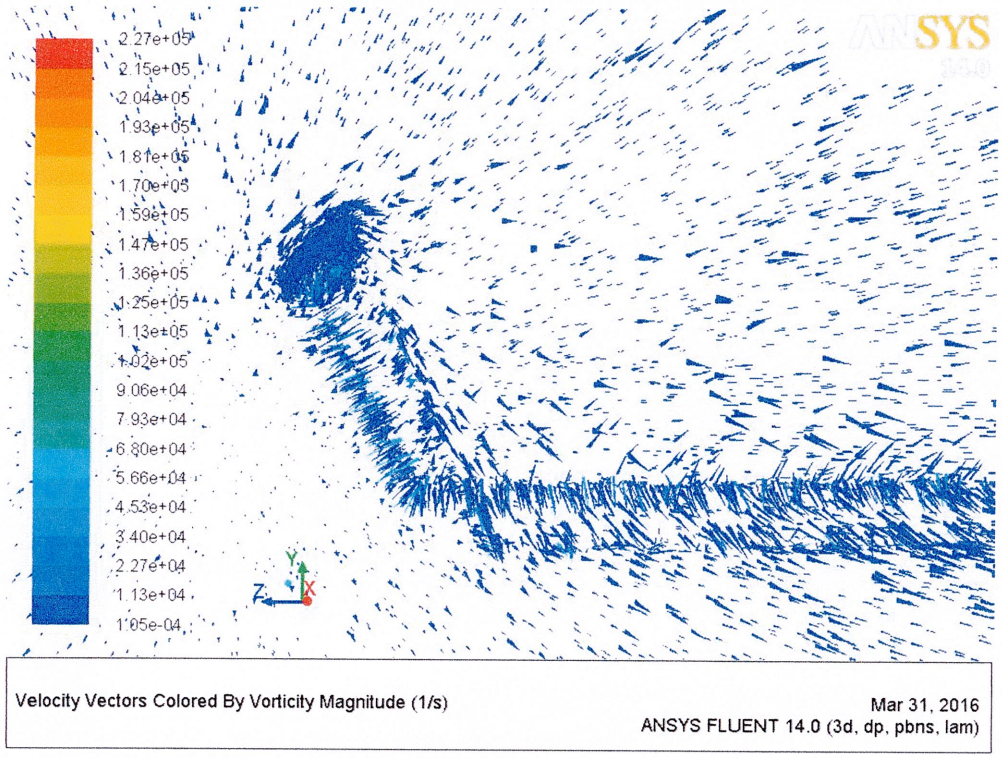


Figure (4.13) Wing with Winglets Velocity Vectors at 10^{o} Angle of Attack

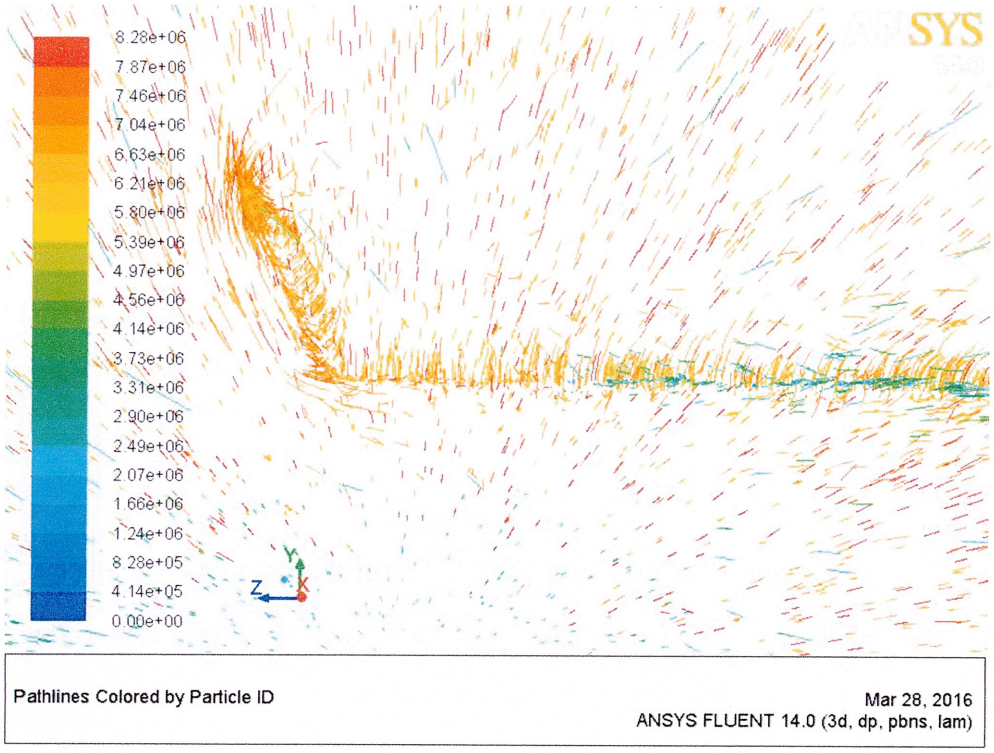


Figure (4.14) Wing with Winglets Pathlines at 10° Angle of Attack

4.2.3 Wing's Pressure Comparison

The total pressure of the wing is a major factor in all aerodynamics studies. As discussed in Chapter 2, the airfoil shape of the wing's cross section divides the pressure into two separate zones: The lower surface of the wing is a high pressure zone, and the upper surface of the wing is a low pressure zone. The difference in the pressure between these zones creates the lift. In the chord's direction (the 2-D direction) it is noticed that the major effect of the winglets is smoothing the pressure gradient on both airfoil surfaces. As seen in Figure (4.14), the lower surface of the plain wing airfoil has significant fluctuations increased at the leading and trailing edges. In Figure (4.15), for wing with winglets both airfoil surfaces show stabilization in the pressures. This stabilization will allow getting the maximum benefit of the pressure difference to generate the lift. This phenomenon is more noticeable at the upper airfoil surface.

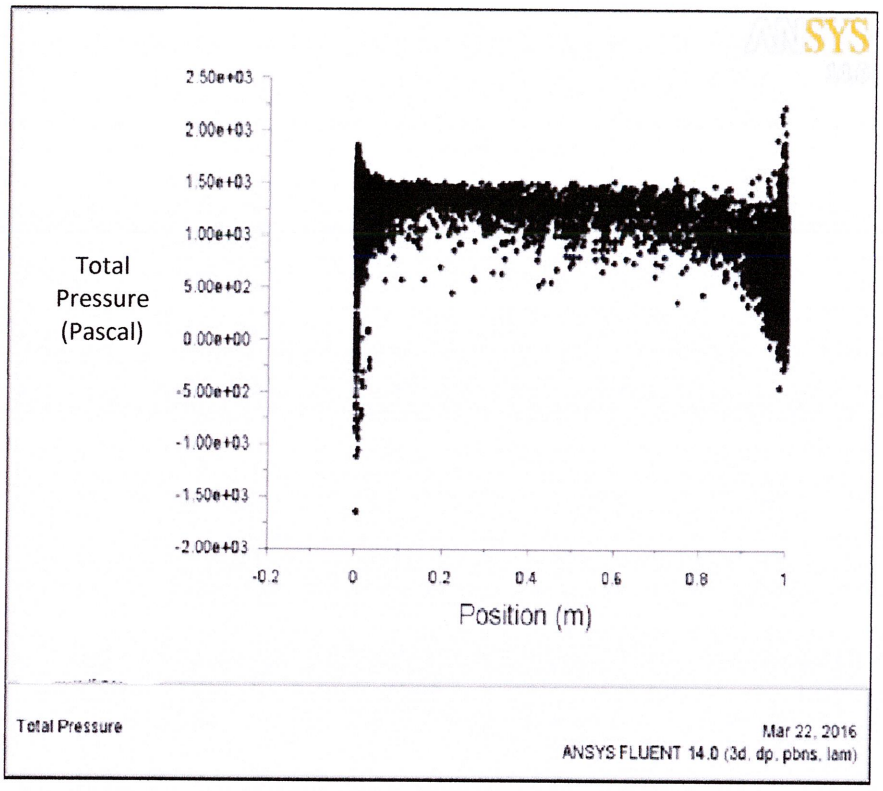


Figure (4.15) Plain Wing Chord's Direction Total Pressure

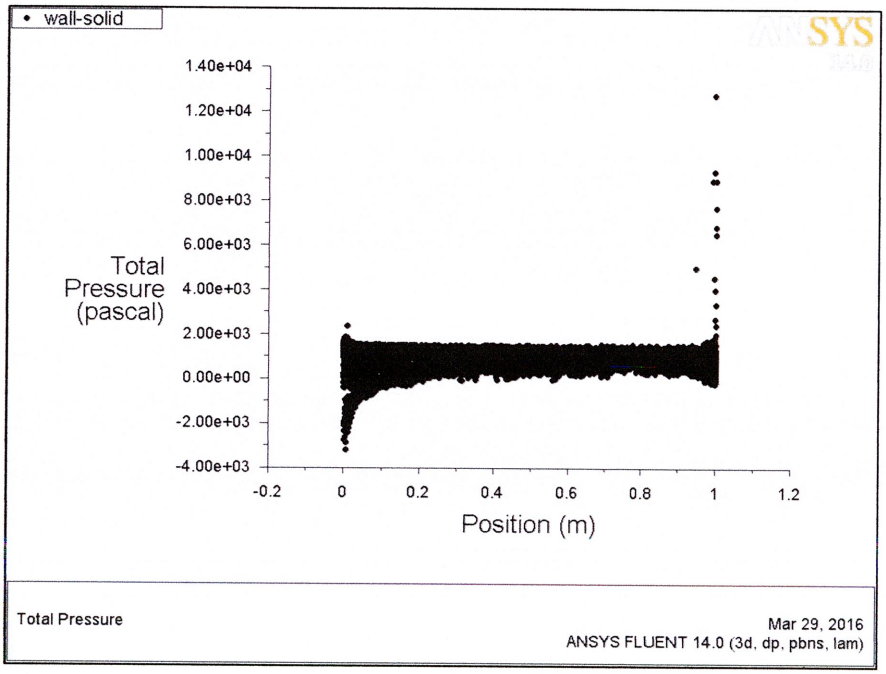


Figure (4.16) Wing with Winglets Chord's Direction Total Pressure

When the total pressure is observed for the plain wing in 3-D view as seen from frontal view in Figure (4.17), the pressure distribution in wing span direction is almost constant from the tip to tip for the plain wing. The 3-D shape of the plain wing shows 246 PSI (1.7 MPa) difference between the upper and lower wing's surfaces. While in Figure (4.18) the pressure difference between upper and lower surfaces for the wing with winglets reaches 290 PSI (2 MPa). This increment in pressure difference means that the lift force generated by wing in the case of wing with winglets is bigger and will result in increasing the lift to drag ratio.

The difference in total pressure at the wing's tips for the wing with winglets is 725 PSI (5 MPa), but in the plain wing wing's tips is only 363 PSI (2.5 MPa). This can be explained by the effect of the winglets as they decrease the wing tip vortices from circulation around the wing's tip. This phenomenon generates high pressure difference between upper and lower tips. This high pressure difference increases the stability of the wing as a new benefit from the winglets design.

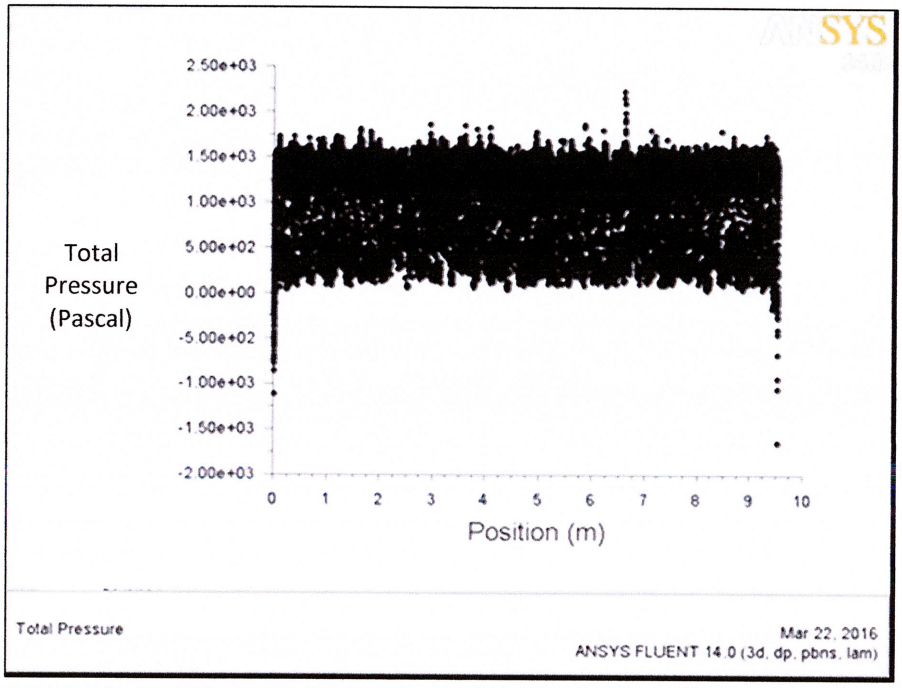


Figure (4.17) Plain Wing's Wing span Direction Total Pressure

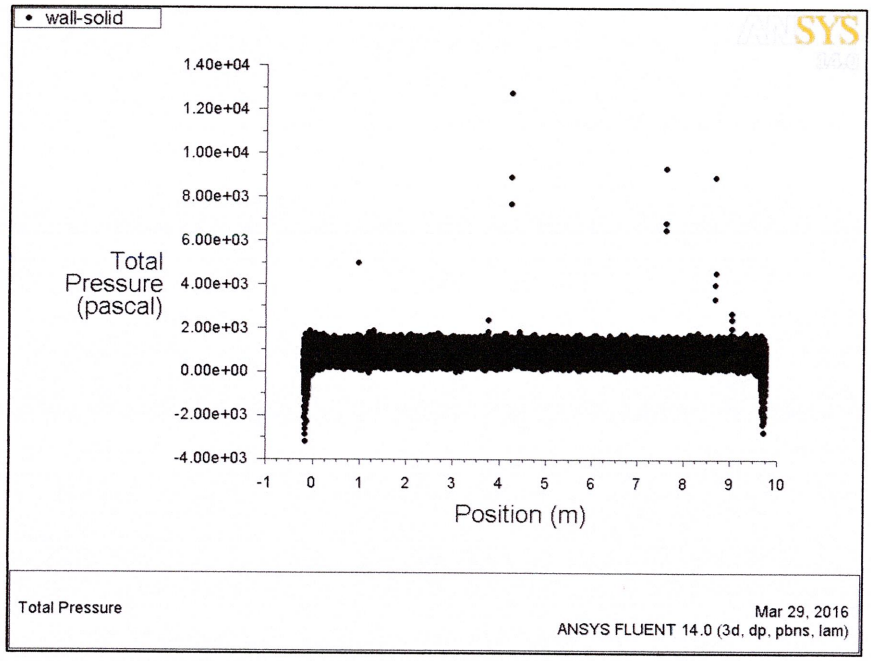


Figure (4.18) Wing with Winglet's Wing Span Direction Total Pressure

4.3 Economical Study

By installing the optimized geometry on the plane, a formidable increase in C_L / C_D has been achieved. Calculations show an increase in flight range equal to 4.96% as calculated from the next formula.

$$Range = V_{t_f} = V \times (\frac{L}{D}) \times I_{sp} \times In(\frac{W_i}{W_f}) \quad (20)$$

where I_{sp} is the overall efficiency, W_i is the initial weight. If W_f is the final weight of vehicle and $t_{initial}$ = 0, the relation between vehicle parameters and flight time, t_f is given by the previous equation also. The above equation is known as the Breguet range equation. It shows the influence of aircraft, propulsion system, and structural design parameters. No changes were observed in pitch stability and stalling. As a first step, a combination of winglet airfoil, chord, height, and cant angle was enough for achieving the initial goals. However, the configuration can be further

improved, as the effect of some parameters, such as toe angle and sweep angle, was not examined.

As the lift to drag ratio $(\frac{L}{D})$ is obtained from our theoretical calculation for lift and drag coefficients at steady level flight of cruise speed of 185 *km/h*, sea level flow parameters. The lift force and drag force equation are:

$$L = \frac{1}{2}\rho V^2 A C_L \tag{21}$$

For plain wing

$$L = 0.5 \times 1.202 \times (51.39)^2 \times 9.528 \times 0.357 = 5398.86\ N$$

For wing with winglets

$$L = 0.5 \times 1.202 \times (51.39)^2 \times 10.328 \times 0.364 = 5966.91\ N$$

$$D = \frac{1}{2}\rho V^2 A C_D \tag{22}$$

For plain wing

$$D = 0.5 \times 1.202 \times (51.39)^2 \times 9.528 \times 0.0123 = 186.01\ N$$

For wing with winglets

$$D = 0.5 \times 1.202 \times (51.39)^2 \times 10.328 \times 0.01195 = 195.89\ N$$

For plain wing, the lift to drag ratio is:

$$\left(\frac{L}{D}\right) = \frac{5398.86}{186.01} = 29.02$$

For wing with winglets, the lift to drag ratio is:

$$\left(\frac{L}{D}\right) = \frac{5966.91}{195.89} = 30.46$$

The initial weight (*Wi*) of the air craft is 600 *kg*, and the fuel capacity is 120.15 *kg*. If considered that landing with minimum of 10 % remaining fuel, the final weight (W_f) will be 491.9 *kg*. The engine overall efficiency I_{sp} is assumed to be 100%, as assumed by manufacturers, therefore the plain wing range will be 1066.5 *km*. And for the wing with winglets, the range is 1119.4 *km*. The resultant increment in the range is 4.96% which can be considered beneficial.

4.4 Summary

The induced drag and lift to drag ratio for both wing with and without winglets are plotted against the different angles of attack. It could be seen from Table (4.8), decrement in drag for the aircraft with winglets is found to be less but of considerable amount for $\alpha=0^{\circ}$. The induced drag reduction observed from the calculation is about 2-14.5 % during the take-off where the contribution of induced drag is very high. The induced drag and the total drag are calculated for different velocities. Based on the calculation, the induced drag at $\alpha=10^{\circ}$ and the percentage of induced drag was calculated. The contribution of the induced drag in total drag is found to be more than 60% when the velocity is given around 50m/s. As the velocity increases the percentage of induced drag is observed to decrease to less than 20% at the velocity of 250 m/s. The result shows that the effect of induced drag would be much higher during the take-off condition and at lesser effect during cruise condition.

The results obtained after the analysis show that the winglet model gives better performance. The C_L coefficients obtained for the wing with winglet are less than those of the plain one at all angles of attack. The best C_L is obtained when the winglet is kept at 10° angle of attack. This

behavior of the lift coefficients can be explained by contribution of induced drag. As known the drag and lift coefficients are depending in each other as listed in Equations (8, 9) in Chapter 3. The induced drag coefficient increases in the plain wing making the lift coefficient increases slightly too. But in the wing with winglets the induced drag decreases and those results in minor lift coefficient decrement.

The C_D coefficients for the wing with winglet are always less than those of the plain one at all angles of attack. The best CD is obtained when the winglet is kept at 10° angle of attack. This is obviously due to the effect of the winglets in eliminating the induced drag effect.

The big decrement in induced drag combined with slight decrement in lift coefficient results in general total lift to drag ratio increment especially at low velocities and high angles of attacks.

Chapter 5

Conclusions and Recommendations

5.1 Conclusions

5.2 Recommendations

Chapter 5

Conclusions and Recommendations

5.1 Conclusions

Experimental as well as numerical works have been performed to examine the efficiency of winglets mounted on an airfoil in subsonic flows. The winglets that are considered here are placed upward at the tip of the wing in order to improve the wing efficiency; decreasing the induced drag and increasing the lift to drag ratio.

Ansys CFD simulation shows that mounting a simple winglet at the tip of the aircraft wing can reduce the induced drag significantly that is always desired. Though this theoretical concept was established by the flow simulation over the same model aircraft wing when one of them was equipped with a winglet at the wing tip and another one is not. Results obtained from flow simulation describe here that, if angle of attack, thermodynamics and other parameters are being kept constant then a conventional aircraft wing having winglet will significantly generate less induced drag compared to other conventional aircraft wing having no winglet. This can be considered as a great achievement from an aerodynamic point of view.

The main results achieved in this study can be listed in the follow points:

1. The theoretical work shows that decrement in the values of induced drag for our designed wing with winglets by 14.9 % at 0^{o} angle of attack, 9.1 % at 5^{o} angle of attack, and 14.5 % at 10^{0}

angle of attack. The values of the lift to drag ratio increased by 5.1 % at 0^{o} angle of attack, 9 % at 5^{o} angle of attack, and 10.5 % at 10^{0} angle of attack.

2. The Numerical work was performed using two different codes. Fluent Ansys 14 verified our results by the most realistic values in simulating the plain wing and wing with winglets. The values of induced drag for the designed wing with winglets decreased 20 % at 5^{o} angle of attack and decreased by only 2 % at 10^{0} angle of attack, but remained constant at 0^{o} angle of attack. The lift to drag ratio decreased by 2.5 % at 0^{o} angle of attack but increased at 5^{o} angle of attack by 0.9 %, and increased again 10^{0} angle of attack by 18.6 %.

3. The other numerical verification method is 3-D Foil Multi-Surfaces Code. In this code, the results are simplified by the developers but still considerable. The values of the induced drag are also decreased 13 % at 0^{o} angle of attack, 9 % at 5^{o} angle of attack and 7.5 % at 10^{0} angle of attack. The lift to drag ratio at 0^{o} angle of attack decreased also in this method by 0.4 % but returned to increase by 3 % at 5^{o} angle of attack and 4.2 % at 10^{o} angle of attack.

4. The experimental verification confirmed that the winglets as designed in our investigations reduce the induced drag and increases the lift to drag ratio. The 2-D wind tunnel adjusted to give the readings at the point exposed to the severest effect of wing tip vortices. So the results may notice little far from other verification methods. The induced drag at 0^{o} angle of attack was reduced by25 % in the designed wing compared to the original

plain wing, reduced by 11 % at 5^{o} angle of attack and reduced by 13.9 % at 10^{o} angle of attack. Moreover, the lift to drag ratio improved in the designed wing. The value increased by 13.1 %, 26.7 % and 12 % for the same angles of attack respectively.

5. The stability and maneuverability improved in our designed wing with winglets. This is noticeable at high angles of attack at low speeds. This presents the condition in take-off, where the induced drag contributes by nearly 80-90 % of the total drag ratio (Kroo, 2005). This benefit emphasizes the safety required for this type of aircraft under study.

6. As a result of decreasing the induced drag and increasing the lift to drag ratio, the resultant increment in the range is 4.96%. This will add a benefit to the ALS aircraft which is mainly owned by its users because it is an economical aircraft.

There are many differences between the four verification methods results used due to several reasons:

a- The human error is somewhat high in the experimental part, in addition to the quality and calibration of the wind tunnel as well. It is observed that the induced drag at 0^{o} angle of attack is reduced by25 % in the experiment, while in theory the value is only 14.9% for the same condition

b- The governing equations used by each numerical method are different due to the designer's code concept and also the selected boundary conditions.

c- The manufacturing of the models is done with the best available methods and resources which are limited to the researcher.

5.2 Recommendations

Since the results presented in this work for induced drag calculation are only through basic formulas which only depend on area of the winglet, a flow analysis could be done in order to determine the lift-off performance, vortices reduction, and also to find the parasite drag associated with size of winglet .

Based on the type of analysis, user interface can be created. If the analysis is to be done it is recommended that MATLAB, and Excel user interface should be linked with MATALAB. Upon changing the values in excel, this should change its geometry and the flow results should be obtained automatically from MATLAB .

Similarly, for CFD method analysis, software like Ansys with CFX should be used. So, an actual drag reduction vortex effects for the respective winglet can be calculated by varying the parameters. Optimization of the geometry for each type of winglet could be done by targeting drag as a minimizing factor .

Moreover, applying a composite material to each winglet and optimizing the drag could be performed. Ribs and spars would be designed for each winglet, and a finite element analysis could be performed to calculate structural integrity using FEA tools like ANSYS .

This work could have been done with Knowledge Pattern approach for automation for better template and view.

References

Allison, C. B., & Dally, B. B. (2007). Effect of a delta-winglet vortex pair on the performance of a tubeâ€“fin heat exchanger. *International Journal of Heat and Mass Transfer, 50*(25), 5065-5072.

Anderson, J. D. (2005). *Introduction to flight* (Vol. 199): McGraw-Hill Boston.

Ardonceau, P., & Trapier, S. (2005). *Réduction de traînée d'une voilure rectangulaire par gestion du décollement marginal.* Paper presented at the Proc. 17Ã¨me CongrÃ¨s FranÃ§ais de MÃ©canique, Troyes, AoÃ»t-Septembre 2005.

Atique, M. S. A., Salam, M. A., Nafi, A. S., Probha, N. N., & Barman, S. (2015). Aerodynamics of Winglet: a Computational Fluid Dynamics Study.

Azlin, M. A., Taib, C. F. M., Kasolang, S., & Muhammad, F. H. (2011). *CFD analysis of winglets at low subsonic flow.* Paper presented at the Proceedings of the World Congress on Engineering.

Babigian, R., & Hayashibara, S. (2009). Computational Study of the Vortex Wake Generated by a Three-Dimensional Wing with Dihedral, Taper, and Sweep: Embry-Riddle Aeronautical University, College of Engineering. Prescott: AIAA.

Babinsky, H. (2003). How do wings work? *Physics Education, 38*(6), 497.

Belferhat, S., Meftah, S. M. A., Yahiaoui, T., & Imine, B. (2013). *Aerodynamic Optimization of a Winglet Design.* Paper presented at the EPJ Web of Conferences.

Beninati, M. L., & Marshall, J. S. (2005). An experimental study of the effect of free-stream turbulence on a trailing vortex. *Experiments in Fluids, 38*(2), 244-257.

Bento Mattos, E., Antonini Macedo, E., & Durval Silva Filho, E. (2003). Considerations about winglet design.

Bojja, A., & Garre, P. (2013). *Analysis on Reducing the Induced Drag Using the Winglet at the Wingtip.* Paper presented at the International Journal of Engineering Research and Technology.

Cosin, R., Catalano, F. M., Correa, L. G. N., & Entz, R. M. U. (2010). *Aerodynamic analysis of multi-winglets for low speed aircraft.* Paper presented at the 27th International congress of the aeronautical sciences.

Fiebig, M., Valencia, A., & Mitra, N. K. (1993). Wing-type vortex generators for fin-and-tube heat exchangers. *Experimental Thermal and Fluid Science, 7*(4), 287-295.

Gimmestad, D. (1981). Aero-elastic tailoring of a composite winglet for KC-135. *AIAA Paper*(81-0607), 373-376.

Hantrais-Gervois, J. L., Grenon, R., Mann, A., & BÃ¼scher, A. (2009). Downward pointing winglet design and assessment within the M-DAW research project. *Aeronautical Journal, 113*(1142), 221-232.

Hossain, A., Rahman, A., Hossen, J., Iqbal, A., & Zahirul, M. I. (2011). Prediction of aerodynamic characteristics of an aircraft model with and without winglet using fuzzy logic technique. *Aerospace Science and Technology, 15*(8), 595-605.

Jacobi, A. M., & Shah, R. K. (1995). Heat transfer surface enhancement through the use of longitudinal vortices: a review of recent progress. *Experimental Thermal and Fluid Science, 11*(3), 295-309.

Jansen, P. W., Perez, R. E., & Ra Martins, J. R. (2010). Aerostructural optimization of nonplanar lifting surfaces. *Journal of Aircraft, 47*(5), 1490-1503.

Joardar, A., & Jacobi, A. M. (2008). Heat transfer enhancement by winglet-type vortex generator arrays in compact plain-fin-and-tube heat exchangers. *International Journal of refrigeration, 31*(1), 87-97.

kevadiya, M., & Vaidya, H. A. (2013). 2-D Analysis of NACA 4412 AIRFOIL. *International Journal of Innovative Research in Science, Engineering and Technology, 2*(5), 1686-1891.

Kontogiannis, S. G., & Ekaterinaris, J. A. (2013). Design, performance evaluation and optimization of a UAV. *Aerospace Science and Technology, 29*(1), 339-350.

Kroo, I. (2005). Nonplanar wing concepts for increased aircraft efficiency. *VKI lecture series on innovative configurations and advanced concepts for future civil aircraft.*

Kwak, K. M., Torii, K., & Nishino, K. (2003). Heat transfer and pressure loss penalty for the number of tube rows of staggered finned-tube bundles with a single transverse row of winglets. *International Journal of Heat and Mass Transfer, 46*(1), 175-180.

Kwak, K. M., Torii, K., & Nishino, K. (2005). Simultaneous heat transfer enhancement and pressure loss reduction for finned-tube bundles with the first or two transverse rows of built-in winglets. *Experimental Thermal and Fluid Science, 29*(5), 625-632.

Manea, A. S., & Galeriu, C. D. (2004). *Laminar – Turbulent transition zone in the boundary layer.* Paper presented at the 6th International

Conference on Hydraulic Machinery and Hydrodynamics, Timisoara, Romania.

Maughmer, M. D. (2003). Design of winglets for high-performance sailplanes. *Journal of Aircraft, 40*(6), 1099-1106.

Maughmer, M. D. (2006). The design of winglets for low-speed aircraft. *Soaring Magazine, 30*(3), 61.

Mccormick, Barens W. (1995). *Aerodynamics Aeronautics and Flight Mechanics* (2nd ed.). John Wiley & SONS, INC.

Meyer Jr, R. R., & Covell, P. F. (1986). *Effects of Winglets on a First-Generation Jet Transport Wing. 7. Sideslip Effects on Winglet Loads and Selected Wing Loads at Subsonic Speeds for a Full-Span Model*: DTIC Document Number)

Min, J., & Xu, W. (2005). Numerical prediction of the performances of the fins with punched delta winglets and the louver fins and their comparison. *Journal of Enhanced Heat Transfer, 12*(4).

Ning, A., & Kroo, I. (2010). Multidisciplinary considerations in the design of wings and wing tip devices. *Journal of Aircraft, 47*(2), 534-543.

Panagiotou, P., Kaparos, P., & Yakinthos, K. (2014). Winglet design and optimization for a MALE UAV using CFD. *Aerospace Science and Technology, 39*, 190-205.

Schubauer, G. B., & Spangenberg, W. G. (1960). Forced mixing in boundary layers. *Journal of Fluid Mechanics, 8*(01), 10-32.

Smith, H. C., & Smith, H. C. (1992). *The illustrated guide to aerodynamics*: Tab Books.

Sohn, M. H., & Chang, J. W. (2012). Visualization and PIV study of wing-tip vortices for three different tip configurations. *Aerospace Science and Technology, 16*(1), 40-46.

Takenaka, K., Hatanaka, K., Yamazaki, W., & Nakahashi, K. (2008). Multidisciplinary design exploration for a winglet. *Journal of Aircraft, 45*(5), 1601-1611.

Torii, K., Kwak, K. M., & Nishino, K. (2002). Heat transfer enhancement accompanying pressure-loss reduction with winglet-type vortex generators for fin-tube heat exchangers. *International Journal of Heat and Mass Transfer, 45*(18), 3795-3801.

Weierman, J., & Jacob, J. D. (2010). *Winglet design and optimization for UAVs.* Paper presented at the 28th AIAA Applied Aerodynamics Conference.

Weierman, J. R., & Jacob, J. D. (2010). *Winglet design and optimization for UAVs.* Oklahoma State University.

Yahaya, N., & Sheriff, J. M. (2012). Flow behavior around winglets. *Jurnal Mekanikal*(34), 95-100.

Appendix (A)

Uncertainty Analysis

A.1 Uncertainty Associated with the Wing's Surface Area

The wing's projected top area is used for calculating the drag and lift coefficients. The next equation presents the wings area formula. S is wing span and C is the chord of the plain wing.

$$A = S \times C \tag{A.1}$$

The uncertainty in A was calculated as follows

$$U_A = \sqrt{(\frac{\partial A}{\partial S} U_S)^2 + (\frac{\partial A}{\partial C} U_C)^2} \tag{A.2}$$

$\frac{\partial A}{\partial S} = 1$, $\frac{\partial A}{\partial C} = 9.528$, and U_S, $U_C = \pm 0.5\ mm$

Thus $U_A = \pm 4.79\ mm^2$

The total uncertainty in the wing's surface for the plain wing is:

$$\frac{U_A}{A} \times 100 = \pm 0.503\ \%$$

The total uncertainty in the wing's surface for the wing with winglets is:

$\frac{\partial A}{\partial S} = 1$, $\frac{\partial A}{\partial C} = 10.328$, and U_S, $U_C = \pm 0.5\ mm$

Thus $U_A = \pm 4.91\ mm^2$

$$\frac{U_A}{A} \times 100 = \pm 0.691\ \%$$

A.2 Uncertainty Associated with the Air flow Velocity at the Inlet of the Wind Tunnel

The free stream air flow velocity at the inlet of the wind tunnel is related to the static pressure inside the wind tunnel by the next formula that based on the density of the air. The velocity given by:

$$V_\infty = \sqrt{\frac{2\Delta P_s}{\rho}} \tag{A.3}$$

For ρ = 1.202 kg/m^3, P_s = 374.74 Pa, the uncertainty was calculated as

$$U_{V_\infty} = \sqrt{(\frac{\partial V_\infty}{\partial P_S} U_{P_S})^2 + (\frac{\partial V_\infty}{\partial \rho} U_P)^2} \tag{A.4}$$

Where

$\frac{\partial V_\infty}{\partial P_S} = \frac{1}{\sqrt{2P_S\rho}}$, and $U_{P_S} = \pm$ 0.981 Pa, and

$\frac{\partial V_\infty}{\partial \rho} = -\sqrt{\frac{P_S}{2\rho^3}}$, and $U_\rho = \pm$ 4.2 × 10^{-4} kg/m^3

Thus $U_{V_\infty} = \pm 0.049\ m/s$

The total uncertainty in the inlet velocity, for $V_\infty = 30\ m/s$ is

$\frac{U_{V_\infty}}{V_\infty} \times 100 = \pm 0.1633\ \%$

A.3 Uncertainty Associated with the Drag Coefficient of the Wing

The drag coefficient at angle of attack of zero α = 0° was obtained from the next formula:

$$C_D = \frac{2F_D}{\rho V_\infty^2 A \cos\alpha} \tag{A.5}$$

For α = 0° , ρ = 1.202 kg/m^3 and for $V_\infty = 30\ m/s$, the drag force was F_D = 0.21 N for the plain wing. And F_D = 0.19 N for the wing with winglets. The uncertainty in C_D was calculated as:

$$U_{C_D} = \sqrt{(\frac{\partial C_D}{\partial F_D} U_{F_D})^2 + (\frac{\partial C_D}{\partial \rho} U_\rho)^2 + (\frac{\partial C_D}{\partial V_\infty} U_{V_\infty})^2 + (\frac{\partial C_D}{\partial A} U_A)^2} \tag{A.6}$$

Where

$$\frac{\partial C_D}{\partial F_D} = \frac{2}{\rho V_\infty^2 A \cos\alpha'} \quad \text{and} \quad U_{F_D} = \pm 0.002\, N\,,$$

$$\frac{\partial C_D}{\partial \rho} = -\frac{2F_D}{\rho^2 V_\infty^2 A \cos\alpha'} \quad \text{and} \quad U_\rho = \pm 3.1 \times 10^{-4}\, kg/m^3\,,$$

$$\frac{\partial C_D}{\partial V_\infty} = -\frac{4F_D}{\rho V_\infty^3 A \cos\alpha'} \quad \text{and} \quad U_{V_\infty} = \pm 0.041\, m/s\,,$$

$$\frac{\partial C_D}{\partial A} = \frac{2F_D}{\rho V_\infty^2 A^2 \cos\alpha'} \quad \text{and} \quad U_A = \pm 6.02 \times 10^{-5}\, m^2$$

Thus, $U_{C_D} = \pm 0.021$

The total uncertainty in the drag coefficient, for the plain wing at $V_\infty = 30\, m/s$ is :

$$\frac{U_{C_D}}{C_D} \times 100 = \pm 2.3\ \%$$

For the wing with winglets, with the same procedures and conditions in calculating the total uncertainty, then got:

$$\frac{U_{C_D}}{C_D} \times 100 = \pm 3.01\ \%$$

A.4 Uncertainty Associated with the Lift Coefficient of the Wing

The lift coefficient at angle of attack of zero $\alpha = 0^\circ$ was obtained from the next formula:

$$C_D = \frac{2F_L}{\rho V_\infty^2 A \cos\alpha} \qquad \text{(A.5)}$$

For $\alpha = 0^\circ$, $\rho = 1.202\ kg/m^3$ and for $V_\infty = 30\, m/s$, the lift force was $F_L = 0.041\ N$ for the plain wing. And $F_D = 0.046\ N$ for the wing with winglets. The uncertainty in C_D was calculated as:

$$U_{C_D} = \sqrt{\left(\frac{\partial C_L}{\partial F_L} U_{F_L}\right)^2 + \left(\frac{\partial C_L}{\partial \rho} U_\rho\right)^2 + \left(\frac{\partial C_L}{\partial V_\infty} U_{V_\infty}\right)^2 + \left(\frac{\partial C_L}{\partial A} U_A\right)^2} \qquad \text{(A.6)}$$

Where

$$\frac{\partial C_L}{\partial F_L} = \frac{2}{\rho V_\infty^2 A \cos \alpha'} \quad \text{and} \quad U_{F_L} = \pm 0.002\, N\,,$$

$$\frac{\partial C_L}{\partial \rho} = -\frac{2F_L}{\rho^2 V_\infty^2 A \cos \alpha'} \quad \text{and} \quad U_\rho = \pm 3.1 \times 10^{-4}\, kg/m^3\,,$$

$$\frac{\partial C_L}{\partial V_\infty} = -\frac{4F_L}{\rho V_\infty^3 A \cos \alpha'} \quad \text{and} \quad U_{V_\infty} = \pm 0.041\, m/s\,,$$

$$\frac{\partial C_L}{\partial A} = \frac{2F_L}{\rho V_\infty^2 A^2 \cos \alpha'} \quad \text{and} \quad U_A = \pm 6.02 \times 10^{-5}\, m^2$$

Thus, $U_{C_L} = \pm 0.0027$

The total uncertainty in the drag coefficient, for the plain wing at $V_\infty = 30\, m/s$ is :

$$\frac{U_{C_L}}{C_L} \times 100 = \pm 4.05\ \%$$

For the wing with winglets, with the same procedures and conditions in calculating the total uncertainty, then got:

$$\frac{U_{C_L}}{C_L} \times 100 = \pm 6.44\ \%$$

Appendix (B)

3-D Foil Multi-Surfaces Optimum Model Trails

Table 1: Winglet length = 0.3m, $\beta=55^{o}$, Chord=1m

	"Case No. 1"	Case No. 2"	Case No. 3"
Total Lift (Newtons)	3,800.34	10,203.92	16,529.84
Total Side Force (Newtons)	2.88E-07	4.69E-07	6.46E-07
Total Drag (Newtons)	128.56	323.19	747.77
Body Lift (Newtons)	0	0	0
Body Side Force (Newtons)	0	0	0
Body Drag (Newtons)	0	0	0
Moment (Newton-m, CG)	1485.9751	1466.6443	1481.2758
Roll Moment (Newton-m, CG)	-3.55E-05	-3.53E-05	-3.45E-05
Yaw Moment (Newton-m, CG)	7.17E-07	1.93E-06	3.03E-06
Lift Coeff.	0.245	0.658	1.07
Side Force Coeff.	1.86E-11	3.02E-11	4.17E-11
Induced CD	0.00211	0.0148	0.0384
Profile CD	0.00618	0.00608	0.00979
Total CD	0.00829	0.0208	0.0482
Cl/CD	29.56	31.57	22.11
CM	-0.0958	-0.0946	-0.0955
Roll Coefficient	-2.29E-09	-2.27E-09	-2.22E-09
Yaw Coefficient	4.62E-11	1.24E-10	1.96E-10
X-Center of Pres. (m)	0.391	0.144	0.0896
Y-Center of Pres. (m)	9.33E-09	3.45E-09	2.09E-09
Z-Center of Pres. (m)	-2.49	-4.12	-4.69
Speed (m/s)	50	50	50
Angle of Attack	0	5	10
Power Usage (kW)	6.43	16.16	37.39

Table 2: Winglet length = 0.3m, $\beta=55^{o}$, Chord=1m

	"Case No. 1"	Case No. 2"	Case No. 3"
Total Lift (Newtons)	3,800.34	10,203.92	16,529.84
Total Side Force (Newtons)	2.88E-07	4.69E-07	6.46E-07
Total Drag (Newtons)	128.56	323.19	747.77
Body Lift (Newtons)	0	0	0
Body Side Force (Newtons)	0	0	0
Body Drag (Newtons)	0	0	0
Moment (Newton-m, CG)	1485.9751	1466.6443	1481.2758
Roll Moment (Newton-m, CG)	-3.55E-05	-3.53E-05	-3.45E-05
Yaw Moment (Newton-m, CG)	7.17E-07	1.93E-06	3.03E-06
Lift Coeff.	0.245	0.658	1.07
Side Force Coeff.	1.86E-11	3.02E-11	4.17E-11
Induced CD	0.00211	0.0148	0.0384
Profile CD	0.00618	0.00608	0.00979
Total CD	0.00829	0.0208	0.0482
Cl/CD	29.56	31.57	22.11
CM	-0.0958	-0.0946	-0.0955
Roll Coefficient	-2.29E-09	-2.27E-09	-2.22E-09
Yaw Coefficient	4.62E-11	1.24E-10	1.96E-10
X-Center of Pres. (m)	0.391	0.144	0.0896
Y-Center of Pres. (m)	9.33E-09	3.45E-09	2.09E-09
Z-Center of Pres. (m)	-2.49	-4.12	-4.69
Speed (m/s)	50	50	50
Angle of Attack	0	5	10
Power Usage (kW)	6.43	16.16	37.39

Table 3: Winglet length = 0.4m, $\beta=55^{o}$, Chord=1m

	"Case No. 1"	Case No. 2"	Case No. 3"
Total Lift (Newtons)	3,912.36	10,516.74	17,041.08
Total Side Force (Newtons)	7.89E-07	2.27E-06	3.73E-06
Total Drag (Newtons)	129.11	319.89	743.75
Body Lift (Newtons)	0	0	0
Body Side Force (Newtons)	0	0	0
Body Drag (Newtons)	0	0	0
Moment (Newton-m, CG)	-1516.4762	-1499.131	-1516.5481
Roll Moment (Newton-m, CG)	-3.16E-05	-1.87E-05	-5.65E-06
Yaw Moment (Newton-m, CG)	9.86E-07	3.24E-06	4.61E-06
Lift Coeff.	0.247	0.665	1.08
Side Force Coeff.	4.99E-11	1.44E-10	2.36E-10
Induced CD	0.00198	0.0142	0.0371
Profile CD	0.00619	0.00606	0.0099
Total CD	0.00816	0.0202	0.047
Cl/CD	30.30	32.88	22.91
CM	-0.0959	-0.0948	-0.0959
Roll Coefficient	-2.00E-09	-1.18E-09	-3.57E-10
Yaw Coefficient	6.24E-11	2.05E-10	2.91E-10
X-Center of Pres. (m)	0.388	0.143	0.089
Y-Center of Pres. (m)	8.08E-09	1.78E-09	3.31E-10
Z-Center of Pres. (m)	-1.25	-1.43	-1.23
Speed (m/s)	50	50	50
Angle of Attack	0	5	10
Power Usage (kW)	6.46	15.99	37.19

Table 4: Winglet length = 0.45m, $\beta=55^{o}$, Chord=1m

	"Case No. 1"	Case No. 2"	Case No. 3"
Total Lift (Newtons)	3,858.17	10,421.89	16,906.29
Total Side Force (Newtons)	2.27E-07	4.12E-07	5.93E-07
Total Drag (Newtons)	132.24	337.37	784.95
Body Lift (Newtons)	0	0	0
Body Side Force (Newtons)	0	0	0
Body Drag (Newtons)	0	0	0
Moment (Newton-m, CG)	-1496.062	-1488.3693	-1517.6617
Roll Moment (Newton-m, CG)	-3.59E-05	-3.57E-05	-3.50E-05
Yaw Moment (Newton-m, CG)	7.39E-07	1.98E-06	3.10E-06
Lift Coeff.	0.242	0.653	1.06
Side Force Coeff.	1.42E-11	2.58E-11	3.71E-11
Induced CD	0.00211	0.0151	0.0394
Profile CD	0.00617	0.00606	0.00974
Total CD	0.00828	0.0211	0.0492
Cl/CD	29.18	30.89	21.54
CM	-0.0937	-0.0932	-0.095
Roll Coefficient	-2.25E-09	-2.24E-09	-2.19E-09
Yaw Coefficient	4.63E-11	1.24E-10	1.94E-10
X-Center of Pres. (m)	0.388	0.143	0.0898
Y-Center of Pres. (m)	9.31E-09	3.43E-09	2.07E-09
Z-Center of Pres. (m)	-3.26	-4.80	-5.23
Speed (m/s)	50	50	50
Angle of Attack	0	5	10
Power Usage (kW)	6.61	16.87	39.25

Table 5: Winglet length = 0.3m, $\beta=60^{o}$, Chord=1m

	"Case No. 1"	Case No. 2"	Case No. 3"
Total Lift (Newtons)	3,795.08	10,182.52	16,492.45
Total Side Force (Newtons)	2.86E-07	4.66E-07	6.43E-07
Total Drag (Newtons)	128.77	324.05	749.02
Body Lift (Newtons)	0	0	0
Body Side Force (Newtons)	0	0	0
Body Drag (Newtons)	0	0	0
Moment (Newton-m, CG)	-1484.5664	-1464.0932	-1477.4734
Roll Moment (Newton-m, CG)	-3.54E-05	-3.52E-05	-3.45E-05
Yaw Moment (Newton-m, CG)	7.19E-07	1.94E-06	3.04E-06
Lift Coeff.	0.245	0.657	1.06
Side Force Coeff.	1.84E-11	3.01E-11	4.15E-11
Induced CD	0.00213	0.0148	0.0385
Profile CD	0.00618	0.00611	0.00978
Total CD	0.0083	0.0209	0.0483
Cl/CD	29.47	31.42	22.02
CM	-0.0957	-0.0944	-0.0953
Roll Coefficient	-2.28E-09	-2.27E-09	-2.22E-09
Yaw Coefficient	4.64E-11	1.25E-10	1.96E-10
X-Center of Pres. (m)	0.391	0.144	0.0896
Y-Center of Pres. (m)	9.34E-09	3.46E-09	2.09E-09
Z-Center of Pres. (m)	-2.52	-4.15	-4.73
Speed (m/s)	50	50	50
Angle of Attack	0	5	10
Power Usage (kW)	6.44	16.20	37.45

Table 6: Winglet length = 0.4m, $\beta=60^{o}$, Chord=1m

	"Case No. 1"	Case No. 2"	Case No. 3"
Total Lift (Newtons)	3,899.48	10,476.18	16,973.15
Total Side Force (Newtons)	8.76E-07	2.51E-06	4.12E-06
Total Drag (Newtons)	129.10	319.41	742.00
Body Lift (Newtons)	0	0	0
Body Side Force (Newtons)	0	0	0
Body Drag (Newtons)	0	0	0
Moment (Newton-m, CG)	-1511.9617	-1495.2202	-1513.104
Roll Moment (Newton-m, CG)	-3.12E-05	-1.83E-05	-5.25E-06
Yaw Moment (Newton-m, CG)	9.65E-07	3.27E-06	4.69E-06
Lift Coeff.	0.247	0.662	1.07
Side Force Coeff.	5.54E-11	1.59E-10	2.61E-10
Induced CD	0.00198	0.0141	0.037
Profile CD	0.00619	0.00606	0.0099
Total CD	0.00816	0.0202	0.0469
Cl/CD	30.21	32.80	22.87
CM	-0.0956	-0.0945	-0.0957
Roll Coefficient	-1.97E-09	-1.16E-09	-3.32E-10
Yaw Coefficient	6.10E-11	2.07E-10	2.97E-10
X-Center of Pres. (m)	0.388	0.143	0.0891
Y-Center of Pres. (m)	8.01E-09	1.75E-09	3.10E-10
Z-Center of Pres. (m)	-1.10	-1.30	-1.14
Speed (m/s)	50	50	50
Angle of Attack	0	5	10
Power Usage (kW)	6.45	15.97	37.10

Table 7: Winglet length = 0.45m, $\beta=60^{o}$, Chord=1m

	"Case No. 1"	Case No. 2"	Case No. 3"
Total Lift (Newtons)	3,844.18	10,389.45	16,847.70
Total Side Force (Newtons)	2.15E-07	4.04E-07	5.85E-07
Total Drag (Newtons)	132.11	337.72	786.84
Body Lift (Newtons)	0	0	0
Body Side Force (Newtons)	0	0	0
Body Drag (Newtons)	0	0	0
Moment (Newton-m, CG)	-1491.0378	-1485.8645	-1514.5453
Roll Moment (Newton-m, CG)	-3.58E-05	-3.57E-05	-3.49E-05
Yaw Moment (Newton-m, CG)	7.32E-07	1.98E-06	3.11E-06
Lift Coeff.	0.241	0.651	1.06
Side Force Coeff.	1.34E-11	2.53E-11	3.66E-11
Induced CD	0.0021	0.0151	0.0395
Profile CD	0.00617	0.00609	0.00974
Total CD	0.00827	0.0212	0.0493
Cl/CD	29.10	30.76	21.41
CM	-0.0934	-0.0931	-0.0948
Roll Coefficient	-2.24E-09	-2.23E-09	-2.19E-09
Yaw Coefficient	4.59E-11	1.24E-10	1.95E-10
X-Center of Pres. (m)	0.388	0.143	0.0899
Y-Center of Pres. (m)	9.31E-09	3.43E-09	2.07E-09
Z-Center of Pres. (m)	-3.41	-4.90	-5.32
Speed (m/s)	50	50	50
Angle of Attack	0	5	10
Power Usage (kW)	6.61	16.89	39.34

Table 8: Winglet length = 0.3m, β=65°, Chord=1m

	"Case No. 1"	Case No. 2"	Case No. 3"
Total Lift (Newtons)	3,795.08	10,159.50	16,452.54
Total Side Force (Newtons)	2.86E-07	4.65E-07	6.42E-07
Total Drag (Newtons)	128.77	325.59	752.74
Body Lift (Newtons)	0	0	0
Body Side Force (Newtons)	0	0	0
Body Drag (Newtons)	0	0	0
Moment (Newton-m, CG)	-1484.5664	-1461.2375	-1473.3308
Roll Moment (Newton-m, CG)	-3.54E-05	-3.52E-05	-3.44E-05
Yaw Moment (Newton-m, CG)	7.19E-07	1.95E-06	3.06E-06
Lift Coeff.	0.245	0.655	1.06
Side Force Coeff.	1.84E-11	3.00E-11	4.14E-11
Induced CD	0.00213	0.0149	0.0388
Profile CD	0.00618	0.0061	0.00978
Total CD	0.0083	0.021	0.0485
Cl/CD	29.47	31.20	21.86
CM	-0.0957	-0.0942	-0.095
Roll Coefficient	-2.28E-09	-2.27E-09	-2.22E-09
Yaw Coefficient	4.64E-11	1.26E-10	1.97E-10
X-Center of Pres. (m)	0.391	0.144	0.0896
Y-Center of Pres. (m)	9.34E-09	3.46E-09	2.09E-09
Z-Center of Pres. (m)	-2.52	-4.19	-4.77
Speed (m/s)	50	50	50
Angle of Attack	0	5	10
Power Usage (kW)	6.44	16.28	37.64

Table 9: Winglet length = 0.4m, $\beta=65^{o}$, Chord=0.3m

	"Case No. 1"	Case No. 2"	Case No. 3"
Total Lift (Newtons)	3,821.72	10,295.57	16,691.06
Total Side Force (Newtons)	-23.79	-53.89	-83.57
Total Drag (Newtons)	126.96	330.06	783.62
Body Lift (Newtons)	0	0	0
Body Side Force (Newtons)	0	0	0
Body Drag (Newtons)	0	0	0
Moment (Newton-m, CG)	-1487.813	-1462.0613	-1472.2303
Roll Moment (Newton-m, CG)	-176.03	-384.42	-583.80
Yaw Moment (Newton-m, CG)	18.51	-32.89	-230.23
Lift Coeff.	0.248	0.669	1.08
Side Force Coeff.	-0.00155	-0.0035	-0.00543
Induced CD	0.00205	0.0154	0.0411
Profile CD	0.00621	0.00609	0.00984
Total CD	0.00825	0.0215	0.0509
Cl/CD	30.10	31.19	21.30
CM	-0.0967	-0.095	-0.0957
Roll Coefficient	-0.0114	-0.025	-0.0379
Yaw Coefficient	0.0012	-0.00214	-0.015
X-Center of Pres. (m)	0.389	0.142	0.0882
Y-Center of Pres. (m)	0.0461	0.0373	0.035
Z-Center of Pres. (m)	0.778	-0.61	-2.75
Speed (m/s)	50	50	50
Angle of Attack	0	5	10
Power Usage (kW)	6.35	16.50	39.18

Table 10: Winglet length = 0.4m, $\beta=65^{o}$, Chord=0.5m

	"Case No. 1"	Case No. 2"	Case No. 3"
Total Lift (Newtons)	3,858.97	10,380.80	16,823.63
Total Side Force (Newtons)	-10.86	-21.37	-31.73
Total Drag (Newtons)	129.96	331.80	776.65
Body Lift (Newtons)	0	0	0
Body Side Force (Newtons)	0	0	0
Body Drag (Newtons)	0	0	0
Moment (Newton-m, CG)	-1492.5115	-1470.3013	-1482.7914
Roll Moment (Newton-m, CG)	-68.09	-126.34	-181.79
Yaw Moment (Newton-m, CG)	4.16	-44.98	-191.82
Lift Coeff.	0.249	0.669	1.08
Side Force Coeff.	-0.0007	-0.00138	-0.00205
Induced CD	0.00218	0.0153	0.0403
Profile CD	0.0062	0.00607	0.00981
Total CD	0.00838	0.0214	0.0501
Cl/CD	29.69	31.29	21.66
CM	-0.0962	-0.0948	-0.0956
Roll Coefficient	-0.00439	-0.00815	-0.0117
Yaw Coefficient	0.000268	-0.0029	-0.0124
X-Center of Pres. (m)	0.387	0.142	0.0881
Y-Center of Pres. (m)	0.0176	0.0122	0.0108
Z-Center of Pres. (m)	0.383	-2.10	-6.05
Speed (m/s)	50	50	50
Angle of Attack	0	5	10
Power Usage (kW)	6.50	16.59	38.83

Table 11: Winglet length = 0.4m, β=65°, Chord=1m (optimum)

	"Case No. 1"	Case No. 2"	Case No. 3"
Total Lift (Newtons)	3,886.23	10,434.56	16,903.47
Total Side Force (Newtons)	9.64E-07	2.73E-06	4.48E-06
Total Drag (Newtons)	129.09	318.93	737.58
Body Lift (Newtons)	0	0	0
Body Side Force (Newtons)	0	0	0
Body Drag (Newtons)	0	0	0
Moment (Newton-m, CG)	-1507.4115	-1491.1614	-1509.3939
Roll Moment (Newton-m, CG)	-3.10E-05	-1.83E-05	-5.50E-06
Yaw Moment (Newton-m, CG)	9.35E-07	3.29E-06	4.77E-06
Lift Coeff.	0.246	0.66	1.07
Side Force Coeff.	6.10E-11	1.73E-10	2.84E-10
Induced CD	0.00198	0.0141	0.0369
Profile CD	0.00619	0.00605	0.00973
Total CD	0.00816	0.0202	0.0466
Cl/CD	30.10	32.72	22.92
CM	-0.0953	-0.0943	-0.0954
Roll Coefficient	-1.96E-09	-1.16E-09	-3.48E-10
Yaw Coefficient	5.91E-11	2.08E-10	3.02E-10
X-Center of Pres. (m)	0.388	0.143	0.0893
Y-Center of Pres. (m)	7.97E-09	1.75E-09	3.25E-10
Z-Center of Pres. (m)	-0.97	-1.20	-1.06
Speed (m/s)	50	50	50
Angle of Attack	0	5	10
Power Usage (kW)	6.45	15.95	36.88

Table 12: Winglet length = 0.45m, $\beta=65^{\circ}$, Chord=1m

	"Case No. 1"	Case No. 2"	Case No. 3"
Total Lift (Newtons)	3,844.18	10,352.00	16,781.03
Total Side Force (Newtons)	2.15E-07	3.99E-07	5.80E-07
Total Drag (Newtons)	132.11	335.61	785.10
Body Lift (Newtons)	0	0	0
Body Side Force (Newtons)	0	0	0
Body Drag (Newtons)	0	0	0
Moment (Newton-m, CG)	-1491.0378	-1481.7371	-1508.5618
Roll Moment (Newton-m, CG)	-3.58E-05	-3.56E-05	-3.49E-05
Yaw Moment (Newton-m, CG)	7.32E-07	1.97E-06	3.10E-06
Lift Coeff.	0.241	0.648	1.05
Side Force Coeff.	1.34E-11	2.50E-11	3.63E-11
Induced CD	0.0021	0.0149	0.0394
Profile CD	0.00617	0.00609	0.00973
Total CD	0.00827	0.021	0.0492
Cl/CD	29.10	30.84	21.37
CM	-0.0934	-0.0928	-0.0945
Roll Coefficient	-2.24E-09	-2.23E-09	-2.18E-09
Yaw Coefficient	4.59E-11	1.23E-10	1.94E-10
X-Center of Pres. (m)	0.388	0.143	0.0899
Y-Center of Pres. (m)	9.31E-09	3.44E-09	2.08E-09
Z-Center of Pres. (m)	-3.41	-4.94	-5.35
Speed (m/s)	50	50	50
Angle of Attack	0	5	10
Power Usage (kW)	6.61	16.78	39.25

Table 13: Winglet length = 0.3m, $\beta=70^{o}$, Chord=1m

	"Case No. 1"	Case No. 2"	Case No. 3"
Total Lift (Newtons)	3,782.68	10,135.35	16,410.89
Total Side Force (Newtons)	2.86E-07	4.66E-07	6.42E-07
Total Drag (Newtons)	130.09	329.24	760.83
Body Lift (Newtons)	0	0	0
Body Side Force (Newtons)	0	0	0
Body Drag (Newtons)	0	0	0
Moment (Newton-m, CG)	-1481.4303	-1458.4107	-1469.5426
Roll Moment (Newton-m, CG)	-3.53E-05	-3.51E-05	-3.44E-05
Yaw Moment (Newton-m, CG)	7.34E-07	1.97E-06	3.10E-06
Lift Coeff.	0.244	0.654	1.06
Side Force Coeff.	1.84E-11	3.00E-11	4.14E-11
Induced CD	0.00221	0.0151	0.0393
Profile CD	0.00618	0.00611	0.00977
Total CD	0.00839	0.0212	0.0491
Cl/CD	29.08	30.78	21.57
CM	-0.0955	-0.094	-0.0948
Roll Coefficient	-2.28E-09	-2.27E-09	-2.22E-09
Yaw Coefficient	4.73E-11	1.27E-10	2.00E-10
X-Center of Pres. (m)	0.392	0.144	0.0895
Y-Center of Pres. (m)	9.34E-09	3.47E-09	2.10E-09
Z-Center of Pres. (m)	-2.57	-4.23	-4.82
Speed (m/s)	50	50	50
Angle of Attack	0	5	10
Power Usage (kW)	6.50	16.46	38.04

Table 14: Winglet length = 0.45m, $\beta=70^{o}$, Chord=1m

	"Case No. 1"	Case No. 2"	Case No. 3"
Total Lift (Newtons)	3,833.06	10,306.46	16,701.42
Total Side Force (Newtons)	2.15E-07	3.99E-07	5.79E-07
Total Drag (Newtons)	131.55	329.98	776.04
Body Lift (Newtons)	0	0	0
Body Side Force (Newtons)	0	0	0
Body Drag (Newtons)	0	0	0
Moment (Newton-m, CG)	-1486.9965	-1475.0542	-1497.8661
Roll Moment (Newton-m, CG)	-3.57E-05	-3.55E-05	-3.48E-05
Yaw Moment (Newton-m, CG)	7.16E-07	1.94E-06	3.06E-06
Lift Coeff.	0.24	0.645	1.05
Side Force Coeff.	1.35E-11	2.50E-11	3.63E-11
Induced CD	0.00206	0.0146	0.0389
Profile CD	0.00617	0.00608	0.00972
Total CD	0.00824	0.0207	0.0486
Cl/CD	29.14	31.23	21.52
CM	-0.0931	-0.0924	-0.0938
Roll Coefficient	-2.24E-09	-2.22E-09	-2.18E-09
Yaw Coefficient	4.48E-11	1.22E-10	1.92E-10
X-Center of Pres. (m)	0.388	0.143	0.0897
Y-Center of Pres. (m)	9.32E-09	3.45E-09	2.08E-09
Z-Center of Pres. (m)	-3.32	-4.87	-5.29
Speed (m/s)	50	50	50
Angle of Attack	0	5	10
Power Usage (kW)	6.58	16.50	38.80

Table 15: Winglet length = 0.4m, $\beta=70^{o}$, Chord=1m

	"Case No. 1"	Case No. 2"	Case No. 3"
Total Lift (Newtons)	3,886.23	10,392.31	16,832.75
Total Side Force (Newtons)	9.64E-07	2.93E-06	4.80E-06
Total Drag (Newtons)	129.09	318.54	735.87
Body Lift (Newtons)	0	0	0
Body Side Force (Newtons)	0	0	0
Body Drag (Newtons)	0	0	0
Moment (Newton-m, CG)	-1507.4115	-1486.9982	-1505.4448
Roll Moment (Newton-m, CG)	-3.10E-05	-1.87E-05	-6.36E-06
Yaw Moment (Newton-m, CG)	9.35E-07	3.29E-06	4.83E-06
Lift Coeff.	0.246	0.657	1.06
Side Force Coeff.	6.10E-11	1.86E-10	3.03E-10
Induced CD	0.00198	0.0141	0.0368
Profile CD	0.00619	0.00606	0.00973
Total CD	0.00816	0.0201	0.0465
Cl/CD	30.10	32.62	22.87
CM	-0.0953	-0.094	-0.0952
Roll Coefficient	-1.96E-09	-1.18E-09	-4.02E-10
Yaw Coefficient	5.91E-11	2.08E-10	3.05E-10
X-Center of Pres. (m)	0.388	0.143	0.0894
Y-Center of Pres. (m)	7.97E-09	1.80E-09	3.78E-10
Z-Center of Pres. (m)	-0.97	-1.12	-1.01
Speed (m/s)	50	50	50
Angle of Attack	0	5	10
Power Usage (kW)	6.45	15.93	36.79

Appendix (C)

Fluent Ansys 14 Solution Iteration

C.1 The plain Wing Simulation

C.1.1 The Plain Wing Script Details

Loading "C:\PROGRA~1\ANSYSI~1\v140\fluent\fluent14.0.0\lib\fl114-64.dmp"
Done.

Welcome to ANSYS FLUENT 14.0.0

Copyright 2011 ANSYS, Inc.. All Rights Reserved.
Unauthorized use, distribution or duplication is prohibited.
This product is subject to U.S. laws governing export and re-export.
For full Legal Notice, see documentation.

Build Time: Oct 25 2011 13:11:26 Build Id: 10398
Loading "C:\PROGRA~1\ANSYSI~1\v140\fluent\fluent14.0.0\lib\flprim1119-64.dmp"
Done.

Host spawning Node 0 on machine "ebrahim-PC" (win64).

You can press CTRL+C to stop the startup process!

WARNING: No cached password or password provided.
use '-pass' or '-cache' to provide password
Platform-MPI licensed for FLUENT.
Host 0 -- ip 192.168.1.7 -- ranks 0 - 3

host | 0
======|======
0 : SHM

Prot - All Intra-node communication is: SHM

ID Comm. Hostname O.S. PID Mach ID HW ID Name

---

host net ebrahim-PC Windows-x64 724 0 488 Fluent Host
n3 pcmpi ebrahim-PC Windows-x64 5452 0 3 Fluent Node
n2 pcmpi ebrahim-PC Windows-x64 5036 0 2 Fluent Node
n1 pcmpi ebrahim-PC Windows-x64 1524 0 1 Fluent Node
n0* pcmpi ebrahim-PC Windows-x64 3216 0 0 Fluent Node

Selected system interconnect: default

Cleanup script file is C:\Users\ebrahim\Documents\Theises\cleanup-fluent-ebrahim-PC-724.bat

> Note: Rank = 2: Process affinity not being set (6).
Note: Rank = 1: Process affinity not being set (6).
Note: Rank = 3: Process affinity not being set (6).
Note: Rank = 0: Process affinity not being set (6).
Reading Settings file
C:\Users\ebrahim\Documents\Theises\wing18decplain_files\dp0\FFF\Fluent\FFF.1.set...
Reading
"C:\Users\ebrahim\Documents\Theises\wing18decplain_files\dp0\FFF\MECH\FFF.1.msh"...
Using buffering for scanning file.

550555 nodes, binary.
129190 nodes, binary.
39670 triangular wall faces, zone 1, binary.
7222764 triangular interior faces, zone 2, binary.
136646 triangular wall faces, zone 6, binary.
40742 triangular velocity-inlet faces, zone 7, binary.
41314 triangular pressure-outlet faces, zone 8, binary.
3675975 tetrahedral cells, zone 3, binary.

Building...
mesh
auto partitioning mesh by Metis (fast),
distributing mesh

parts....,

faces....,

nodes....,

cells....,

materials,

interface,

domains,

mixture

zones,

pressure-outlet

velocity-inlet

duct-inlt

solid

interior-solid

wall-solid

Applying mesh operation "Rename Zone duct-inlt to duct-wall "

Applying mesh operation "Change Zone Type"

Setting zone id of solid to 3.

Setting zone id of duct-wall to 6.

Setting zone id of wall-solid to 1.

Setting zone id of interior-solid to 2.

Setting zone id of velocity-inlet to 7.

Setting zone id of pressure-outlet to 8.

Done.

Setting solid (mixture) ... Done.

Setting duct-wall (mixture) ... Done.

Setting wall-solid (mixture) ... Done.

Setting interior-solid (mixture) ... Done.

Setting velocity-inlet (mixture) ... Done.

Setting pressure-outlet (mixture) ... Done.

parallel,

Done.

Preparing mesh for display...

Done.

Setting Post Processing and Surfaces information ... Done.

Writing Settings file...

writing rp variables ... Done.

writing domain variables ... Done.

writing fluid (type fluid) (mixture) ... Done.

writing duct-wall (type velocity-inlet) (mixture) ... Done.

writing wall-solid (type wall) (mixture) ... Done.

writing interior-solid (type interior) (mixture) ... Done.

writing velocity-inlet (type velocity-inlet) (mixture) ... Done.

writing pressure-outlet (type pressure-outlet) (mixture) ... Done.

writing zones map name-id ... Done

C.1.2 The Plain Wing at Zero Degree Angle of Attack Iterations

C.1.2.1 The First Ten Iterations in the Unstable Stage

iter continuity x-velocity y-velocity z-velocity Cl-1 Cd-1 time/iter

1 1.0000e+00 9.7960e-09 2.1267e-09 5.8651e-11 1.6606e-01 5.8440e-01 2:46:30 999

2 1.0000e+00 3.9275e-04 3.9682e-04 2.4687e-04 2.4848e-01 8.7674e-02 2:43:00 998

3 5.6730e-01 2.1515e-04 2.1530e-04 1.6869e-04 2.0958e-01 7.9348e-02 2:36:52 997

4 4.1665e-01 1.3077e-04 1.4941e-04 1.2680e-04 2.1206e-01 3.8822e-02 2:35:15 996

5 2.1156e-01 7.2776e-05 7.4264e-05 5.7103e-05 2.1012e-01 1.7587e-02 2:30:36 995

6 1.4464e-01 5.4502e-05 5.1031e-05 3.5016e-05 2.1997e-01 1.0245e-02 2:26:52 994

7 1.3408e-01 5.2554e-05 5.1022e-05 3.6167e-05 2.1811e-01 1.3476e-02 2:27:10 993

8 9.0007e-02 4.2440e-05 3.8641e-05 2.3576e-05 2.2553e-01 1.6248e-02 2:24:04 992

9 9.1437e-02 4.1728e-05 3.9151e-05 2.4468e-05 2.2778e-01 1.6657e-02 2:21:34 991

10 6.4664e-02 3.7837e-05 3.3914e-05 1.8381e-05 2.3403e-01 1.7047e-02 2:19:32 990

11 5.5638e-02 3.6813e-05 3.2718e-05 1.7102e-05 2.4098e-01 1.7094e-02 2:17:53

iter continuity x-velocity y-velocity z-velocity Cl-1 Cd-1 time/iter

980 1.2469e-03 2.5349e-07 1.7229e-07 1.5125e-07 3.4216e-01 1.4439e-02 0:02:41

C.1.2.2 The Last Ten Iterations with the Final Solution

10

iter continuity x-velocity y-velocity z-velocity Cl-1 Cd-1 time/iter

991 1.2371e-03 2.5153e-07 1.7380e-07 1.5249e-07 3.4220e-01 1.4446e-02 0:01:12 9

992 1.2536e-03 2.5416e-07 1.7473e-07 1.5301e-07 3.4219e-01 1.4441e-02 0:01:04 8

993 1.2719e-03 2.5711e-07 1.7661e-07 1.5436e-07 3.4220e-01 1.4447e-02 0:00:56 7

994 1.2868e-03 2.5972e-07 1.7869e-07 1.5629e-07 3.4219e-01 1.4446e-02 0:00:48 6

995 1.2768e-03 2.5790e-07 1.7940e-07 1.5704e-07 3.4220e-01 1.4451e-02 0:00:40 5

996 1.2676e-03 2.5702e-07 1.8007e-07 1.5687e-07 3.4219e-01 1.4448e-02 0:00:32 4

997 1.2799e-03 2.5827e-07 1.7995e-07 1.5738e-07 3.4219e-01 1.4454e-02 0:00:24 3

998 1.2700e-03 2.5956e-07 1.8034e-07 1.5714e-07 3.4218e-01 1.4449e-02 0:00:16 2

999 1.2646e-03 2.5980e-07 1.7956e-07 1.5666e-07 3.4218e-01 1.4453e-02 0:00:08 1

1000 1.2646e-03 2.6043e-07 1.7885e-07 1.5644e-07 3.4218e-01 1.4446e-02 0:00:00 0

C.1.3 The Plain Wing at Five Degrees Angle of Attack Iterations

C.1.3.1 The First Ten Iterations in the Unstable Stage

iter continuity x-velocity y-velocity z-velocity Cl-1 Cd-1 time/iter

1 1.0000e+00 1.0057e-08 2.4558e-09 5.8698e-11 2.0961e+00 7.8218e-01 2:16:33 999

2 1.0000e+00 5.5008e-04 5.7877e-04 3.6202e-04 5.6841e-01 1.1389e-01 2:19:04 998

3 5.5110e-01 2.7979e-04 3.0657e-04 2.3166e-04 4.6478e-01 1.0972e-01 2:17:44 997

4 3.8050e-01 1.6274e-04 1.9816e-04 1.6168e-04 4.1744e-01 5.9507e-02 2:16:38 996

5 1.9085e-01 8.9960e-05 1.0302e-04 7.0969e-05 4.1354e-01 3.2206e-02 2:15:44 995

6 1.5431e-01 9.0862e-05 9.2349e-05 6.0065e-05 4.2130e-01 3.4797e-02 2:14:59 994

7 9.8058e-02 7.6710e-05 7.3805e-05 4.0587e-05 4.4695e-01 3.6668e-02 2:14:21 993

8 7.9903e-02 7.2074e-05 6.8831e-05 3.5215e-05 4.9693e-01 4.2844e-02 2:13:50 992

9 8.5469e-02 7.6961e-05 7.6585e-05 3.9497e-05 5.0110e-01 4.3209e-02 2:13:23 991

10 6.2164e-02 7.3104e-05 7.1432e-05 3.3778e-05 5.1799e-01 4.4226e-02 2:13:00 990

C.1.3.2 The Last Ten Iterations with the Final Solution

iter continuity x-velocity y-velocity z-velocity Cl-1 Cd-1 time/iter

991 1.1773e-03 3.1060e-07 2.3300e-07 1.8708e-07 7.6824e-01 3.2900e-02 0:01:13 9

992 1.1822e-03 3.1173e-07 2.3435e-07 1.8714e-07 7.6821e-01 3.2892e-02 0:01:06 8

993 1.1805e-03 3.1099e-07 2.3561e-07 1.8767e-07 7.6820e-01 3.2891e-02 0:00:58 7

994 1.1808e-03 3.1102e-07 2.3691e-07 1.8804e-07 7.6817e-01 3.2884e-02 0:00:49 6

995 1.1883e-03 3.1257e-07 2.4033e-07 1.9081e-07 7.6816e-01 3.2887e-02 0:00:42 5

996 1.1822e-03 3.1230e-07 2.4044e-07 1.9177e-07 7.6814e-01 3.2881e-02 0:00:33 4

997 1.1767e-03 3.1227e-07 2.4005e-07 1.9231e-07 7.6813e-01 3.2880e-02 0:00:25 3

998 1.1735e-03 3.1122e-07 2.4075e-07 1.9216e-07 7.6812e-01 3.2876e-02 0:00:16 2

999 1.1850e-03 3.1417e-07 2.4317e-07 1.9342e-07 7.6812e-01 3.2881e-02 0:00:08 1

1000 1.1814e-03 3.1788e-07 2.4161e-07 1.9513e-07 7.6810e-01 3.2874e-02 0:00:00 0

C.1.4 The Plain Wing at ten Degrees Angle of Attack Iterations

C.1.4.1 The First Ten Iterations in the Unstable Stage

iter continuity x-velocity y-velocity z-velocity Cl-1 Cd-1 time/iter

1 1.0000e+00 9.6572e-09 3.1956e-09 5.9421e-11 3.9793e+00 1.3156e+00 2:13:12 999

2 1.0000e+00 8.2825e-04 8.9324e-04 5.5972e-04 8.1515e-01 1.8161e-01 2:16:24 998

3 5.5692e-01 3.9770e-04 4.6780e-04 3.5045e-04 7.6791e-01 1.8740e-01 2:15:36 997

4 3.5448e-01 2.2821e-04 2.8413e-04 2.2479e-04 6.4964e-01 1.1494e-01 2:14:55 996

5 1.7893e-01 1.2687e-04 1.5340e-04 9.9490e-05 5.9423e-01 7.3514e-02 2:17:41 995

6 1.4620e-01 1.3256e-04 1.3790e-04 8.7043e-05 6.2276e-01 7.9452e-02 2:16:32 994

7 9.3135e-02 1.1398e-04 1.1163e-04 5.9894e-05 6.7813e-01 8.6428e-02 2:12:18 993

8 7.6286e-02 1.0896e-04 1.0540e-04 5.2680e-05 7.6217e-01 1.0089e-01 2:15:29 992

9 8.0623e-02 1.1650e-04 1.1859e-04 5.7994e-05 7.6974e-01 1.0009e-01 2:14:42 991

10 5.9637e-02 1.1112e-04 1.1207e-04 5.0589e-05 7.9527e-01 1.0089e-01 2:10:45 990

C.1.4.2 The Last Tten Iterations with the Final Solution

iter continuity x-velocity y-velocity z-velocity Cl-1 Cd-1 time/iter

991 1.1013e-03 4.1334e-07 3.2367e-07 2.6527e-07 1.1653e+00 6.9728e-02 0:01:06 9

992 1.1038e-03 4.1723e-07 3.2573e-07 2.6714e-07 1.1653e+00 6.9716e-02 0:01:00 8

993 1.1011e-03 4.1287e-07 3.2412e-07 2.6535e-07 1.1653e+00 6.9720e-02 0:00:52 7

994 1.0944e-03 4.1413e-07 3.2339e-07 2.6543e-07 1.1652e+00 6.9709e-02 0:00:45 6

995 1.0828e-03 4.1327e-07 3.2291e-07 2.6618e-07 1.1652e+00 6.9717e-02 0:00:38 5

996 1.0757e-03 4.1250e-07 3.2445e-07 2.6776e-07 1.1652e+00 6.9704e-02 0:00:30 4

997 1.0702e-03 4.1249e-07 3.2587e-07 2.6653e-07 1.1652e+00 6.9711e-02 0:00:22 3

998 1.0802e-03 4.1558e-07 3.2472e-07 2.6719e-07 1.1652e+00 6.9705e-02 0:00:15 2

999 1.0770e-03 4.1613e-07 3.2717e-07 2.6915e-07 1.1652e+00 6.9708e-02 0:00:07 1

1000 1.0577e-03 4.1581e-07 3.2787e-07 2.7044e-07 1.1652e+00 6.9706e-02 0:00:00 0

C.2 The Wing with Winglets Simulation

C.2.1 The Wing with Winglets Script Details

Loading "C:\PROGRA~1\ANSYSI~1\v140\fluent\fluent14.0.0\lib\fl114-64.dmp"

Done.

Welcome to ANSYS FLUENT 14.0.0

Copyright 2011 ANSYS, Inc.. All Rights Reserved.

Unauthorized use, distribution or duplication is prohibited.

This product is subject to U.S. laws governing export and re-export.

For full Legal Notice, see documentation.

Build Time: Oct 25 2011 13:11:26 Build Id: 10398

Loading "C:\PROGRA~1\ANSYSI~1\v140\fluent\fluent14.0.0\lib\flprim1119-64.dmp"

Done.

Host spawning Node 0 on machine "ebrahim-PC" (win64).

You can press CTRL+C to stop the startup process!

WARNING: No cached password or password provided.

use '-pass' or '-cache' to provide password

Platform-MPI licensed for FLUENT.

Host 0 -- ip 192.168.1.10 -- ranks 0 - 3

host | 0

======|======

0 : SHM

Prot - All Intra-node communication is: SHM

ID Comm. Hostname O.S. PID Mach ID HW ID Name

---

host net ebrahim-PC Windows-x64 5816 0 488 Fluent Host

n3 pcmpi ebrahim-PC Windows-x64 3420 0 3 Fluent Node

n2 pcmpi ebrahim-PC Windows-x64 4308 0 2 Fluent Node

n1 pcmpi ebrahim-PC Windows-x64 3412 0 1 Fluent Node

n0* pcmpi ebrahim-PC Windows-x64 3176 0 0 Fluent Node

Selected system interconnect: default

Cleanup script file is C:\Users\ebrahim\AppData\Local\Temp\cleanup-fluent-ebrahim-PC-5816.bat

> Note: Rank = 0: Process affinity not being set (6).

Note: Rank = 2: Process affinity not being set (6).

Note: Rank = 1: Process affinity not being set (6).

Note: Rank = 3: Process affinity not being set (6).

Reading Settings file C:\Users\ebrahim\Documents\Theises\wingwinglet65D0.4m_files\dp0\FFF\Fluent\FFF.set...

Reading "C:\Users\ebrahim\Documents\Theises\wingwinglet65D0.4m_files\dp0\FFF\MECH\FFF.msh"...

Using buffering for scanning file.

635767 nodes, binary.

137743 nodes, binary.

50612 triangular wall faces, zone 1, binary.

8284919 triangular interior faces, zone 2, binary.

182248 triangular velocity-inlet faces, zone 6, binary.

42618 triangular pressure-outlet faces, zone 7, binary.

4211329 tetrahedral cells, zone 3, binary.

Building...

mesh

auto partitioning mesh by Metis (fast),

distributing mesh

parts....,

faces....,

nodes....,

cells....,

materials,

interface,

domains,

mixture

zones,

pressure-outlet

velocity-inlet

solid

interior-solid

wall-solid Setting zone id of solid to 3.

Setting zone id of wall-solid to 1.

Setting zone id of interior-solid to 2.

Setting zone id of velocity-inlet to 6.

Setting zone id of pressure-outlet to 7.

Done.

Setting solid (mixture) ... Done.

Setting wall-solid (mixture) ... Done.

Setting interior-solid (mixture) ... Done.

Setting velocity-inlet (mixture) ... Done.

Setting pressure-outlet (mixture) ... Done.

parallel,

Done.

Preparing mesh for display...

Done.

Setting Post Processing and Surfaces information ... Done.

Writing Settings file...

writing rp variables ... Done.

writing domain variables ... Done.

writing solid (type fluid) (mixture) ... Done.

writing wall-solid (type wall) (mixture) ... Done.

writing interior-solid (type interior) (mixture) ... Done.

writing velocity-inlet (type velocity-inlet) (mixture) ... Done.

writing pressure-outlet (type pressure-outlet) (mixture) ... Done.

writing zones map name-id ... Done

C.2.2 The Wing with Winglets at Zero Degree Angle of Attack Iterations

C.2.2.1 The First Ten Iterations in the Unstable Stage

iter	continuity	x-velocity	y-velocity	z-velocity	Cl-1	Cd-1	time/iter
1	1.0000e+00	1.0552e-08	2.1686e-09	2.8027e-10	1.7711e-01	5.5000e-01	3:03:09 999
2	1.0000e+00	3.8655e-04	3.8873e-04	2.4436e-04	2.4939e-01	8.0254e-02	3:02:58 998
3	5.7729e-01	2.1392e-04	2.1439e-04	1.6712e-04	1.9997e-01	7.5463e-02	3:02:47 997
4	4.2085e-01	1.2889e-04	1.4816e-04	1.2618e-04	2.0672e-01	3.5966e-02	2:59:17 996
5	2.1311e-01	7.1243e-05	7.2800e-05	5.6740e-05	2.0523e-01	1.7351e-02	2:56:27 995
6	1.4355e-01	5.3828e-05	4.9428e-05	3.4948e-05	2.1471e-01	1.1337e-02	2:54:09 994
7	1.2906e-01	5.0733e-05	4.9910e-05	3.4710e-05	2.1304e-01	1.4062e-02	2:48:58 993
8	8.8347e-02	4.1350e-05	3.8858e-05	2.2756e-05	2.1871e-01	1.5795e-02	2:48:06 992
9	8.1000e-02	3.8921e-05	3.6172e-05	2.1087e-05	2.2145e-01	1.6431e-02	2:47:23 991
10	6.1544e-02	3.6544e-05	3.2749e-05	1.7172e-05	2.2829e-01	1.6853e-02	2:43:28 990

C.2.2.2 The Last Ten Iterations with the Final Solution

iter continuity x-velocity y-velocity z-velocity Cl-1 Cd-1 time/iter

991 1.2749e-03 2.4328e-07 1.8848e-07 1.6250e-07 3.2883e-01 1.4186e-02 0:01:24 9

992 1.2746e-03 2.4291e-07 1.8826e-07 1.6136e-07 3.2884e-01 1.4183e-02 0:01:14 8

993 1.2713e-03 2.4309e-07 1.8844e-07 1.6113e-07 3.2885e-01 1.4188e-02 0:01:05 7

994 1.2705e-03 2.4238e-07 1.8761e-07 1.6121e-07 3.2886e-01 1.4183e-02 0:00:56 6

995 1.2753e-03 2.4308e-07 1.8706e-07 1.6120e-07 3.2886e-01 1.4188e-02 0:00:47 5

996 1.2796e-03 2.4315e-07 1.8723e-07 1.6114e-07 3.2887e-01 1.4185e-02 0:00:37 4

997 1.2713e-03 2.4206e-07 1.8672e-07 1.6061e-07 3.2887e-01 1.4189e-02 0:00:28 3

998 1.2722e-03 2.4156e-07 1.8598e-07 1.5986e-07 3.2888e-01 1.4187e-02 0:00:19 2

999 1.2653e-03 2.4120e-07 1.8512e-07 1.5912e-07 3.2887e-01 1.4189e-02 0:00:09 1

1000 1.2672e-03 2.4080e-07 1.8453e-07 1.5850e-07 3.2887e-01 1.4186e-02 0:00:00 0

C.2.3 The Wing with Winglets at Five Degrees Angle of Attack Iterations

C.2.3.1 The First Ten Iterations in the Unstable Stage

iter continuity x-velocity y-velocity z-velocity Cl-1 Cd-1 time/iter

1 1.0000e+00 1.0522e-08 2.5413e-09 2.8330e-10 2.0259e+00 7.4239e-01 3:03:09 999

2 1.0000e+00 5.4056e-04 5.6663e-04 3.5574e-04 5.4748e-01 1.0443e-01 3:02:58 998

3 5.5702e-01 2.7760e-04 3.0073e-04 2.2735e-04 4.6190e-01 1.0465e-01 2:59:28 997

4 3.7673e-01 1.5956e-04 1.9158e-04 1.5717e-04 4.1669e-01 5.6489e-02 2:53:18 996

5 1.9055e-01 9.0999e-05 1.0094e-04 7.0413e-05 3.9319e-01 3.4497e-02 2:51:40 995

6 1.3017e-01 7.5479e-05 7.6425e-05 4.4909e-05 4.2539e-01 3.1784e-02 2:50:20 994

7 1.3560e-01 9.3499e-05 9.0079e-05 5.6758e-05 4.3747e-01 3.5425e-02 2:49:14 993

8 8.7168e-02 8.0754e-05 7.5515e-05 4.0238e-05 4.7106e-01 3.9771e-02 2:48:19 992

9 7.8321e-02 7.2051e-05 7.1409e-05 3.5621e-05 4.8164e-01 4.1052e-02 2:44:15 991

10 5.9884e-02 6.9392e-05 6.7594e-05 3.1106e-05 5.0336e-01 4.2756e-02 2:44:16 990

C.2.3.2 The Last Ten Iterations with the Final Solution

iter continuity x-velocity y-velocity z-velocity Cl-1 Cd-1 time/iter

991 1.2439e-03 3.2693e-07 2.8008e-07 2.3035e-07 7.4701e-01 3.1799e-02 0:01:23 9

992 1.2358e-03 3.2557e-07 2.7888e-07 2.2725e-07 7.4701e-01 3.1792e-02 0:01:13 8

993 1.2325e-03 3.2448e-07 2.7709e-07 2.2604e-07 7.4702e-01 3.1801e-02 0:01:04 7

994 1.2411e-03 3.2408e-07 2.7574e-07 2.2450e-07 7.4700e-01 3.1788e-02 0:00:55 6

995 1.2361e-03 3.2088e-07 2.7196e-07 2.2204e-07 7.4701e-01 3.1798e-02 0:00:45 5

996 1.2402e-03 3.2030e-07 2.7016e-07 2.1892e-07 7.4699e-01 3.1785e-02 0:00:36 4

997 1.2551e-03 3.2008e-07 2.6811e-07 2.1859e-07 7.4702e-01 3.1799e-02 0:00:27 3

998 1.2473e-03 3.1594e-07 2.6711e-07 2.1663e-07 7.4700e-01 3.1787e-02 0:00:18 2

999 1.2495e-03 3.1449e-07 2.6578e-07 2.1507e-07 7.4704e-01 3.1803e-02 0:00:09 1

1000 1.2982e-03 3.4176e-07 2.9081e-07 2.2955e-07 7.4694e-01 3.1766e-02 0:00:00 0

C.2.4 The Wing with Winglets at Ten Degrees Angle of Attack Iterations

C.2.1.1 The First ten Iterations in the Unstable Stage

iter	continuity	x-velocity	y-velocity	z-velocity	Cl-1	Cd-1	time/iter
1	1.0000e+00	1.0399e-08	3.3480e-09	2.9501e-10	3.8249e+00	1.2555e+00	3:03:09 999
2	1.0000e+00	8.0865e-04	8.7186e-04	5.4735e-04	7.9468e-01	1.6939e-01	3:02:58 998
3	5.5841e-01	3.9019e-04	4.5336e-04	3.4330e-04	7.9323e-01	1.8614e-01	2:56:08 997
4	2.5760e-01	2.1163e-04	2.3050e-04	1.6860e-04	5.5931e-01	7.9131e-02	2:53:58 996
5	2.9633e-01	1.9928e-04	2.3084e-04	1.7451e-04	5.8743e-01	8.2052e-02	2:52:12 995
6	1.5094e-01	1.3281e-04	1.3568e-04	8.3154e-05	6.0374e-01	7.4041e-02	2:50:45 994
7	1.0141e-01	1.1245e-04	1.1106e-04	5.7869e-05	6.7921e-01	8.7216e-02	2:49:34 993
8	1.1703e-01	1.3064e-04	1.3275e-04	7.6913e-05	6.9685e-01	8.8059e-02	2:45:17 992
9	7.5599e-02	1.1608e-04	1.1398e-04	5.5813e-05	7.5376e-01	9.5886e-02	2:48:26 991
10	7.2377e-02	1.1256e-04	1.0909e-04	5.2667e-05	7.6220e-01	9.5293e-02	2:44:18 990

C.2.4.2 The Last Ten Iterations with the Final Solution

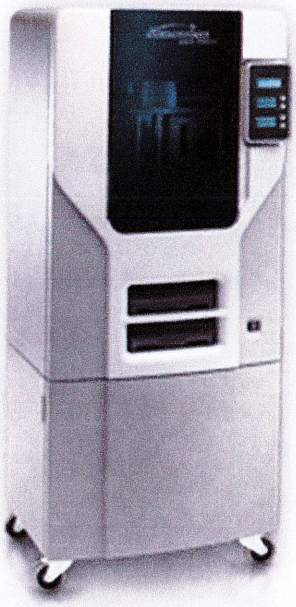
iter	continuity	x-velocity	y-velocity	z-velocity	Cl-1	Cd-1	time/iter
991	1.4446e-03	5.6447e-07	4.5118e-07	3.7523e-07	1.1330e+00	6.7248e-02	0:01:26 9
992	1.4649e-03	5.7229e-07	4.5781e-07	3.8243e-07	1.1329e+00	6.7233e-02	0:01:17 8
993	1.4486e-03	5.6787e-07	4.5409e-07	3.7892e-07	1.1329e+00	6.7238e-02	0:01:07 7
994	1.4215e-03	5.6151e-07	4.4954e-07	3.7374e-07	1.1329e+00	6.7244e-02	0:00:56 6
995	1.4087e-03	5.6033e-07	4.4785e-07	3.7340e-07	1.1329e+00	6.7246e-02	0:00:48 5
996	1.3924e-03	5.5765e-07	4.4380e-07	3.7215e-07	1.1329e+00	6.7255e-02	0:00:38 4
997	1.3973e-03	5.5379e-07	4.4524e-07	3.7278e-07	1.1329e+00	6.7258e-02	0:00:28 3
998	1.4126e-03	5.5349e-07	4.4500e-07	3.6931e-07	1.1329e+00	6.7260e-02	0:00:19 2
999	1.4257e-03	5.5676e-07	4.4661e-07	3.7137e-07	1.1330e+00	6.7268e-02	0:00:09 1
1000	1.4239e-03	5.5587e-07	4.4574e-07	3.6992e-07	1.1330e+00	6.7260e-02	0:00:00 0

Appendix (D)

Dimension 1200es 3-D Printer Specifications

Print large, durable 3-D models right in your office. See your designs come to life with the Dimension SST 1200es™ and BST 1200es 3D Printers. They turn 3-D CAD files into functional, durable 3D models that you can not only discuss but test. The large build capacity of Dimension 1200es 3D Printers gives you the room to print models at the size you need. And they're simple to operate: Just click "print" to prep the CAD file and print the model, then remove the support material to reveal your design in three dimensions. Bundle & Save Order the Dimension 3-D Print Pack and you'll get everything you need to start printing 3-D models affordably – as soon as you unbox it. You get a:

- Dimension 1200es SST 3D Printer
- SCA-1200 support removal system
- Startup supply of materials.



Model material: ABSplus in ivory, white, black, red, olive green, nectarine, fluorescent yellow, blue or gray

Support material: Soluble Support Technology (SST) or Breakaway Support Technology (BST)

Build size: 254 x 254 x 305 mm (10 x 10 x 12 in)

Layer thickness .254 mm (.010 in) or .330 mm (.013 in) of precisely deposited ABSplus model and support material

Workstation compatibility: Windows XP/Windows 7

Network connectivity: Ethernet TCP/IP 10/100Base-T

Size and weight: 838 x 737 x 1143 mm (33 x 29 x 45 in) 148 kg (326 lbs)

Power requirements: 110–120 VAC, 60 Hz, minimum 15A dedicated circuit; or 220–240 VAC 50/60 Hz, minimum 7A dedicated circuit

Regulatory compliance: CE/ETL

Special facility requirements: None

Appendix (E)

C-15 Computer Controlled Subsonic Wind Tunnel



C15-10 Computer Controlled Subsonic Wind Tunnel Ordering Specification

- Small computer controlled wind tunnel for undergraduate teaching
- Clear acrylic working section (150mm x 150mm x 455mm) for excellent visibility
- Inverter controlled AC fan for accurate speed control up to 34m/s air velocity

- Wide range of optional models and instrumentation
- Multi-way or single-way quick release connectors between models and manometers
- Models mounted in side wall of working section incorporate quick release catches
- Complete with data logging and educational software
- Removable base to working section to allow the insertion of large or complex models
- Flow visualization facility included
- Air flow studies option available including Bernoulli apparatus

Appendix (F)

Wind Tunnel Results

Wind Tunnel (C-15) Test 1: Plain Wing

Test 1: Plain Wing	Fan Speed [%]	Rotation r [°]	Lift Force L [N]	Drag Force D [N]	Static Pressure H [mm]	Ambient Temperature T [°C]	Density of Air [kg/m³]	Air Velocity v [m/s]	Reynolds Number Re	C_L	C_D	C_{DL}
1	96	0.0	0.001611	0.001665	65.2	18.0	1.211	32.5	2111635	0.133	0.011	0.0013
2	96	5.0	0.003330	0.053281	69.1	18.0	1.211	33.5	2111635	0.211	0.022	0.0023
3	96	9.9	0.006660	0.056611	72.8	18.0	1.211	34.3	2111635	0.301	0.054	0.0210
4	96	14.1	0.006660	0.056611	66.4	18.0	1.211	32.8	2111635	0.301	0.054	0.0443
5	68	0.0	0.003330	0.003330	28.1	18.0	1.211	21.3	1407757	0.301	0.009	0.0017
6	68	5.2	0.003277	0.003992	33.7	18.0	1.211	23.4	1407757	0.205	0.014	0.0080
7	68	9.9	0.004995	0.004995	32.8	18.0	1.211	23.0	1407757	0.223	0.032	0.0290
8	68	14.8	0.016658	0.001665	26.2	18.0	1.211	20.6	1407757	0.133	0.011	0.0441
9	31	0.0	0.001006	0.002110	6.1	18.0	1.211	10.0	703878	0.005	0.013	0.0022
10	31	4.9	0.001121	0.003002	6.9	18.0	1.211	10.5	703878	0.008	0.051	0.0076
11	31	10.2	0.002308	0.005904	7.0	18.0	1.211	10.6	703878	0.017	0.021	0.0241
12	31	14.8	0.007111	0.012211	6.7	18.0	1.211	10.4	703878	0.027	0.040	0.0455
13	96	0.0	0.001665	0.003112	60.6	18.0	1.211	31.3	2111635	0.133	0.008	0.0075
14	96	5.0	0.001665	0.054433	63.3	18.0	1.211	32.0	2111635	0.133	0.031	0.0073
15	96	10.1	0.008325	0.066607	73.2	18.0	1.211	34.4	2111635	0.034	0.042	0.0088
16	96	14.9	0.008325	0.083250	73.6	18.0	1.211	34.5	2111635	0.065	0.046	0.0210
17	68	0.0	0.003554	0.004344	26.8	18.0	1.211	20.8	1407757	0.329	0.010	0.0044
18	68	5.1	0.004995	0.006660	33.4	18.0	1.211	23.2	1407757	0.433	0.038	0.0021
19	68	10.1	0.006660	0.008325	32.0	18.0	1.211	22.8	1407757	0.544	0.036	0.0098
20	68	14.9	0.004995	0.008325	31.7	18.0	1.211	22.7	1407757	0.466	0.067	0.0311

Experimental results

Wind Tunnel (C-15) Test2: Plain Wing

Test2: Plain Wing	Fan Speed [%]	Rotation r [°]	Lift Force L [N]	Drag Force D [N]	Static Pressure H [mm]	Ambient Temperature T [°C]	Density of Air [kg/m³]	Air Velocity v [m/s]	Reynolds Number Re	C_L	C_D	C_{DL}
1	31	0.0	0.0016650	0.0016650	6.3	18.0	1.211	10.1	703878	0.121	0.0098	0.0011
2	31	4.9	0.0049951	0.0033301	6.7	18.0	1.211	10.4	703878	0.440	0.0087	0.0012
3	31	10.0	0.0033301	0.0016650	6.9	18.0	1.211	10.5	703878	0.466	0.0133	0.0075
4	31	15.1	0.0016650	0.0016650	6.6	18.0	1.211	10.4	703878	0.788	0.0599	0.0066
5	63	0.0	0.0020021	0.0043300	25.2	18.0	1.211	20.2	1407757	0.221	0.0218	0.0065
6	63	5.0	0.0059901	0.0055606	28.3	18.0	1.211	21.4	1407757	0.471	0.0086	0.0114
7	63	15.0	0.0039987	0.0088093	28.3	18.0	1.211	21.4	1407757	0.866	0.0640	0.0155
8	94	0.0	0.0004430	0.0016650	60.8	18.0	1.211	31.4	1407757	0.410	0.0066	0.0033
9	94	5.0	0.0016650	0.0033301	68.4	18.0	1.211	33.3	2111635	0.611	0.0034	0.0096
10	94	9.8	0.0049951	0.0066602	70.5	18.0	1.211	33.8	2111635	0.390	0.0098	0.0290
11	94	15.0	0.0070051	0.0066602	70.0	18.0	1.211	33.7	2111635	0.599	0.0311	0.0551

Experimental results

Wind Tunnel (C-15) Test 3: Plain Wing

Test3: Plain Wing	Fan Speed [%]	Rotation r [°]	Lift Force L [N]	Drag Force D [N]	Static Pressure H [mm]	Ambient Temperature T [°C]	Density of Air [kg/m³]	Air Velocity v [m/s]	Reynolds Number Re	C_L	C_D	C_{DL}
1	31	0.0	0.0016650	0.0001222	6.0	18.0	1.211	9.9	703878	0.2111207	0.0075521	0.000122
2	31	5.0	0.0016650	0.0016650	6.6	18.0	1.211	10.4	703878	0.3932964	0.0098035	0.0011457
3	31	10.0	0.0016650	0.0049951	7.0	18.0	1.211	10.6	703878	0.3690011	0.0133967	0.0029306
4	31	15.2	0.0016650	0.0088771	6.6	18.0	1.211	10.4	703878	0.3809331	0.0345202	0.0045204
5	64	0.0	0.0016650	0.0016650	26.9	18.0	1.211	20.9	1407757	0.0970012	0.0970811	0.0213666
6	64	4.8	0.0006650	0.0016650	28.8	18.0	1.211	21.6	1407757	0.4211678	0.0907177	0.0690009
7	64	10.1	0.0016650	0.0033301	28.8	18.0	1.211	21.6	1407757	0.8930012	0.0986000	0.0209962
8	64	14.9	0.0049951	0.0033301	29.3	18.0	1.211	21.8	1407757	2.5009987	0.1083109	0.0713331
9	93	0.0	0.0099073	0.0099902	59.1	18.0	1.211	30.9	2111635	0.0081223	0.0265308	0.0112210
10	93	5.0	0.0066602	0.0682666	67.0	18.0	1.211	33.0	2111635	0.1552052	0.1024888	0.0500860
11	93	10.2	0.0016650	0.0649365	67.3	18.0	1.211	33.0	2111635	0.3820511	0.1222206	0.0442988
12	93	14.8	0.0066602	1.1871729	66.3	18.0	1.211	32.8	2111635	1.5239880	0.2978441	0.1907560

Experimental results

Wind Tunnel (C-15) Test 4: Wing with winglets

Test 4: Wing with winglets	Fan Speed [%]	Rotation r [°]	Lift Force L [N]	Drag Force D [N]	Static Pressure H [mm]	Ambient Temperature T [°C]	Density of Air [kg/m³]	Air Velocity v [m/s]	Reynolds Number Re	C_L	C_D	C_{DL}
1	31	0.0	0.0017650	0.0001821	7.0	18.0	1.211	10.6	703878	0.144	0.0053	0.0021
2	31	5.0	0.0018640	0.000877	6.6	18.0	1.211	10.4	703878	0.012	0.0036	0.0011
3	31	10.1	0.0019880	0.0049951	6.9	18.0	1.211	10.5	703878	0.321	0.0059	0.0031
4	31	15.0	0.0016333	0.0088771	6.6	18.0	1.211	10.4	703878	0.101	0.0322	0.0098
5	63	0.0	0.0016322	0.0033650	24.1	18.0	1.211	19.8	1407757	0.109	0.0048	0.0013
6	63	5.1	0.0023344	0.0033301	30.3	18.0	1.211	22.2	1407757	0.344	0.0042	0.0011
7	63	10.1	0.0078833	0.0053991	31.1	18.0	1.211	22.5	1407757	0.569	0.0040	0.0009
8	63	15.0	0.0122322	0.0099902	30.5	18.0	1.211	22.2	1407757	1.032	0.0528	0.0189
9	90	0.0	0.0067743	0.0682666	54.2	18.0	1.211	29.6	2111635	0.488	0.0917	0.0477
10	90	5.1	0.0032650	0.0649365	66.2	18.0	1.211	32.8	2111635	0.251	0.0908	0.0451
11	90	9.9	0.0089602	1.1871729	53.9	18.0	1.211	29.5	2111635	1.687	0.2557	0.1004
12	90	15.1	0.0122650	0.0001222	51.8	18.0	1.211	29.0	2111635	1.810	0.0042	0.0011

Experimental results

Wind Tunnel (C-15) Test 5: Wing with winglets

Test 5: Wing with winglets	Fan Speed [%]	Rotation r [°]	Lift Force L [N]	Drag Force D [N]	Static Pressure H [mm]	Ambient Temperature T [°C]	Density of Air [kg/m³]	Air Velocity v [m/s]	Reynolds Number Re	C_L	C_D	C_{DL}
1	31	0.0	0.0014880	0.0001963	7.0	18.0	1.211	10.6	703878	0.209	0.0063	0.0030
2	31	5.0	0.0019648	0.0007558	6.6	18.0	1.211	10.4	703878	0.344	0.0089	0.0033
3	31	10.1	0.0024880	0.0009360	6.9	18.0	1.211	10.5	703878	0.589	0.0109	0.0052
4	31	15.0	0.0032333	0.0078876	6.6	18.0	1.211	10.4	703878	0.321	0.0370	0.0162
5	63	0.0	0.0015874	0.0041654	24.1	18.0	1.211	19.8	1407757	0.592	0.0071	0.0034
6	63	5.1	0.0023344	0.0063891	30.3	18.0	1.211	22.2	1407757	0.883	0.0078	0.0034
7	63	10.1	0.0066863	0.0083309	31.1	18.0	1.211	22.5	1407757	0.784	0.0233	0.0101
8	63	15.0	0.0142002	0.0099015	30.5	18.0	1.211	22.2	1407757	1.282	0.0769	0.0321
9	90	0.0	0.0067743	0.0682225	54.2	18.0	1.211	29.6	2111635	0.388	0.0122	0.0056
10	90	5.1	0.0038740	0.0758830	66.2	18.0	1.211	32.8	2111635	0.691	0.0428	0.0288
11	90	9.9	0.0083058	1.2171729	53.9	18.0	1.211	29.5	2111635	1.081	0.0896	0.0433
12	90	15.1	0.0137855	1.2220188	51.8	18.0	1.211	29.0	2111635	1.466	0.0755	0.0246

Experimental results

Wind Tunnel (C-15) Test 6: Wing with winglets

Test 6: Wing with winglets	Fan Speed [%]	Rotation r [°]	Lift Force L [N]	Drag Force D [N]	Static Pressure H [mm]	Ambient Temperature T [°C]	Density of Air [kg/m³]	Air Velocity v [m/s]	Reynolds Number Re	C_L	C_D	C_{DL}
1	32	0.0	0.0009221	0.0016650	6.4	18.0	1.211	10.2	703878	0.136	0.009	0.002
2	32	4.9	0.0016650	0.0023308	7.0	18.0	1.211	10.6	703878	0.355	0.021	0.009
3	32	9.9	0.0035509	0.0045509	7.7	18.0	1.211	11.1	703878	0.866	0.043	0.026
4	32	15.0	0.0072099	0.0087661	7.3	18.0	1.211	10.9	703878	0.988	0.045	0.034
5	60	0.0	0.0015539	0.0018852	23.2	18.0	1.211	19.4	1407757	0.211	0.009	0.004
6	60	5.0	0.0033301	0.0038221	26.1	18.0	1.211	20.6	1407757	0.423	0.027	0.011
7	60	10.0	0.0096662	0.0056629	26.4	18.0	1.211	20.7	1407757	0.879	0.051	0.038
8	60	14.8	0.0123301	0.0092074	26.9	18.0	1.211	20.9	1407757	1.002	0.063	0.046
9	91	0.0	0.0014442	0.0023110	54.6	18.0	1.211	29.7	2111635	0.311	0.011	0.005
10	91	4.8	0.0066509	0.0056618	65.4	18.0	1.211	32.5	2111635	0.538	0.034	0.013
11	91	9.9	0.0108776	0.0090011	65.6	18.0	1.211	32.6	2111635	0.903	0.076	0.037
12	91	15.1	0.0377730	0.0165537	47.6	18.0	1.211	27.8	2111635	1.226	0.082	0.044

Abstract (Arabic)

ملخص الرسالة

تم التحقق نظريا ومختبريا في خصائص الديناميكا الهوائية لجناح هوائي عند إضافة جوينحات جانبية في أطرافه. وتعد قوة الرفع وقوة المقاومة هما العاملان المحددان لنتائج هذه الدراسة.

تمت دراسة جناح طائرة رياضية خفيفة بقياساته الحقيقية. ويتميز بأنه مستطيل الشكل بسيط التصميم. ويتكون مقطعه الطولي من أطوال متساوية من NACA 4412 بينما أطراف الجوينحات الخارجية تتكون من المقطع NACA 0012 المرجع الدولي المعتمد لوكالة الطيران والفضاء الأمريكية. علما بأن هذه الطائرة لا تحوي جوينحات إضافية جانبية في تصميمها الأصلي. تمت دراسة التأثيرات و التغيرات في قوة الرفع وقوة المقامة بهدف التوصل للشكل الأمثل للجوينحات الاضافية بالإضافة لجدوى اضافتها من عدمه. وهذا كله سينعكس على الأهداف الرئيسية والمتمثلة بالتالي:

١. تقليل قوة المقاومة الناتجة من قوة الرفع.

٢. تقليل نسبة استهلاك الوقود وبالتالي زيادة مدى الطائرة نتيجة لتقليل المقاومة.

٣. زيادة معايير السلامة أثناء الطيران.

تم اعتماد نموذج ثلاثي الأبعاد عن طريق تكرار المحاولات في برنامج 3-D Foil Multi-Surfaces. حيث حصلنا على نموذج جناح بجوينح مساحته ٩,٥٢٨ م^{٢} للنموذج الأصلي و١٠,٣٢٨ م^{٢} للنموذج المعدل بالزوائدة الجوينحية. قمنا بمعالجة المرسومات حسب المعطيات القياسية للظروف المحيطة في كل من برنامج Fluent Ansys 14 وبرنامج 3-D Foil Multi-Surfaces. لمحاكاة ظروف إقلاع الطائرة والتي تتجلى فيها هذه الظاهرة بشكل كبير تم اعتماد سرعة طيران ٥٠ متر\ ثانية في درجة حرارة ١٥ درجة سيليزية على مستوى سطح البحر. وتم معالجة البيانات لثلاث مرات، كل منها لزاوية هجوم مختلفة كالآتي: صفر، خمس درجات و١٠ درجات. ثم قمنا بمقارنة النتائج المتحصل عليها بالمعادلات النظرية. وقد حصلنا على نتائج مرضية متقاربة تدعم فرضيتنا بجدوى تركيب الجوينحات لهذا النوع من الطائرات.

وقد قمنا بعد ذلك بعمل تجربة عملية في النفق الهوائي الخاص بجامعة البحرين C-15 Computer Controlled Subsonic Wind Tunnel .و تم الحصول على نتائج مرضية دعمت فرضيتنا المذكورة أعلاه. جرت التجربة في سرعات مختلفة بلغ أقصاها حوالي ٣٠ متر/ ثانية. وتم تكرار التجربة لكل من النموذجين في زوايا هجوم بلغت: صفر، خمس، عشر و خمسة عشر درجة.

ووصلنا ختاما إلى نتائج تم التحقق منها نظريا، عمليا وتشبيهيا عبر إجمالي ٣ وسائل تحقيق تفيد بأن تركيب الجوينحات لهذا النوع من الطائرات مجدي ويحقق مقاصد البحث. وقمنا بالتوصية بمواصلة البحث في هذا المجال مستقبلا ليشمل أنواعا أكثر من الطائرات وتصاميم أكثر من الجوينحات كذلك.

University Of Bahrain



كلية الهندسة

قسم الهندسة الميكانيكية

دراسة قوة الرفع و قوة المقاومة لجناح طائرة هوائية عند إضافة جوينحات

بحث لاستكمال متطلبات الحصول على درجة (الماجستير) في برنامج الهندسة الميكانيكية

إعداد

إبراهيم كمال صديق

الرقم الجامعي: ٢٠١٢١٠٠٣

إشراف

الأستاذ المشارك د. محمد نبهان

جامعة البحرين

مملكة البحرين

أكتوبر ٢٠١٦